# LATE QUATERNARY CLIMATE HISTORY ON THE NORTHEAST TIBETAN PLATEAU: MULTI-PROXY INVESTIGATION OF LAKE QINGHAI SEDIMENTS, CHINA

A DISSERTATION
SUBMITTED TO THE FACULTY OF THE GRADUATE SCHOOL
OF THE UNIVERSITY OF MINNESOTA
BY

Xiuju Liu

IN PARTIAL FULFILLMENT OF THE REQUIREMENTS
FOR THE DEGREE OF
DOCTOR OF PHILOSOPHY

Dr. Steven M. Colman
Dr. Erik T. Brown

September, 2011

# ACKNOWLEDGEMENTS

Financial support for the dissertation work described here was provided by National Science Foundation grant EAR-0602412 to Steven M. Colman.

Field work for this research was conducted with help from the Institute of Earth Environment Chinese Academy of Sciences in Xi'an and the Ministry of Education Key Laboratory of Western China's Environmental Systems, Research School of Arid Environment and Climate Change at Lanzhou University. Dr. Erik Brown, Dr. Doug Ricketts, Dr. Andrew Henderson, Dr. Shiyong Yu, Dr. Fahu Chen, Dr. Juzhi Hou, Mr. Jixiu Cao are especially thanked for their efforts in the field work.

Laboratory analyses greatly benefited from the interactions with staff and technicians of the Limnological Research Center (LRC) including Amy Mybro, Kristina Brady, and Anders Noren; the Large Lakes Observatory (LLO) including Sarah Grosshuesch and Yvonne Chan; the Institute for Rock Magnetism (IRM) including Julie Bowles, Mike Jackson, and Ioan Lascu; the Department of Geological Sciences at the University of Minnesota Duluth including Penny Morton. I would like to thank all of them for providing full access to the laboratories, valuable discussions and amazing help with lab work.

I am very thankful for the constant support and invaluable feedback from my dissertation committee members Dr. Emi Ito and Dr. Josef P. Werne. A special thanks also goes to Dr. Emi Ito for her great help during my application for a PhD program back in 2006 when I first met her in China. It is my privilege to thank my advisor Dr. Steven M. Colman for providing an opportunity to work in the Lake Qinghai Drilling Project, guiding and supporting me over the years. He is not only my research advisor but also my life mentor. I would never forget his solid advice and guidance when I went through hard times. I would really like to address special thanks to my co-advisor Dr. Erik T. Brown for his constant support and encouraging comments, and for being the most enthusiastic,

knowledgeable, and patient geochemist that I have had the pleasure of working with. I have been truly lucky to have them as my PhD advisors.

I am grateful to have had the opportunity to work with and learn from the faculty and staff at the LLO including Dr. Thomas Johnson, Dr. Elizabeth Minor, Dr. Sergei Katsev, Dr. Nigel Wattrus, Dr. Doug Ricketts, Ms. Yvonne Chan and Ms. Kathy Oliver.

I would like to thank all my fellow graduate students, colleagues, and friends, for providing intellectual and emotional support, and for making my stay in Duluth and in Minneapolis. I give my special thanks to Martijn Woltering, Prosper Zigah, Melissa Berke, Jessica Gary, Marian Kramer, Miao Du, April Abbott, Jiying Li, Hongyu Li, Meg Rubesch, Sergio Contreras Quintana**,** Marian Colman, Caihong Liu, Jun Ma, Peng Li, Gai Geng, Sharon Kressler, Lauren Idelman, Roxanne Renedo, Jennifer Wright, Patrick Hastings, Erkan Toraman, Feng Luo, Xiaoyi Cui, Arda Özdemir, Peng Li and Nicholas Palmquist. I enjoy my life so much in Minnesota largely because of them.

Finally, I deeply and sincerely thank my family for putting up with me and taking care of me always. A special thank you also goes out to my master's advisor Dr. Yan Zhao and many dear friends in China. Without their love and support, I would not be the person I am today.

# DEDICATION

This dissertation is dedicated to my parents for their endless love, unlimited support and encouragement, as well as to all those people, on whose shoulders I stand.

# ABSTRACT

The objective of this dissertation is to reconstruct the history of the Asian monsoon and to examine the controls of the climate system on the Tibetan Plateau, using lake sediment cores from Lake Qinghai, China. Lake Qinghai is the largest inland water body in China, situated on the northeastern margin of the Tibetan Plateau, where the climate conditions are mainly controlled by the interaction of the East Asian monsoon and the Westerlies. It lies near the limit of penetration of the Asian summer monsoon, and is thus sensitive to climate changes. Yet the climate history in this region is not fully understood. This dissertation contributes to our understanding of a detailed Holocene and late glacial climate history in western China.

A set of Lake Qinghai sediment cores, including a 18.6-m-long drill core (LQDP05-1F), a 3.5-m-long Uwitec sediment core (QH07-1A), and a 0.85-m-long mini-Mackereth core (QH07-1B-1MM), provide a record of climate that extends further back in time than that from any other records for Lake Qinghai.

Results from multiple proxies derived from the composite 2007 core (QH07) are internally consistent and reveal a distinct Holocene and Late Pleistocene climate record. Carbonate content and total organic carbon in sediments are interpreted as proxies for the strength of the Asian summer monsoon. During the glacial period (~14,600 to ~20,000 yrs), the summer monsoon intensity remained low and relatively constant, suggesting cool, dry, and relatively stable climatic conditions. The Holocene (~11,500 yrs to present) was a time of enhanced summer monsoon strength and greater variability, indicating relatively wetter but more unstable climatic conditions than those of the Late Pleistocene. The warmest, wettest part of the Holocene occurred from ~9,000 to ~11,500 yrs. The transition between the Holocene and the Late Pleistocene, about 11,500 years ago, was abrupt. A cool Younger Dryas appears to be recorded in the record, but its onset is not as distinct as it is in cave records from Dongge and Sanbao. Evidence of a warm interval

correlative with the Bølling–Allerød oscillation is weak in the QH07 record. We propose that changes in the contrast of summer insolation between the continent and the ocean are the primary control on the Asian monsoon system over the glacial/interglacial time scales. Secondary influences may include ice sheet size (albedo) and sea level (distance from moisture source). A climate threshold for arrival of monsoonal rainfall is suggested at the northeastern Tibetan Plateau.

Magnetic properties and geochemistry of sediments were determined for an 18.6 m u-channel sample of core LQDP05-1F and several selected discrete samples. These results provide clues to changes in magnetic mineral concentration, grain-size distribution, mineralogy, and geochemical composition, as well as having implications for paleoclimatology. The relative abundances of iron and concentration-dependent magnetic parameters reflect higher concentrations of magnetic minerals during glacial times than the Holocene. Hysteresis measurements of the discrete samples show larger proportions of single domain (SD) minerals relative to multiple domain (MD) particles in Late Pleistocene sediment compared to Holocene sediment, suggesting that the glacial period was dominated by deposition of fine-grained aeolian materials, whereas the Holocene was characterized by increased riverine transport of coarse materials to the lake. Furthermore, greater variability of magnetic parameters and geochemical composition during the Holocene suggests complex and multiple sediment sources. Magnetite has been identified as the primary ferrimagnetic mineral throughout the core, suggesting relatively constant mineralogy. Relatively low magnetite concentration during the Holocene is mainly due to dilution by increased authigenic carbonate that is strongly associated with riverine Ca delivery. The presence of monoclinic pyrrhotite implies reducing depositional environment associated with remineralization of organic matter in the lake. Several lines of evidence suggest the occurrence of greigite, which may indicate relatively dry climate conditions during the glacial period. Results from the elemental composition and magnetic properties of the Lake Qinghai sediments are consistent with records derived from lithological and sedimentological proxies.

Fourier Transform Infrared Spectroscopy (FTIR) and X-ray Fluorescence (XRF) scanning techniques were evaluated, using sediments from Lake Qinghai and Lake Malawi (Africa). The results show statistically significant correlations between conventionally measured concentrations of carbonate (%$CaCO_3$), total organic carbon (%TOC), and biogenic silica (%BSi), and absorbance in the corresponding FTIR spectral regions, as well as between conventional measurements and XRF elemental ratios including calcium: titanium (Ca/Ti), incoherent: coherent X-ray scatter intensities (Inc/Coh), and silicon: titanium (Si/Ti). Both FTIR and XRF techniques exhibit great potential to quantitatively assess concentrations of inorganic and organic components of lacustrine sediments.

These results provide evidence that climate on the Tibetan Plateau has varied considerably, suggesting a relatively stable, cold, and dry Late Pleistocene along with a weak Asian summer monsoon, versus a relatively unstable, warm, and wet Holocene with a relatively strong summer monsoon. The results also highlight that the Asian monsoon system is driven by changes in the contrast of summer insolation between the continent and the ocean over the glacial/interglacial time scales.

## TABLE OF CONTENTS

# LIST OF FIGURES

## Chapter 1



## Chapter 2



## Chapter 3



## Chapter 4

## Appendix

# DISSERTATION OVERVIEW

The major objective of this dissertation is to document the history and the dynamics of past climate, especially the Asian summer monsoon, during the late Quaternary using multi-proxy analyses of sediment cores from Lake Qinghai, China. The study aims to provide a better understanding of the history of local climate conditions and environment in western China. Its findings help to improve our ability to anticipate future climate and to deal with the consequences.

The results of this dissertation are organized into an introductory and three results chapters, each of which constitutes an individual paper, with its own introduction, methodology, results, discussion and conclusions. These three papers are currently being revised for submission for publication. Some repetition of introductory and methodological materials is necessitated by this format.

Chapter 1 presents background information about the Asian monsoon and Lake Qinghai.

Chapter 2 presents data from the composite core QH07, showing multi-proxy evidence for climate history since the Last Glacial Maximum (LGM). The multiple proxies include not only lithological and sedimentological properties of sediments, but also their geochemical characteristics, such as bulk elemental chemistry, and stable isotope compositions.

Chapter 3 presents the geochemical and magnetic characteristics of Lake Qinghai sediments, providing information about changes in magnetic mineral concentration, grain-size distribution, mineralogy, and geochemical composition, as well as implications for paleoclimatology.

Chapter 4 presents results from determination of carbonate, total organic matter, and biogenic silica contents by FTIR and XRF techniques, using sediments from Lake Qinghai and Lake Malawi. Both FTIR and XRF techniques exhibit great potential to quantitatively assess concentrations of inorganic and organic contents of lacustrine sediments.

The Appendix presents a brief summary of the Lake Qinghai Drilling Project.

# Chapter 1: The Asian monsoon and Lake Qinghai

## Introduction

The Asian monsoon is of crucial importance, not only because it provides the rainfall that sustains more than half of the world's human population, as well as the ecosystem of much of the Asian continent, but also because it plays a key role in global climate (Wang et al., 2005). Climate changes in the Asian interior, to a large extent, are determined by changes in the Asian monsoon system. Lakes on the Tibetan Plateau, especially large lakes, are rich sources of information about past climatic and environmental changes, particularly the dynamics of the Asian monsoon system over geologic time (Ruddiman and Kutzbach, 1989; Raymo and Ruddiman, 1992).

Previous studies on ice cores, loess-paleosol sequences, speleothems, tree rings as well as lacustrine sediments have focused on the climate history of the Tibetan Plateau region, especially on changes in the strength of the Asian monsoon (Porter and An, 1995; Wang et al., 2001; Zhang et al., 2003; Zhang et al., 2009). However, details of climatic variations and Asian monsoon behavior are still not adequately defined (Wang et al., 2008). Besides, ongoing aridification and degradation of the sensitive ecosystems in the Asian interior means that there is an urgent need to understand the dynamics and mechanisms of the Asian monsoon system and its connections to global climate patterns.

Sediments from large lakes potentially contain long, continuous, and high-resolution paleoclimate records, applicable for various time scale studies, including glacial-interglacial, millennial, to centennial, decadal, or even annual time scales. One such lake is Lake Qinghai, the largest inland water body in China, northeastern Tibetan Plateau, which lies near the limit of penetration of the modern Asian summer monsoon precipitation. It is one of the best regional paleoenvironmental and paleoclimatic

archives. This chapter includes a brief summary of the previous studies of the Asian monsoon history, and background information about Lake Qinghai including geography, geology, limnology, hydrochemistry, and climatology.

## Previous studies on Asian monsoon history

Ice core records from high latitude/altitude sites are believed to be one of the most robust sources of paleoclimatic proxies. A handful ice cores have been recovered from the Tibetan Plateau. Among these, some well-known records include Gulia (6200 m a.s.l.) (Thompson et al., 1997), Dunde (5325 m a.s.l.) (Liu et al., 1998), and Dasuopu (7200 m a.s.l.) (Thompson et al., 2000). Variations in oxygen isotopic compositions of the ice cores have been initially interpreted as mostly due to changes in temperature. Alternatively, Ramirez et al. (2003) suggest that these oxygen-isotope measurements more likely reflect changes in precipitation rather than temperature.

Loess-paleosol sequences, mostly east of the Tibetan Plateau, constitute an excellent long-term proxy record. For example, the grain-size of loess at the Luochuan section has been interpreted as a proxy of the changing strength of the Asian winter monsoon, showing evidence of the North Atlantic "Heinrich events," supporting the idea that the climates of the North Atlantic and China were linked by the Westerlies (Porter and An, 1995). Records from Xifeng section reveal orbital variations in Asian monsoon system including a 41-ka frequency with low-amplitude fluctuations, and a 100-ka frequency with large-amplitude fluctuations (Liu et al., 2001). Such loess records are detailed enough to trace continental climate changes during the Quaternary on orbital time scales. However, study of millennial-scale climate events has been hampered due to the relatively low accumulation rate of loess deposition.

The tree ring record from Dulan, northeastern Tibetan plateau, has been related to regional spring precipitation during the last two millennia (Zhang et al., 2003). This

record has also been interpreted as an annual temperature signal by Feng and Hu (2005), who generated a composite record from ice cores and tree rings, suggesting that the surface heating over the Tibetan Plateau has played a dominant role in changes of the summer monsoon intensity (Feng and Hu, 2005).

Oxygen isotopes of cave speleothems have been widely used as a proxy for intensity of the Asian monsoon. The Hulu cave record from eastern China has been used to link the East Asian monsoon with North Atlantic climate (Wang et al., 2001). The Dongge cave record from southern China contains a history of the Asian monsoon and low latitude precipitation over the past 160,000 years (Yuan et al., 2004). However, recently published results derived from a numerical climate model with an embedded oxygen-isotope model argue that changes in oxygen isotopic compositions in the Chinese caves, including Hulu and Dongge, associated with Heinrich events, reflect changes in the intensity of Indian rather than East Asian monsoon precipitation (Pausata et al., 2011). It has also been suggested that precipitation in China originates in the Indian Ocean and that there is a significant phase lag between insolation maxima and monsoon maxima (Clemens et al., 2010). The Sanbao cave record from southeast of China contains millennial-scale strong summer monsoon events (so called Chinese interstadials) in addition to orbital-scale variations, suggesting that global ice volume is one of the main factors that influences millennial-scale events (Wang et al., 2008). A relatively short record from Wanxiang cave, northwest of China, which covers the past 1810 years, shows correlations between the summer monsoon, inferred from oxygen isotope variations, and solar variability, Northern Hemisphere and Chinese temperature, Alpine glacial retreat, and Chinese cultural changes (Zhang et al., 2008). This record also implies that the anthropogenic forcing superseded natural forcing as the major driver of the monsoon variations in the late 20th century.

A number of paleolimnological studies in the monsoonal area have focused on the variations and dynamics of the Asian monsoon system. For example, high-resolution

sediment record from Lake Huguang Maar, in coastal southeast China, using magnetic properties and titanium content as proxies for the strength of the winter monsoon, suggests stronger winter monsoon before the Bølling/Allerød warming, during the Younger Dryas episode and during the middle and late Holocene (Yancheva et al., 2007). A recently published sediment record from Heqing basin, southwestern China, presents that the modern Indian summer monsoon (ISM) variability is driven by interhemispheric processes (An et al., 2011a). The interhemispheric forcing also controls the ISM variability over the orbital time scales, i.e., interglacial ISM maxima are associated with global ice volume minima, but the glacial ISM minimum precedes the global ice volume maximum due to an enhanced cross-equatorial pressure gradient from Southern Hemisphere high-latitude cooling.

At Lake Qinghai, oxygen isotopes of ostracoda from sediments suggest cold and arid climate conditions before 14,500 cal yrs, a strong summer monsoon around 10,000 cal yrs, and a weakening of summer monsoon intensity towards the late Holocene (Lister et al., 1991). Results from a multi-proxy record of Lake Qinghai sediments show similar features of the monsoonal precipitation pattern, suggesting that the likely driving force of the Asian monsoon is solar insolation changes on the ten-thousand-year time scale (Shen et al., 2005b). A record of redness from the same core, related to iron oxide content and hence fluvial transport, shows evidence of the Little Ice Age, the Medieval Warm Period, the Dark Ages Cool Period, and the Roman Warm Period (Ji et al., 2005). These data also suggest orbital variations as well as a 200-yr frequency related to the de Vries solar cycle. In contrast, the pollen record from Hurleg Lake, 300 km west of Lake Qinghai, appears to show the opposite pattern of the moisture history (Zhao et al., 2007). This suggests importance of the interaction between the monsoon system and the Westerlies, as well as local topography, in determining regional climate.

Overall, these archives, including loess-paleosol sequences, ice cores, speleothems, tree rings, and lacustrine sequences give a general picture of postglacial history in the Asian

monsoon system and its associated paleoenvironmental changes. These records reveal several climate events such as the Medieval Warm Period (~1000 AD), Little ice age (~1400- ~1850 AD), 8.2 ka cooling events, Younger Dryas (~11.5- ~12.9 ka), Bølling/ Allerød (~12.9- ~14.7 ka), part of Dansgaard-Oeschger Events and Heinrich Events. However, the details of the behavior of the monsoon system have still not been adequately defined.

The strength of the monsoon is determined by a number of forcing mechanisms operating over a variety of time scales. The evolution and variability of the monsoon circulation can be attributed to cyclical changes in solar radiation induced by orbital parameters, the orography of mountain-plateau (tectonic forcing), ice or snow cover (glacial surface boundary conditions), sea surface temperature (SST), and linkages with the ENSO system. These may affect the monsoon by amplifying or dampening the seasonal processes of heating, latent heat transport, and moisture convergence over land, and thereby influence the strength of the monsoon (Prell and Kutzbach, 1992; Yu, 2005). But so far, the details of the factors that control the intensity of the monsoon remain elusive, and the dynamics and mechanisms of the monsoon system is still not completely understood (Wang et al., 2008).

## Unresolved questions on Asian monsoon history and dynamics

Among the paleoclimate questions addressed in this study of Lake Qinghai sediments are the following: What was the glacial-interglacial climate history in this area, in terms of changes in the Asian monsoon? Was the transition from the late-glacial to the Holocene gradual or abrupt? How stable was the climate during the glacial period versus the Holocene and why? Were the climate events, such as Bølling/Alleröd oscillation, and Younger Dryas, recorded at the northern limits of monsoonal circulation? What did they look like? When did the wettest condition occur during the Holocene? What controlled the climatic variations on different time scales (e.g., orbital or millennial)?

## Lake Qinghai: Geography, geology, limnology, hydrochemistry, and climatology

Lake Qinghai (36°32' to 37°15' N, 99°36' to 100°47' E), the largest inland water body in China, at an elevation of 3194 m, is situated on the northeastern margin of the Tibetan Plateau (Fig. 1). It is a "piggy-back" basin, sitting above a thrust sheet (Fig. 2 and Fig. 3). The basin is closed, surrounded by three mountain ranges, the Qilian Shan (Datong Shan to the north and Riyue Shan to the east), and the Qinghai Nan Shan to the south. The elevations of these mountains are above 4000 m on average (Yu, 2005). Tectonic movement along the Qinghai Nan Shan fault began during the Late Miocene to early Pliocene (Metivier et al., 1998).

The drainage area of the lake is about 30,000 $km^2$ (LZCAS, 1994), from which five major rivers discharge to the lake basin. The Buha River, on the northwestern side of the lake contributes more than 60% of the total runoff. Its drainage area is dominated by Late Paleozoic sedimentary rocks (marine limestones and sandstones). Triassic volcanics and Mesozoic granodiorites are common in catchments of smaller tributaries (Yan et al., 2002; Yu and Zhang, 2008). The surrounding mountain glaciers are generally small in size, and glacial melt water only accounts for 0.3% of the total inflow to the lake. No surface outflow is observed. However, groundwater through-flow is thought to be substantial (Jin et al., 2010). Based on the estimates from previous studies, groundwater input accounts for 11%-25% of the lake water budget (Table 1).

The lake has a surface area of 4400 $km^2$, and an average water depth of 21 m, with a maximum depth of 27 m. It is composed of three sub-basins based on its bathymetry: the northern basin, the southern basin and the southeastern basin (Fig. 4). The lake floor is extremely flat. The mean annual precipitation in this semi-arid region is ~360 mm, most of which falls in summer, while the potential evaporation is up to 1000 mm per year on lake surface. About 75% of the total precipitation occurs in the summer time. The

catchment is mainly semi-arid grassland. Annual mean temperature is –0.7℃and monthly means exhibit remarkable seasonality, varying from –11℃ in winter to 12℃ in summer (Lister et al., 1991; Shen et al., 2005a; Henderson et al., 2010).

The lake water is brackish (average salinity = 15.5 g/l; pH = 9.06), dominated by sodium, magnesium, potassium, chlorine, bicarbonate, and sulphate ions (Table 2). These dissolved constituents of the lake water are mainly contributed by silicate and carbonate weathering in the catchment through the rivers (the Buha river is the largest contributor), partly by atmospheric deposition (7.4-44%), and only modestly by groundwater input (3.7-4.7%) (Jin et al., 2010). The lake is supersaturated with respect to carbonates including aragonite, calcite, and dolomite (Sun et al., 1991; Yu and Zhang, 2008). Magnesium is remarkably abundant in the lake water, currently with a Mg/Ca ratio of 61 (by weight), which promotes aragonite to precipitate directly from the lake water. Lake Qinghai is dimictic. During summer it is intermittently thermally stratified. In winter, inverse stratification occurs after ice covers the lake. The entire water column is oxic but pore water becomes suboxic a few centimeters below the water/sediment interface.

Plankton appears to be abundant in the pelagic zone. Diatoms are common in the lake but they are not preserved in the sediments due to the high pH of the lake water, which causes dissolution of biogenic silica. Macrophytes are generally rare in the lake system. Chironomides and ostracoda are abundant on the lake floor (Yu and Zhang, 2008).

Climatically, Lake Qinghai area is generally considered to be at the intersection of the East Asian monsoon and the Westerlies on the Tibetan Plateau (Fig. 5). Its unique geographical settings make Lake Qinghai very sensitive to environmental and climatic changes and thus an ideal site to study the behavior of the East Asian monsoon and the Westerlies at different time scales (Zhang, 1997; Henderson et al., 2010; An et al., 2011b).

Fig. 1 Map showing the location of Lake Qinghai in China (from Google Earth)

Fig. 2 Satellite image of the Lake Qinghai catchment showing its major rivers and surrounding mountains

Fig. 3 Cross section (north-south) of Lake Qinghai, a “piggy-back” basin above a major thrust sheet, which is located on the southwest side of the Qinghai Nan Shan.

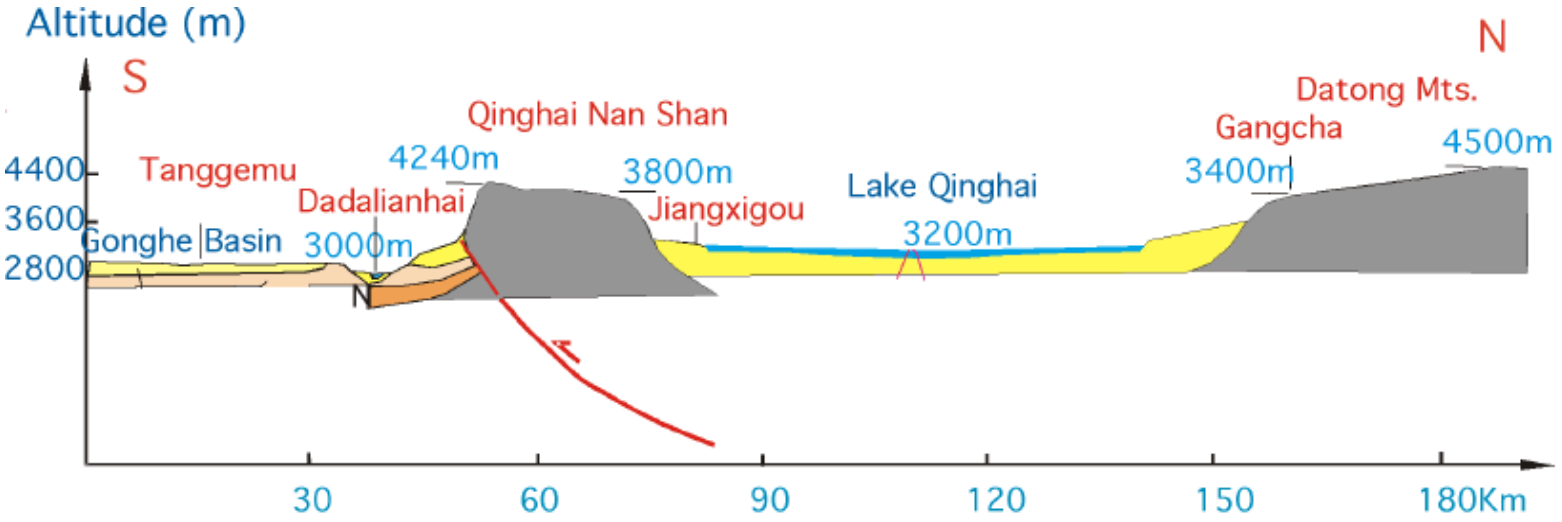

Fig.4 Bathymetry of Lake Qinghai

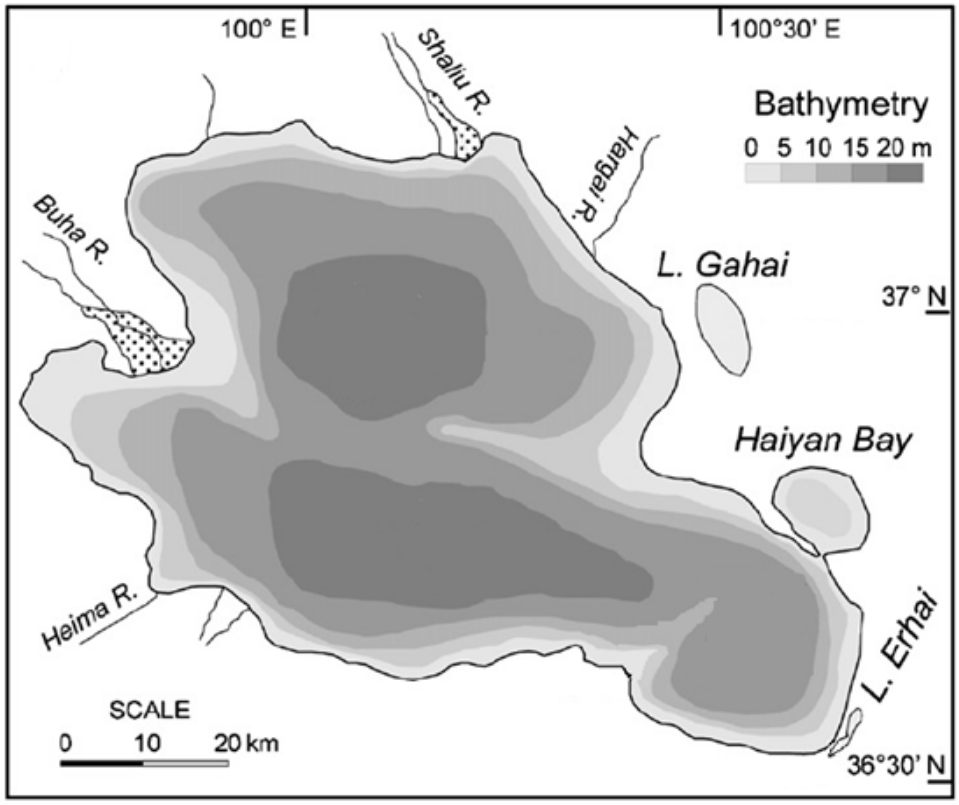

Fig. 5 Climate systems in the Lake Qinghai region

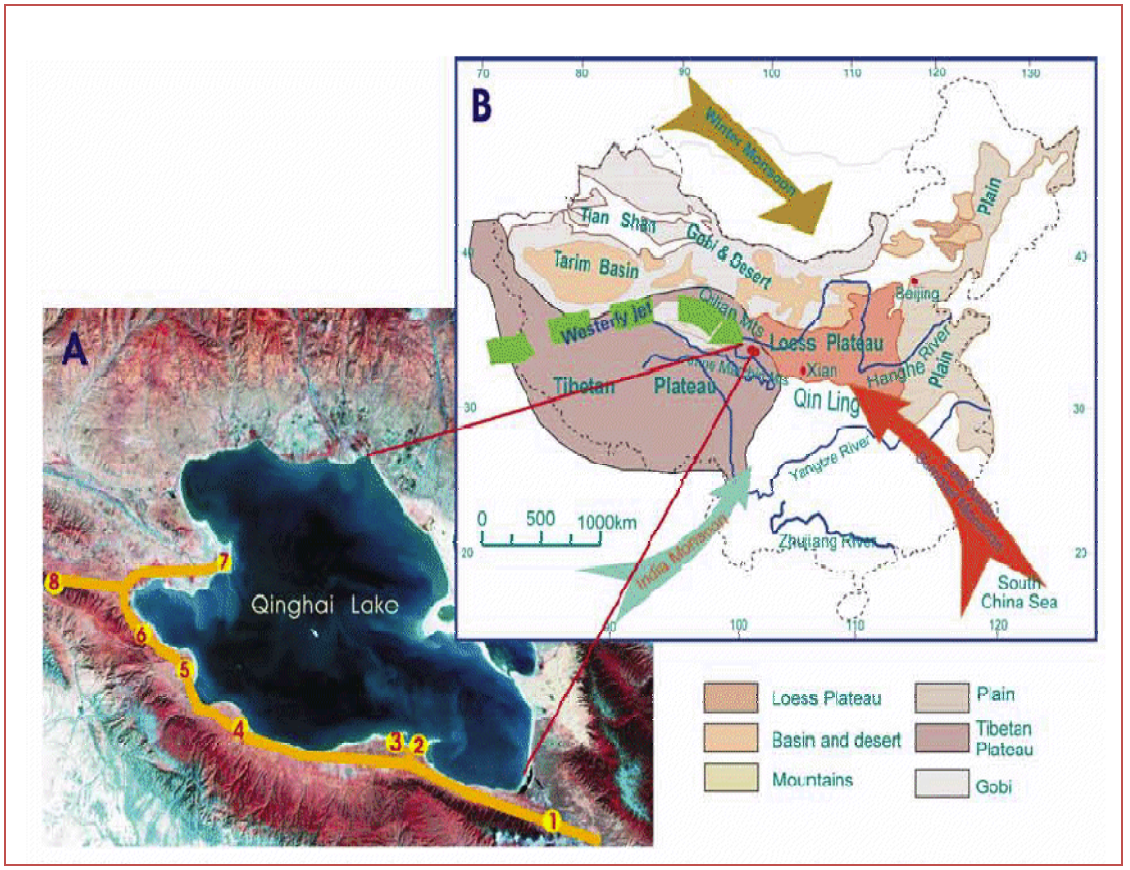

Table 1 Summary of the water budget of Lake Qinghai (Jin et al., 2010)

| Item of the budget | | 1958–1984 Gao and Tang (1992) | | 1958–1986 Qin and Shi (1992) | | 1959–1988 Qu (1994) | | 1959–1999 Liu (2001) | | 1959–2000 Li et al. (2007) | |
|---|---|---|---|---|---|---|---|---|---|---|---|
| | | $km^3/y$ | % | $km^3/y$ | % | $km^3/y$ | % | $km^3/y$ | % | $km^3/y$ | % |
| Input | From atmosphere [a] | 1.440 | 40 | 1.809 | 46.8 | 1.457 | 41.1 | 1.561 | 42.2 | 1.561 | 42.3 |
| | With rivers | 1.764 | 49 | 1.600 | 41.4 | 1.215 | 34.2 | 1.613 | 43.7 | 1.526 | 41.3 |
| | Groundwater | 0.396 | 11 | 0.456 | 11.8 | 0.876 | 24.7 | 0.522 | 14.1 | 0.606 | 16.4 |
| | Total | 3.6 | 100 | 3.865 | 100 | 3.548 | 100 | 3.696 | 100 | 3.693 | 100 |
| Output | Evaporation [b] | 4.1 | 113.9 | 4.244 | 109.8 | 4.006 | 112.9 | 4.051 | 109.6 | 4.050 | 109.7 |
| | Total | 4.1 | | 4.244 | | 4.006 | | 4.051 | | 4.050 | |
| Loss (inputs – output) | | −0.5 | −13.9 | −0.467 | −9.8 | −0.458 | −12.9 | −0.355 | −9.6 | −0.357 | −9.7 |

[a] Mean annual precipitation over the lake.
[b] Evaporation from the lake.

Table 2 Water chemistry about rainfall, input rivers, groundwater, and lake water of Lake Qinghai (Jin et al., 2010)

| Sources | Concentration (ppm) | | | | | | |
|---|---|---|---|---|---|---|---|
| | $Cl^-$ | $Na^+$ | $Mg^{2+}$ | $K^+$ | $Si^{4+}$ | $Ca^{2+}$ | DIC |
| Rain | 1.8 ± 1.1 | 1.8 ± 0.9 | 1.0 ± 0.6 | 1.1 ± 0.9 | 1.0 ± 0.9 | 18.2 ± 10.9 | 15.6 ± 10.3 |
| Buha River | 21.7 ± 7.9 | 16.6 ± 1.8 | 12.5 ± 0.6 | 1.5 ± 0.2 | 2.4 ± 0.0 | 58.8 ± 1.2 | 34.9 ± 3.7 |
| Shaliu River | 7.1 ± 1.3 | 10.2 ± 0.7 | 11.9 ± 0.7 | 1.3 ± 0.2 | 2.5 ± 0.1 | 56.8 ± 2.9 | 37.2 ± 5.1 |
| Hargai River | 7.0 ± 1.5 | 7.5 ± 0.6 | 18.5 ± 0.5 | 1.5 ± 0.2 | 2.8 ± 0.3 | 59.1 ± 2.7 | 41.8 ± 4.4 |
| Quanji River | 12.2 ± 2.6 | 7.9 ± 0.4 | 10.7 ± 0.6 | 1.7 ± 0.2 | 2.5 ± 0.2 | 63.7 ± 1.7 | 36.6 ± 3.4 |
| Heima River | 35.2 ± 9.1 | 21.3 ± 4.7 | 13.9 ± 1.3 | 3.2 ± 0.3 | 1.9 ± 0.3 | 69.6 ± 5.7 | 38.3 ± 4.3 |
| Groundwater | 24.8 ± 16.3 | 16.9 ± 6.9 | 15.6 ± 3.5 | 2.7 ± 1.2 | 4.0 ± 1.3 | 86.3 ± 26.5 | 51.9 ± 15.3 |
| Main lake | 6307.0 ± 40.9 | 4083.1 ± 54.8 | 798.1 ± 14.7 | 227.0 ± 3.8 | 0.5 ± 0.0 | 11.0 ± 0.3 | 291.0 ± 43.8 |

# Chapter 2: Multi-proxy evidence for climate history since the LGM from Lake Qinghai sediments

**Liu, Xiuju[1,2], Colman, Steve M.[1,3], Brown, Erik T.[1,3], Henderson, Andrew C. G.[4], Werne, Josef P.[1,5], Holmes, Jonathan A.[6]**

1 Large Lakes Observatory, University of Minnesota Duluth, Duluth MN 55812, USA

2 Department of Earth Sciences, University of Minnesota Twin Cities, Minneapolis MN 55455, USA

3 Department of Geological Sciences, University of Minnesota Duluth, Duluth MN 55812, USA

4 Department of Geographical & Earth Sciences, University of Glasgow, Glasgow G12 8QQ, UK

5 Department of Chemistry and Biochemistry, University of Minnesota Duluth, Duluth, MN 55812, USA

6 Environmental Change Research Centre, University College London, London WC1E 6BT, UK

Post glacial Central Asian climate history was reconstructed using sediments from the southeastern basin of Lake Qinghai, situated on the northeastern margin of the Tibetan Plateau. Results from multiple proxies are internally consistent and reveal a distinct Holocene and Late Pleistocene climate record.

Carbonate content and total organic carbon in Lake Qinghai sediments are interpreted as proxies for the strength of the Asian summer monsoon. During the glacial period (~14,600 to ~20,000 yrs), the summer monsoon intensity remained low and relatively constant, suggesting cool, dry, and relatively stable climatic conditions. The Holocene (~11,500 yrs to present) was a time of enhanced summer monsoon strength and greater variability, indicating relatively wetter but more unstable climatic conditions than those of the Late Pleistocene. The warmest, wettest part of the Holocene (marked by maximum organic matter and carbonate contents) occurred from ~9,000 to ~11,500 yrs, consistent with maximum summer insolation contrast between the continent and the ocean. Gradually reduced monsoonal precipitation (weakened summer monsoon) is inferred from decreased carbonate content through the course of the Holocene. The transition between the Holocene and the Late Pleistocene, about 11,500 years ago, was abrupt. A cool Younger Dryas appears to be recorded in the record, but its onset is not as distinct as it is in cave records from Dongge and Sanbao. Evidence of a warm interval correlative with the Bølling–Allerød oscillation is weak in all the proxies in the QH07 record.

We propose that changes in the contrast of summer insolation between the continent and the ocean are the primary control on the Asian monsoon system over the glacial/interglacial time scales. Secondary influences may include ice sheet size (albedo) and sea level (distance from moisture source). A climate threshold for arrival of monsoonal rainfall is suggested at the northeastern Tibetan Plateau.

## 1 Introduction

The Tibetan Plateau has experienced the Late Cenozoic tectonic movement, and its uplift has significant influence on the global atmospheric circulation, especially on the pattern of the Asian monsoon system (Harrison et al., 1992; Molnar et al., 1993; An et al., 2001; Liu and Yin, 2002). The Asian monsoon system is of crucial importance because it plays a key role in the global climate system. It provides the rainfall that sustains more than half of the world's population, as well as vast natural ecosystems. Knowledge of the climate history of the Tibetan Plateau, at the inland edge of monsoon influence, will lead to a better understanding of the dynamics of the Asian monsoon system. Various paleoclimatic records, including those derived from ice cores, tree rings, speleothems, and lacustrine sediments have been applied in efforts to reconstruct Tibetan climate history.

Oxygen-isotope measurements on ice cores from Gulia (Thompson et al., 1997), Dunde (Liu et al., 1998), and Dasuopu (Thompson et al., 2000) have been interpreted as temperature signals. However, others have argued that the oxygen isotope values may reflect changes in monsoonal precipitation (Ramirez et al., 2003).

Interpretations of tree ring records also have been variable. The Dulan tree-ring record from the northeastern Tibetan plateau has been related to variations in regional spring precipitation during the last two millennia (Zhang et al., 2003b; Zhang et al., 2009), but this record has also been interpreted as an annual temperature signal (Feng and Hu, 2005).

Oxygen isotopes of cave speleothems have been widely used as a proxy for intensity of the Asian monsoon. The Hulu Cave record has been used to link the East Asian Monsoon with North Atlantic climate (Wang et al., 2001). The Dongge cave record contains a history of the Asian monsoon and low latitude precipitation over the past 160,000 years (Yuan et al., 2004). However, recently published results derived from a numerical climate

model with an embedded oxygen-isotope model show that changes in oxygen isotopic compositions in the Chinese caves including Hulu and Dongge, associated with Heinrich events reflect changes in the intensity of Indian rather than East Asian monsoon precipitation (Pausata et al., 2011). The Sanbao cave record characterizes millennial-scale strong summer monsoon events (Chinese interstadials) in addition to orbital-scale variations, suggesting that global ice volume is the main factor that influences millennial-scale events (Wang et al., 2008). A short record, covering the past 1810 years, from Wanxiang Cave, shows correlations between the summer monsoon and solar variability, Northern Hemisphere and Chinese temperature, Alpine glacial retreat, and Chinese cultural changes (Zhang et al., 2008).

Lake sediments contain proxy records of past water temperature, biology, and chemistry, that provide information about climatic variations, glacial/interglacial history, vegetation alternations, and their connections with global change (Peck et al., 1994; Colman et al., 1999; Muller et al., 2001; Huang et al., 2002; Johnson et al., 2002; Hodgson et al., 2005; Russell and Johnson, 2007; Conroy et al., 2008; Henderson et al., 2010; Zhao et al., 2010; Anderson, 2011; Stager et al., 2011). Sediments from large lakes often provide long, continuous, and high-resolution paleoclimate records, applicable for various time scales including glacial-interglacial, millennial, centennial, decadal, or even annual time scales.

Lake Qinghai (36°32’ to 37°15’ N, 99°36’ to 100°47’ E), the largest inland water body in China, at an elevation of 3194 m, is situated on the northeastern margin of the Tibetan Plateau, where the climate conditions are mainly controlled by the interaction of the East Asian monsoon and the Westerlies. It lies near the limit of penetration of the Asian Summer monsoon, i.e., the transition from arid to semi-arid zones. Its location makes it a promising candidate for exploring past changes in continental climate and the relationship between the East Asian monsoon and the Westerlies. Several studies including Lake Qinghai catchment surveys, water column samples, and sediment cores, investigated various proxies, for example, pollen assemblages (Shan et al., 1993; Shen et

al., 2005), grain size (Zhang et al., 2003a), ostracod morphology and trace element geochemistry (Zhang et al., 2004), stable isotope composition of authigenic carbonate and organic matter (Henderson et al., 2003; Xu et al., 2006), and long-chain alkenones (Liu et al., 2006; Liu et al., 2011a). These studies, from various perspectives including focus on geological, geochemical, geophysical, biological, and hydrological processes, provide information on paleoenvironmental and paleoclimatic changes and the associated climatic forcings at various time scales (Colman et al., 2007; Henderson and Holmes, 2009).

However, only a handful of studies on the sediments of Lake Qinghai (e.g., Shen et al., 2005) have applied multiple biogeochemic analyses of the sediments to interpret the regional climatic and environmental changes. Most of the previous sediment studies focused on the influence of the Asian Summer monsoon and most had relatively limited chronological constraints. Radiocarbon dating of Lake Qinghai sediment is difficult because macro-organic matter is scarce and because of carbon reservoir effects in the lake (An et al., 2011).

Lister et al. (1991) applied oxygen isotope analysis of fossil ostracod valves in core QH85-14B from Lake Qinghai and provided a record of changes in the isotopic chemistry of the lake waters, which could be related to the water balance of the lake and to paleo-lake levels. They suggested that the climate conditions (dry or wet) in the Lake Qinghai region were largely determined by the Asian monsoon system (Lister et al., 1991).

A multi-proxy analysis of a sediment core (QH-2000) from the southeastern basin of Lake Qinghai, similar in duration to the record discussed here, was used to reconstruct the past 18 kyrs of monsoon precipitation patterns (Shen et al., 2005). This record suggests that the likely driving force of the summer monsoon was solar insolation changes on the ten-thousand-year scale. The redness record from QH-2000, which is

related to iron oxide content, shows evidence of the Little Ice Age, the Medieval Warm Period, the Dark Ages Cool Period, and the Roman Warm Period. It has been interpreted as showing orbital cycles as well as the de Vries solar cycle (Ji et al., 2005).

Several scientific questions remain in the Lake Qinghai area: What was the glacial-interglacial climate history in this area, in terms of changes in the Asian Summer monsoon and the Westerlies? Was the transition from the late-glacial to the Holocene gradual or sharp? Were abrupt global climate events such as Bølling/Alleröd oscillation, Younger Dryas, and 8.2 ka cooling recorded in the sediments? When did the Holocene climatic optimum occur? What controlled the climatic variations on different time scales (e.g., orbital or millennial)? We aim to answer these questions through multi-proxy investigations on Lake Qinghai sediments.

The Lake Qinghai Drilling Project (LQDP), under the auspices of the International Continental Drilling Program (ICDP) and the Chinese Academy of Science (CAS), addressed past variations in the climate system that involves the Asian monsoon and the Westerlies, as well as their dynamics, on both orbital and millennial to centennial time scales. A set of drill cores were collected from Lake Qinghai in 2005 (An et al., 2006). As a complementary study to this drilling project, short cores (a Uwitec piston core and a mini-Mackereth core) were collected in 2007 from the southeastern basin of Lake Qinghai, at LQDP site 2 (Fig. 1), in order to focus on the youngest part of the record.

## 2 Study site

Lake Qinghai is a closed basin, surrounded by two mountain ranges, the Qilian Shan (Datong Shan) to the north, and the Qinghai Nan Shan to the south (Yu, 2005). The drainage area of the lake is about 30,000 $km^2$ (LZCAS, 1994), in which five major rivers discharge to the lake basin. The Buha River, on the western side of the lake contributes more than 60% of the total runoff. Its drainage area is dominated by Late Paleozoic

sedimentary rocks (marine limestones and sandstones). Triassic volcanics and Mesozoic granodiorites are common in catchments of smaller tributaries (Yan et al., 2002; Yu and Zhang, 2008). The surrounding mountain glaciers are generally small in size, from which the melt water only accounts for 0.3% of the total inflow to the lake, thus, the influence of the melt water on the water budget is relatively trivial. Although there is no surface outflow, groundwater through-flow may be substantial (Jin et al., 2010).

The lake has a surface area of 4400 $km^2$, and an average water depth of 21 m, with a maximum depth of 27 m. It is composed of three sub-basins based on its bathymetry: the northern basin, the southern basin and the southeastern basin. The lake floor is extremely flat. The mean annual precipitation in this semi-arid region is ~360 mm, most of which falls in summer, while the potential evaporation is up to 1000 mm on lake surface per year. About 75% of the total runoff occurs in the summer time. The catchment is mainly semi-arid grassland. Annual mean temperature is –0.7℃and monthly means exhibit remarkable seasonality, varying from –11℃ in winter to 12℃ in summer (Lister et al., 1991; Shen et al., 2005; Henderson et al., 2010).

The lake water is brackish (average salinity = 15.5 g/l; pH = 9.06), dominated by sodium, magnesium, potassium, chlorine, carbonate, and sulphate ions. These dissolved constituents of the lake water are mainly contributed by silicate and carbonate weathering in the catchment through the rivers (the Buha river is the largest contributor), partly by atmospheric deposition (7.4-44%), and only modestly by groundwater input (3.7-4.7%) (Jin et al., 2010). The lake is supersaturated with respect to carbonates including aragonite, calcite, and dolomite (Sun et al., 1991; Yu and Zhang, 2008). Magnesium is remarkably abundant in the lake water, currently with a Mg/Ca of 61, which promotes aragonite to precipitate directly from the lake water. Lake Qinghai is dimictic. During summer it is intermittently thermally stratified. In winter the inverse stratification occurs after the ice covers the lake. The entire water column is oxic but pore water becomes suboxic a few centimeters below the water/sediment interface.

Plankton appears to be abundant in pelagic zone. Diatoms are common in the lake but they are not preserved in the sediments due to the high pH of the lake water, which causes dissolution of biogenic silica. Macrophytes are generally rare in the lake system. Chironomides and ostracoda are abundant on the lake floor (Yu and Zhang, 2008).

Climatically, Lake Qinghai area is generally considered to be at the intersection of the East Asian monsoon and the Westerlies on the Tibetan Plateau. Its unique geographical settings make Lake Qinghai very sensitive to environmental and climatic changes and thus an ideal site to study the behavior of the East Asian monsoon and the Westerlies at different time scales (Zhang, 1997; Henderson et al., 2010; An et al., 2011)

# 3 Materials and methods

## 3.1 Sediment cores and sampling

A 3.55-m-long Uwitec piston core (QH07-1A) and an 85-cm-long mini-Mackereth core (QH07-1B-1MM) were collected from the southeastern basin of Lake Qinghai, at LQDP site 2 (36° 43′ 36.7" N, 100° 29′ 28.1" E; Fig. 1). The top 15 cm of QH07-1B-1MM was soupy and was extruded and sampled at 0.5 cm intervals in the field. Discrete samples were taken continuously at 1.5 cm intervals from the mini-Mackereth core and at 3 cm intervals from the Uwitec core, for the purpose of measuring water content, carbonate content, organic carbon and nitrogen content and their stable isotopes, and grain size.

## 3.2 Methods

A number of studies have used Lake Qinghai sedimentary records to reconstruct the climate history (Huang and Sun, 1989; Kelts et al., 1989; Lister et al., 1991; Henderson et al., 2003; Zhang et al., 2003a; Shen et al., 2005; Liu et al., 2006; Xu et al., 2006; Liu et al., 2007; Ji et al., 2009). Shen et al. (2005) applied multiple methods for revealing the

paleoclimatic changes during the last 18 kyrs by using pollen assemblages and concentrations, contents of authigenic carbonate, total organic carbon (TOC), total nitrogen (TN) and stable isotopes of organic matter ($\delta^{13}C_{OM}$). In our study, we also utilized a multiple-analysis approach. In addition to carbonate content, TOC, TN and $\delta^{13}C_{OM}$, other analyses such as water content, bulk density, $\delta^{15}N_{OM}$, bulk geochemical composition, magnetic susceptibility, and grain size, were conducted on the sediments from QH07-1A and QH07-1B-1MM cores. These analyses together with a relatively robust age model provide information about the behavior of the climate system over time, and more importantly, the associated climatic controls in Lake Qinghai area.

### 3.2.1 Magnetic susceptibility and bulk density analyses

Measurements of magnetic susceptibility at 1 cm intervals were performed on split cores using an automated core logger (Geotek MSCL-XYZ) with a point sensor in contact with the surface of the sediment. The susceptibility reading was reported as volume-normalized susceptibility in units of $10^{-6}$ SI. In addition, the split cores were scanned using a Geotek MSCL-S to measure gamma-ray density, which provided an estimate of bulk density ($g/cm^3$), an indicator of lithology and porosity.

### 3.2.2 Bulk geochemical element analysis

The bulk elemental composition of the sediments in split cores was analyzed using an ITRAX X-ray Fluorescence (XRF) Core Scanner (Cox Analytical Instruments). The measurements were taken at 2-mm intervals with a sampling time of 90 seconds using a molybdenum X-ray source set to 30 kV and 30 mA. Initial XRF spectral data were reprocessed in a standard fitting procedure using the Q-Spec spectral analysis software to refine the individual elemental peak areas (Croudace et al., 2006). Final XRF results were reported as counts per second (cps), representing relative element concentrations.

### 3.2.3 Carbonate analysis

Total inorganic carbon in the sediments was measured by coulometry. Samples were freeze-dried and ground into fine, homogeneous powder and desiccated overnight. Carbon dioxide gas evolved by reaction of carbonates in the powdered sample with acid (30 mg sediment and 5 ml 2N HCl) was swept by a gas stream into a coulometer cell and was detected and recorded as micrograms of carbon. Blanks and standards were run between every 10 samples. The amount of carbonate was calculated using the conversion: Carbonate content = (μg carbon in sample − μg carbon in blank) / (μg sample weight) × 100/12 by assuming all inorganic carbon is present as calcium carbonate.

### 3.2.4 Analysis of TOC, TN and their isotopic ratios

Samples were freeze-dried, ground into fine powder, oven-dried at 60˚C overnight, and treated by acid fumigation for 6 hrs to remove carbonate in the sediments. Fumigated samples wrapped in tin capsules were placed in a desiccator until EA-IRMS (Elemental Analysis-Isotope Ratio Mass Spectrometry) analyses. TOC and TN were reported as weight percentages. C/N ratios were converted to atomic ratios. Carbon and nitrogen isotopic ratios of the organic matter were determined by a Finnigan Delta Plus XP isotope-ratio mass spectrometer. The isotope ratios were reported in δ values relative to Vienna PeeDee Belemnite (VPDB), using equation $\delta = [(R_{sample}-R_{standard})/R_{standard}]*1000$.

### 3.2.5 Grain size analysis

About 1 cubic centimeter wet bulk sediment was collected directly from split cores and was first pretreated with 50 ml 30% $H_2O_2$ and then with 20 ml 10% HCl solution in a water bath (85℃), to remove organic matter, carbonate, and iron oxides, leaving aluminosilicates behind (Konert and Vandenberghe, 1997). Then samples were mixed with 5 ml sodium hexametaphosphate to disperse the sediments. Further, a shaker was

used to suspend and mix the treated samples thoroughly right before they were transferred to the measuring vessel. Measurements of grain size distribution were performed on a Beckman Coulter LS 13 320 Particle Size Analyzer, which uses the principles of laser light scattering. Grain-size distribution was reported in 93 size classes between 0.375 and 2000 μm.

## 4 Chronology

The Uwitec sediment core (QH07-1A) and the mini-Mackereth core (QH07-1B-1MM) were 3.5 m and 0.85 m long, respectively. Based on field observations, we believe that the mini-Mackereth core sampled the sediment-water interface. Comparison of magnetic susceptibility and elemental chemistry profiles among the mini-Mackereth core, the Uwitec piston core, and the LQDP drill core at this site allows a composite depth scale for the cores. The composite depth scale indicates a gap of about 2 m between the mini-Mackereth and the Uwitec core, probably due to overpenetration by the latter. The age model for the composite record (QH07-1B-1MM and QH07-1A) was established on the basis of 17 AMS $^{14}C$ ages (5 ages from QH07-1B-1MM and 12 ages from QH07-1A). Two of the radiocarbon ages were from samples of seeds of the aquatic plant *Ruppiaceae*. The rest were determined on bulk organic matter due to the lack of terrestrial plant macrofossils in the sediments.

Radiocarbon ages of aquatic material need to be corrected for lake reservoir effects, which relate to the presence of old dissolved inorganic carbon, mobilized by chemical weathering of carbonate rocks, in the lake. Ages for bulk organic matter may also be affected by the residence time of terrestrial organic matter in the drainage basin before its final sequestration in the sediments. Previous studies have shown that the organic matter in the Lake Qinghai sediments is mainly aquatic (Shen et al., 2005; Yu and Zhang, 2008). So, terrestrial residence times are likely to have only a negligible influence on bulk radiocarbon ages.

Shen et al. (2005) estimated an average reservoir effect for core QH-2000 based on 10 AMS $^{14}$C ages of bulk organic carbon by using linear regression, which yielded an intercept of 1039 yrs at the surface sediment. Yu et al. (2007) applied a two-box model of the radiocarbon mass balance in the lake water and in the early diagenetic zone at Lake Qinghai, suggesting a 1500 yr reservoir age and that the old carbon was mainly introduced by two components: riverine and ground water input. If the old carbon is controlled by river discharge and/or the lake hydrological state, it is unlikely that the reservoir effect is constant through time. An et al. (2011) measured 65 AMS $^{14}$C samples from LQDP05-1F core. Based on the lithologic differences in the core, separate linear regressions were applied to three sections and three different reservoir ages were assigned to each of the three sections from young to old, 135 (0~10 ka), 1143 (10~20 ka) and 2523 yrs (30~40 ka), respectively. Hou et al. (2010) obtained three lignin phenol radiocarbon ages, which were consistently younger than bulk organic carbon ages during the late glacial and the Holocene, i.e., the last ~12,000 yrs. Age differences between lignin and bulk organic carbon were 700, 1230 and 1581 yrs, suggesting a variable reservoir effect in Lake Qinghai (Hou et al., 2010). Finally, Henderson et al. (2010) estimated reservoir effects for core QING6 by determining $^{14}$C ages for the dissolved organic carbon in lake water, for bulk organic carbon in surface sediment, and for authigenic carbonate in surface sediment. These three fractions, all reflecting a reservoir age, averaged 658 yrs. Linear surface intercepts applied to down-core ages provided an estimated reservoir age of 737 yrs (Henderson et al., 2010). Both estimates are consistent with ages inferred from $^{210}$Pb-based age models (Henderson et al., 2010). We use a reservoir age of about 700 yrs, consistent with the multiple cross-checked approaches of Henderson et al. (2010), as the most reasonable single estimate of the average reservoir effect in Lake Qinghai.

The age model (Fig. 2) was generated by CLAM software (‘classical’ age-depth modeling) based on probability sampling methods in order to take into account multi-modal and asymmetric distributions of calibrated radiocarbon dates (Blaauw, 2010). Five

out of the 17 AMS $^{14}C$ ages were considered outliers, either because they created apparent age reversals, were far removed from regression fits, or were incompatible with multiple other nearby estimates. The surface sediment of QH07-1B-1MM was given a modern age. Ages were weighted inversely with the error in their calibrated probabilities. The smooth-spline method in CLAM was adopted with a smoothing level of 0.4. This age modeling produced a 'best' age-model (black line in Fig. 2) as well as uncertainty ranges (95% confidence interval grey area in Fig. 2) by finding the highest posterior probability density of the array of age-depth curves. Confidence intervals were calculated at 2 standard deviation (95%) level based on 10,000 iterations. The age-depth model provides a robust fit to the individual calibrated ages, particularly at the glacial/Holocene transition, and indicates that our sedimentary record reaches back close to the Last Glacial Maximum (LGM) (Fig. 2). Sedimentation rates inferred from this age model for our composite core QH07 varied through the sequence, from about 0.37 mm/yr in the Holocene to a much lower rate of ~0.14 mm/yr during the late glacial period. Sedimentation rates derived from our age-depth model for QH07 are consistent with those for QH85-14B (from the south basin, Holocene sedimentation rate, 0.3-0.4 mm/yr) (Lister et al., 1991), QH-2000 (from the southeastern basin, Holocene sedimentation rate, 0.32-0.64 mm/yr) (Shen et al., 2005) and LQDP05-1F (from the south basin, Holocene sedimentation rate, 0.43 mm/yr) (An et al., 2011). Overall, the south basin cores have higher accumulation rates than those from the southeastern basin during the glacial time: ~0.67 mm/yr in LQDP05-1F and ~0.5 mm/yr in QH85-14B, versus 0.29-0.77 mm/yr in QH-2000 and ~0.14 mm/yr in QH07 (Lister et al., 1991; Shen et al., 2005; Jin et al., 2010; An et al., 2011).

## 5 Results and interpretation of individual paleoenvironmental proxies

Parameters measured for QH07 include water content, bulk density, carbonate content, TOC, TN and $\delta^{13}C_{OM}$ and $\delta^{15}N_{OM}$, bulk geochemical composition, magnetic susceptibility, and grain size. These proxies are highly consistent with each other.

### 5.1 Lithological and sedimentologic proxies (Fig. 3)

5.1.1 Water content, density and Cl/Ti

Water content shows a sharp change at the Late Pleistocene/Holocene transition, at ~11.5 ka, increasing from 20% to 50% (Fig. 3). The density data are in agreement with the water content record, exhibiting low values (~1.7 g/cm$^3$) in the Holocene and high values (~2.3 g/cm$^3$) in glacial times. The effects of compaction below ~15 cm (upper watery sediments) are not apparent. Taken together, this implies a higher bulk density for glacial sediments. The Cl/Ti profile based on XRF measurements also is highly consistent with water content and density profiles, as expected, since most Cl is present as ions in pore water. Increased water content, high Cl/Ti, and relatively low density, all reflect the increased porosity in Holocene sediments.

5.1.2 Carbonate content (Ca/Ti)

The carbonate content profile is similar to water content pattern (low in the late Pleistocene and high in the Holocene) and it varies from about 20% to 60% (by weight) throughout the core (Fig. 3). Late Holocene sediments contain ~30% carbonate. Early to mid-Holocene sediments have the highest concentrations and the most variability (as low as 30% and as high as 60%, average ~45%). During the glacial period, carbonate content is low and remains relatively stable, fluctuating slightly in a narrow range between 20% and 28%. The carbonate minerals in the sediment of Lake Qinghai are mainly aragonite with minor calcite and dolomite (Shen et al., 2005). Other than these, nodular siderite ($FeCO_3$) was also identified by smear slides, but only at a few intervals in Holocene sediments. Therefore, the Ca/Ti calculated from XRF data should indicate the relative abundance of carbonate. The Ca/Ti profile indeed correlates well with the carbonate content determined by coulometry (Fig. 3).

Carbonate precipitation in lakes (provided that $CaCO_3$ is the dominant carbonate) can be controlled by several climate-related factors (Talbot and Kelts, 1986). First, carbonate precipitation can occur by evaporative concentration in lake water, because the products of $Ca^{2+}$ and $CO_3^{2-}$ ion activities exceed saturation. Under these conditions, high carbonate content implies relatively dry climate conditions. Second, the solubility of calcium carbonate decreases with temperature, so that sedimentary carbonate content is enhanced by warm water. Third, photosynthesis and respiration can affect the equilibrium of the carbonate system through losses and gains of dissolved $CO_2$. High primary production in lake system causes removal of aqueous $CO_2$ in the process of photosynthesis, increasing pH and promoting carbonate precipitation. Fourth, if one of the ions, either the cations ($Ca^{2+}$) or the anions ($CO_3^{2-}$) present in excess of saturation, the other becomes limiting to carbonate precipitation in the lake system. The addition of the limiting ion would result in enhanced carbonate precipitation and rapid removal of the limiting ion.

$Ca^{2+}$ concentrations in modern lake water are low (~11 ppm), compared to that in major input rivers (~58.8 ppm in Buha River; ~69.6 ppm in Heima River; ~56.8 ppm in Shaliu River). In contrast, total dissolved inorganic carbon concentration in the lake is relatively high (~291 ppm) (Jin et al., 2010). Results from MINEQL, a program that performs to calculate equilibrium composition of an aqueous system, show that the lake water is saturated with respect to calcite and near saturated with respect to aragonite. Moreover, carbonate content in recent sediments covaries with the observed water discharge of the Buha River, the largest input river for Lake Qinghai, for the last 50 yrs (An et al., 2011). Thus it appears that the carbonate chemistry of the lake is calcium limited, so that carbonate precipitation closely relates to river runoff, which in turn relates to precipitation in this region. Because Lake Qinghai apparently was always a closed basin, this relationship applies to our entire record. Therefore, carbonate content (and/or Ca/Ti) in Lake Qinghai sediments can be used as a proxy for the river runoff.

For conceivable glacial-interglacial temperature change, the change in calcium carbonate solubility is small compared to the change in carbonate content in Lake Qinghai sediments. In addition, although primary productivity in Lake Qinghai increases from the Late Pleistocene to the Holocene, it is still relatively low even in the Holocene, as judged from TOC contents. Increased productivity would add to the effect of increased $Ca^{2+}$ delivering to the lake in runoff.

**5.2 Organic geochemical proxies (Fig. 4)**

5.2.1 TOC, Inc/coh, and TN

Regardless of organic carbon respiration/oxidation during early diagenesis, TOC content in sediments generally reflects lake primary productivity and the input of terrestrial organic matter. TOC values in QH07 (Fig. 4) are generally consistent with the previous studies, including LQDP05-1F (An et al., 2011) and QH86-14B (Yu and Zhang, 2008) but are much lower than those in QH2000 (Shen et al., 2005). TOC in our record is relatively low (~0.6%) and relatively constant during the glacial period, suggesting low primary production in the lake. An abrupt change at ~11.5 ka is marked by much higher TOC (~2% on average, as much as 3%), presumably resulting from increased biological productivity and greater riverine input of terrestrial organic matter. Both lacustrine production and terrestrial inputs are likely linked with increased precipitation and warm temperature, probably because fresh water input decreases lake water salinity and thereby enhances aquatic productivity (Henderson and Holmes, 2009). Thus, we suggest that TOC is an indicator of monsoonal precipitation.

Measurements of incoherent and coherent scattering were produced during XRF scanning. The ratio (inc/coh) is dependent on the average atomic number of material in the sediment. Because organic matter generally has a lower average atomic mass than other constituents, such as carbonates, aluminosilicates, or quartz, this ratio increases with organic carbon content. Therefore inc/coh can be used as a qualitative indicator of

total organic matter concentrations (Burnett, 2010), provided that the inorganic composition of sediments is relatively invariant. Inc/coh ratios from QH07 cores appear to correlate well with TOC (Fig. 4).

The TN profile closely follows the TOC profile, displaying high values (~0.2%) in the Holocene, and low values (~0.07%) during glacial times. This pattern suggests higher primary productivity in the lake during the Holocene relative to the low production in the Late Pleistocene.

### 5.2.2 C/N

The C/N ratio of organic matter is extensively used as a source indicator of organic matter because it can help differentiate original proportions of aquatic and terrestrial material, despite diagenetic alteration (Meyers, 1994). Aquatic plants have low C/N, typically in the range of 4-10, whereas land plants have C/N of 20 and greater (Meyers and Ishiwatari, 1993). C/N in QH07 is relatively constant. The late Pleistocene shows lower C/N (<10) than does the Holocene (about 12 or greater). Higher C/N suggests increased contribution of organic matter from land plant debris and/or aquatic macrophytes in the shallow parts of the lake. The results suggest that organic matter deposited during glacial times was mainly from aquatic sources, whereas organic matter in the Holocene sediments is a mixture of aquatic and terrestrial material, but mostly aquatic.

### 5.2.3 $\delta^{13}C_{OM}$

Bulk organic carbon stable isotopic composition ($\delta^{13}C_{OM}$) is affected by many factors, including the quantity and isotopic composition of the organic matter source (terrestrial or aquatic), fractionations during carbon assimilation, metabolism, and synthesis, and microbial reworking of organic matter during early diagenesis (Hayes, 1993; Meyers and

Ishiwatari, 1993; Werne and Hollander, 2004). $\delta^{13}C$ of land-derived organic matter has a relatively large range, as terrestrial plants can be divided into three groups on the basis of their distinct photosynthetic pathways: $C_3$, $C_4$ and CAM. The carbon isotope range of $C_3$ plants is -22‰−-35‰, with a mean of ~-28‰; that of $C_4$ is -9‰−-16‰, with a mean of ~-14‰. CAM plants have a large range of $\delta^{13}C$ that covers the range of the $C_3$ and $C_4$ pathways (DeNiro, 1987; O'Leary, 1988). Lake-derived organic matter is isotopically indistinguishable from land-derived organic matter such as $C_3$ or possibly CAM (Meyers and Ishiwatari, 1993). This makes $\delta^{13}C_{OM}$ difficult to use to identify the predominant source of the organic matter.

$\delta^{13}C$ of aquatic organic matter is affected by the $\delta^{13}C$ of the dissolved inorganic carbon ($\delta^{13}C_{DIC}$) in lake water, which is linked to $CO_2$ equilibrium exchange between the lake water and the atmosphere (relatively long term), and by aquatic productivity (relatively short term). Aquatic plants preferentially take up $^{12}C$ during photosynthesis and leave the remaining dissolved inorganic carbon pool enriched in $^{13}C$. Enhanced primary productivity thereby leads to a more positive $\delta^{13}C_{OM}$ (Meyers and Lallier-Verges, 1999).

The pattern of $\delta^{13}C_{OM}$ in QH07 is somewhat different from the TOC record, ranging from -28‰ to -20‰, comparable with down core $\delta^{13}C_{OM}$ records in previous studies (Shen et al., 2005; Henderson and Holmes, 2009). During glacial times, $\delta^{13}C_{OM}$ varies slightly about -24‰. It drastically shifts to a more positive value (as much as -20‰) in early Holocene, gradually decreasing to a more depleted level of about -24‰ during middle Holocene, and decreasing to even more negative values (~-27‰) during late Holocene.

### 5.2.4 $\delta^{15}N_{OM}$

Interpretation of the nitrogen isotopic composition of organic matter ($\delta^{15}N_{OM}$) is complex (Schulz and Zabel, 2009). Terrestrial plants have a wide range of $\delta^{15}N$, from –5‰ to +18‰. Aquatic plants have a similar range, but generally are isotopically heavier on

average than terrestrially-derived plants (Hoefs, 1988). Similar to $\delta^{13}C_{OM}$, $\delta^{15}N$ of aquatic source was suggested to be associated with primary productivity (Meyers and Ishiwatari, 1993). The $\delta^{15}N_{OM}$ in QH07 falls in the range of +3‰ to +10‰, and it shows relatively constant values (~5‰) during glacial times, suggesting low aquatic productivity. The $\delta^{15}N_{OM}$ in the Holocene is heavier and more variable on average than that in the glacial, indicating relatively higher lake production and more complex sources. Despite complications in interpreting $\delta^{15}N_{OM}$, we suggest that low-frequency variations in $\delta^{15}N_{OM}$ record reflect the aquatic production, whereas high-frequency variations imply relative proportion of terrestrial vs. aquatic sources.

In sum, the organic geochemical proxies measured in QH07 are highly consistent with each other as well as with the lithological and sedimentologic proxies. All of them show a distinctly more variable Holocene relative to the late Pleistocene. More organic material and carbonate are present in Holocene sediments than in glacial-age deposits, suggesting relatively high primary productivity and increased river runoff during the Holocene vs. relatively low aquatic production and diminished river runoff during glacial times. Moreover, the sharp changes in all the proxies indicate that an abrupt late-glacial/Holocene transition occurred at about 11.5 ka.

### 5.2.5 Correlations between TOC and TN, C/N, and $\delta^{13}C_{OM}$

In general, all the organic geochemical proxy records show low primary production during the glacial period, highest lake productivity in early Holocene, decreasing to late Holocene.

TN shows a linear relationship with the TOC (Fig. 5a). The C/N shows linear correlation with the TOC during glacial times, but not in the Holocene (Fig. 5b). A cross plot of $\delta^{13}C_{OM}$ vs. TOC (Fig. 5c) shows that the $\delta^{13}C_{OM}$ values in glacial sediments have a narrow range, while the $\delta^{13}C_{OM}$ data in Holocene sediments are rather scattered. We

conclude that during glacial times, the $\delta^{13}C_{OM}$ not only reflects the $\delta^{13}C$ values of algae (C/N <10, aquatic source), but also indicates low primary productivity. More positive values of $\delta^{13}C_{OM}$ in early Holocene likely indicate enhanced lake production as well as an increased terrestrial input of organic matter, although the terrestrial organic matter might be only a minor proportion in the total organic matter (C/N ~12). More negative values of $\delta^{13}C_{OM}$ in middle Holocene and late Holocene compared to the early Holocene likely are caused by the introduction of terrestrial organic matter delivered into the lake system by runoff. The sources of the terrestrial organic matter during early-, mid-, and late-Holocene might have been different from each other.

**5.3 Proxies derived from terrigenous sediment (Fig. 6)**

5.3.1 Si/Ti, K/Ti

Biogenic silica content is very low in Lake Qinghai sediment. Measurements of biogenic silica were attempted by Liu et al. (2010), but no observation of individual diatom shells in the sediment was reported (Liu et al., 2010). The Si/Ti, therefore, likely reflects relative quartz content, i.e., high Si/Ti suggests high quartz contents. Because K is much more soluble than Ti, K/Ti reflects the degree of weathering condition of detrital sediment, i.e., high K/Ti suggests less-altered, fresher sediment sources. In QH07, high Si/Ti and low K/Ti during the glacial period are followed by low Si/Ti and high K/Ti during the Holocene, which indicates that less quartz and fresher silicates are present in Holocene sediments compared to glacial deposits. The greater variability during the Holocene in Si/Ti and K/Ti may suggest multiple sediment sources. This is consistent with what is inferred from the lithological and sedimentologic data.

5.3.2 Grain size

The grain size of aeolian sediment has been used to reconstruct past variations of the Asian winter monsoon on Loess Plateau (Porter and An, 1995), in the North Pacific (Rea

et al., 1998), and in Lake Biwa (Xiao et al., 1997). However, terrigenous sediment in most lakes is made up of materials from a combination of sources including both aeolian and riverine load. Grain-size data from Lake Qinghai sediments show multi-modal distribution patterns. By assuming multiple end members present in terrigenous sediments, the aeolian component potentially can be separated from the riverine component.

An et al. (2011) suggested that the <25 μm fraction in Lake Qinghai sediments is derived mostly from riverine input, whereas the >25 μm fraction is primarily aeolian dust. This suggestion was based on the observation of distinct grain-size characteristics of modern dust, loess, surface sediments, and suspended particles in river water. Accordingly, suspended river particles are finer than modern dust and loess deposits in the surrounding region. For the drill core in the southern basin of Lake Qinghai, the average grain-size distribution is bimodal, partitioned at 25 μm, with one peak at 9 μm and the other at 60 μm, which correspond to riverine and aeolian contributions, respectively (An et al., 2011).This work suggested that the content of >25 μm fraction is an indicator of aeolian sediment flux related to the intensity of Westerly winds. Their results show high contents of >25 μm fraction in glacial time versus low contents in the Holocene, suggesting strengthened versus weakened westerly winds (An et al., 2011).

However, the grain-size record from QH07 (in the southeastern basin) appears quite different from that of LQDP05-1F in the southern basin. First, the grain-size record of QH07 shows three or more distinct size modes in both Holocene and glacial samples. The typical Holocene sediment grain-size distribution has three major modes, centered at 9 μm, 28 μm, and 160 μm, and two minor modes, centered at 80 μm and 500 μm. The typical glacial sediment grain-size distribution has three similar major modes but does not contain the two minor modes. This difference in size distribution indicates more complex and variable sources in the Holocene than in the glacial. Compared with LQDP05-1F, the coarse fraction (16-116 μm) in the size record from QH07 cores shows an opposite trend,

i.e. higher contents of coarse fraction in the Holocene than in the glacial. Therefore, the coarse fraction in QH07 can not be simply interpreted as a signal of the strength of the Westerlies.

The southeastern basin is shallower and QH07 is closer to the lake shore than the core from the southern basin (LQDP05-1F). QH07 is also located offshore from the Erlangjian terrace, a hook-shaped sand spit prograding into the southeastern basin of Lake Qinghai. Therefore, the coarse fraction in QH07 record may not simply reflect aeolian process. The content of the >116 μm fraction (fine sand) increased during the Holocene compared to the late glacial. This may indicate higher lake levels during the Holocene, which would result in greater fetch. Since the fetch of the lake determines the size of waves (Wetzel, 2001), larger waves would occur in the Holocene, transporting coarse grains to the southeastern basin (QH07).

Medium/coarse sand (500-μm-size) sporadically occurs in a few Holocene samples. This seems anomalously coarse for this offshore site. The sand may have been frozen into nearshore ice in the winter. During ice break-up fragments may have rafted to offshore locations where ice melted and dropped the coarse sand. Another possibility is that the coarse sand was blown by winter winds onto the surface of the ice and was released offshore during spring melt and incorporated into the sediments, which are otherwise fine grained.

The mean grain-size profile shows similar trends as that for the content of the >116 μm fraction. Coarser and more variable materials of the Holocene may reflect a more complex and variable combination of sources, including aeolian dust, riverine load and longshore current transport, compared to sites in the deeper south basin of the lake.

### 5.3.2 Magnetic susceptibility and Fe, and Ti content

Magnetic susceptibility has been used for core-to-core correlation in many studies, but it also contains important paleoclimatic information (An et al., 1991; Verosub et al., 1993; Porter and An, 1995; Xiao et al., 1995; An, 2000). Ferromagnetic minerals such as magnetite, hematite, and greigite, have strong positive susceptibility. Paramagnetic and diamagnetic minerals, however, exhibit weak positive and negative values of magnetic susceptibility, respectively. Magnetic susceptibility values in lake sediments generally reflect the concentration of Fe-bearing magnetic minerals, mostly ferromagnetic (Evans and Heller, 2003). Secondarily, susceptibility also depends on magnetic grain size (Thompson and Oldfield, 1986; Evans and Heller, 2003). Therefore, susceptibility in lake sediments, by itself, is difficult to interpret in terms of mineralogy or even climatic implications. However, chemical composition data provide useful information for a better understanding of susceptibility variations.

Magnetic susceptibility, iron, and titanium profiles from QH07 exhibit parallel changes. The correlation coefficient (R) between Fe content and susceptibility is 0.76. This highly positive correlation indicates that the magnetic susceptibility reflects the relative concentration of Fe-bearing magnetic minerals in Lake Qinghai. Magnetic susceptibility values, Fe content, and Ti content are higher in pre-Holocene sediments than in the Holocene, suggesting that the relative input of detrital material was reduced in the Holocene. The relatively low susceptibility values in the Holocene result from the combined effect of higher concentrations of paramagnetic and diamagnetic materials as well as dilution with authigenic carbonate. Also, mineralogical changes in Fe-bearing magnetic minerals are likely associated with changes in anoxic/reducing conditions of the lake due to higher primary productivity, and the possible presence of magnetotactic bacteria (Liu et al., 2011b).

## 6 Climatic implications

Paleoclimate studies on the Tibetan Plateau have been focusing on various time scales (An, 2000; Chen et al., 2001; Zhao et al., 2009; Chen et al., 2010; Zhao et al., 2010). Chen et al. (2008) synthesized climatic proxy records from lake sediments at many sites in central Asia. They found an out-of-phase relationship in moisture change during the Holocene, between the records from the northwest and the southeast of Tibetan Plateau. The former showed a dry early Holocene, a less dry mid-Holocene, and a moderately wet late Holocene, whereas the latter, monsoonal region, showed a humid early Holocene and a relatively dry late Holocene (Chen et al., 2008). Herzschuh (2006) reconstructed moisture conditions in central Asia during the last 50 ka using 75 paleoclimatic records. According to this synthesis, the middle and late marine isotope stage 3 was wet, while the LGM was dry. Following the LGM, relatively wet climate conditions returned. Among the 75 records, some (e.g. records from the southeastern Tibetan Plateau) show that, the warmest, wettest Holocene climate conditions occurred during the early Holocene. Others (in north-western and north-central China and in Mongolia), however, show a mid-Holocene, rather than the early-Holocene temperature maximum. The majority of these paleoclimatic records suggest reduced moisture since the mid Holocene (Herzschuh, 2006).

In general, our lacustrine sediment record QH07 is consistent with the climate history of the southeastern Tibetan Plateau and eastern China since the Younger Dryas cold interval. The multiple proxies we measured in the QH07 core from Lake Qinghai are compatible with each other and capture a distinct Holocene and latest Pleistocene climate record. The major first-order change in the record occurs at the transition between the Holocene and the latest Pleistocene, about 11,500 years ago, temporally correlative with the end of the Younger Dryas.

Our interpretation that the carbonate content (also the Ca/Ti) in Lake Qinghai sediments closely relates to river runoff allows us to use carbonate content as a proxy for the Asian summer monsoon, assuming a direct relation between precipitation and runoff. Another

index of the summer monsoon strength is TOC, because TOC reflects lake primary productivity and/or contribution of land-derived organic matter, probably both. For better comparison, we calculated the fluxes of total organic matter and carbonate, respectively. These two proxies of the summer monsoon intensity (Fig.7) remain low and relatively constant during the glacial period (~14,600 to ~ 20,000 yrs). During Holocene period (~11,500 yrs to present), the proxies show higher values and greater variability in contrast to the glacial time. Compared to our summer monsoon record (QH07), the Chinese cave records are remarkably similar (Fig.7), although some differences in detail are apparent. The Dongge and Sanbao cave records show major changes in the late glacial, such as the Bølling–Allerød oscillation, whereas the QH07 record suggests that largely glacial conditions persisted from the LGM to the end of the Younger Dryas. The Younger Dryas (~11,600 to 12,900 yr**s**) is recorded in QH07 as LGM-like conditions. However, in contrast to the cave records, the beginning of the Younger Dryas in QH07 is indistinct. Evidence of the Bølling–Allerød oscillation (~12,900 to 14,600 yrs BP) is weak in all of the proxies in QH07. Moreover, the cave records suggest a relatively gradual Younger Dryas/Holocene transition, whereas the equivalent change in QH07 is relatively abrupt. These differences between QH07 and the Chinese cave records may be related to the fact that Lake Qinghai is further inland and at higher elevation than the Dongge and Sanbao caves (Fig. 1).

The Asian summer monsoon is mainly driven by the differential heating between the Asian landmass and the Pacific Ocean especially the South China Sea (Li and Yanai, 1996). Thus, the June insolation difference between 30˚N and 15˚N (Huybers, 2006) is conceptually an index of this difference, so we compare it to the monsoon proxy records of QH07. The pattern of relatively weak summer monsoon in the glacial time, greatly enhanced summer monsoon in the early Holocene, and weakening of the monsoon in the late Holocene broadly matches the insolation-difference record (Fig.7). This accord implies that the major control on the variations of the summer monsoon is orbitally-induced insolation difference between the continent and the ocean, on glacial-interglacial

time scales. Feedbacks for the weak summer monsoon during the glacial period may include lower sea level (more distant shoreline) and decreased continental albedo from expanded continental ice masses. In the early Holocene, maximum organic matter and carbonate contents signify the strongest summer monsoon, suggesting the occurrence of the warmest, wettest part of the Holocene, at time of the insolation-difference maximum (Fig. 7). Gradually reduced monsoonal precipitation, i.e., a weakened summer monsoon, since the mid-Holocene, is marked by a decrease in the carbonate content, and total organic matter content. The greater variability in the records of the Holocene implies complex and multiple sediment sources that include atmospheric deposition and riverine input. The Younger Dryas interval is an anomaly, as it is in many records, compared to the insolation-difference curve. More anomalous still is the period from ~13,000 - ~15,000 yrs, which appears only slightly wetter than the LGM and the Younger Dryas, in contrast to many records that show warming (Bølling–Allerød) during this interval.

The relatively stable glacial, abrupt Late Pleistocene/Holocene transition, and unstable Holocene suggest a climate threshold for arrival of monsoonal precipitation at Qinghai. Due to the high elevation of the Tibetan Plateau, the westerly jet stream (high altitude wind) is divided into two, passing to the north and south of the Himalayas. The northerly jet stream and the southerly jet stream join on the lee side of the mountain range over eastern China. However, the locations of the two jet streams are variable over time. Modern climatic data show that during winter the westerly jet stream is located to the south of the Tibetan Plateau, i.e., the northerly jet stream moves to the south, whereas in the summer, it is located to the north, i.e., the southerly jet stream weakens and moves to the north (Schiemann et al., 2009). Results of PMIP2 coupled simulations show that during the LGM, the Asian monsoon prevailed on the northeastern Tibetan Plateau in summer, while the westerly jet stream dominated in winter (Braconnot et al., 2007). During glacial times, ice sheet growth and low North Atlantic sea surface temperature lead to southward shift of polar front and the westerly jet stream; Asian monsoon did not reach this area. In contrast, during the Holocene, ice sheet retreat and the associated

increase in sea level moved the westerly jet stream northward, allowing more northwesterly penetration of the Asian monsoon. The abrupt transition between late glacial and the Holocene indicates the time when the Asian monsoon crossed this climate threshold.

# 7 Conclusions

A multi-proxy approach was applied to the paleoenvironmental interpretations from the sediments in Lake Qinghai. These proxies include water content, bulk density, carbonate content, TOC, TN and $\delta^{13}C_{OM}$, $\delta^{15}N_{OM}$, bulk geochemical composition, magnetic susceptibility, and grain size. The results from these proxies, which are highly consistent with each other, plus a relatively robust age model, reveal the climatic variations on the northeastern Tibetan Plateau since the LGM. In particular, the carbonate and TOC contents are interpreted as proxies for the strength of the Asian summer monsoon, reflecting distinct Late Pleistocene and Holocene climatic changes.

- Summer monsoon was relatively weak and constant during the entire LGM and late glacial time, suggesting relatively cool, dry and stable climatic conditions. In contrast, during the Holocene, the summer monsoon was relatively strong and showed greater variability, implying relatively wet but less stable climatic conditions than those during the Late Pleistocene. The strongest summer monsoon, marked by maximum organic matter and carbonate contents, occurs in the earliest Holocene.
- Gradually reduced monsoonal precipitation, i.e., a weakened summer monsoon, is inferred from decreased carbonate content through the course of the Holocene.
- All of the paleoenvironmental proxies provide evidence of abrupt changes across the Late-Pleistocene/Holocene transition, about 11,500 years ago.
- The Younger Dryas appears to be recorded in the sediment, marked by low carbonate content and low total organic matter content, but compared to the

Chinese cave records, its onset is indistinct.

- Evidence of significant climate change equivalent to the Bølling–Allerød oscillation is weak in the proxies in the QH07 record.
- By comparing our Lake Qinghai record QH07 with the Northern Hemisphere insolation-difference record (between June 30˚N and June 15˚N), we propose that the changes in insolation contrast between the continent and the ocean is the major control on the Asian monsoon system over the glacial/interglacial time scales. Secondary influence may include ice sheet size (albedo) and sea level (distance from moisture source).
- A climate threshold for arrival of monsoonal rainfall is suggested at the northeastern Tibetan Plateau.

**Acknowledgement:** This work was supported by National Science Foundation grant EAR-0602412 to Steve Colman. UK NERC Program supported some of the $^{14}C$ dating. We thank LacCore (National Lacustrine Core Facility), Limnological Research Center, University of Minnesota-Twin Cities for laboratory assistance. We also thank MOE Key Laboratory of Western China's Environmental Systems, Research School of Arid Environment and Climate Change at Lanzhou University, for field assistance.

Fig. 1 The map of China shows the setting of Lake Qinghai on the Tibetan Plateau and the sites of speleothem records discussed in the text (blue square A: Lake Qinghai; B: Dongge Cave; C: Sanbao Cave). The white square in the southeastern basin of Lake Qinghai indicates the core site location of QH07.

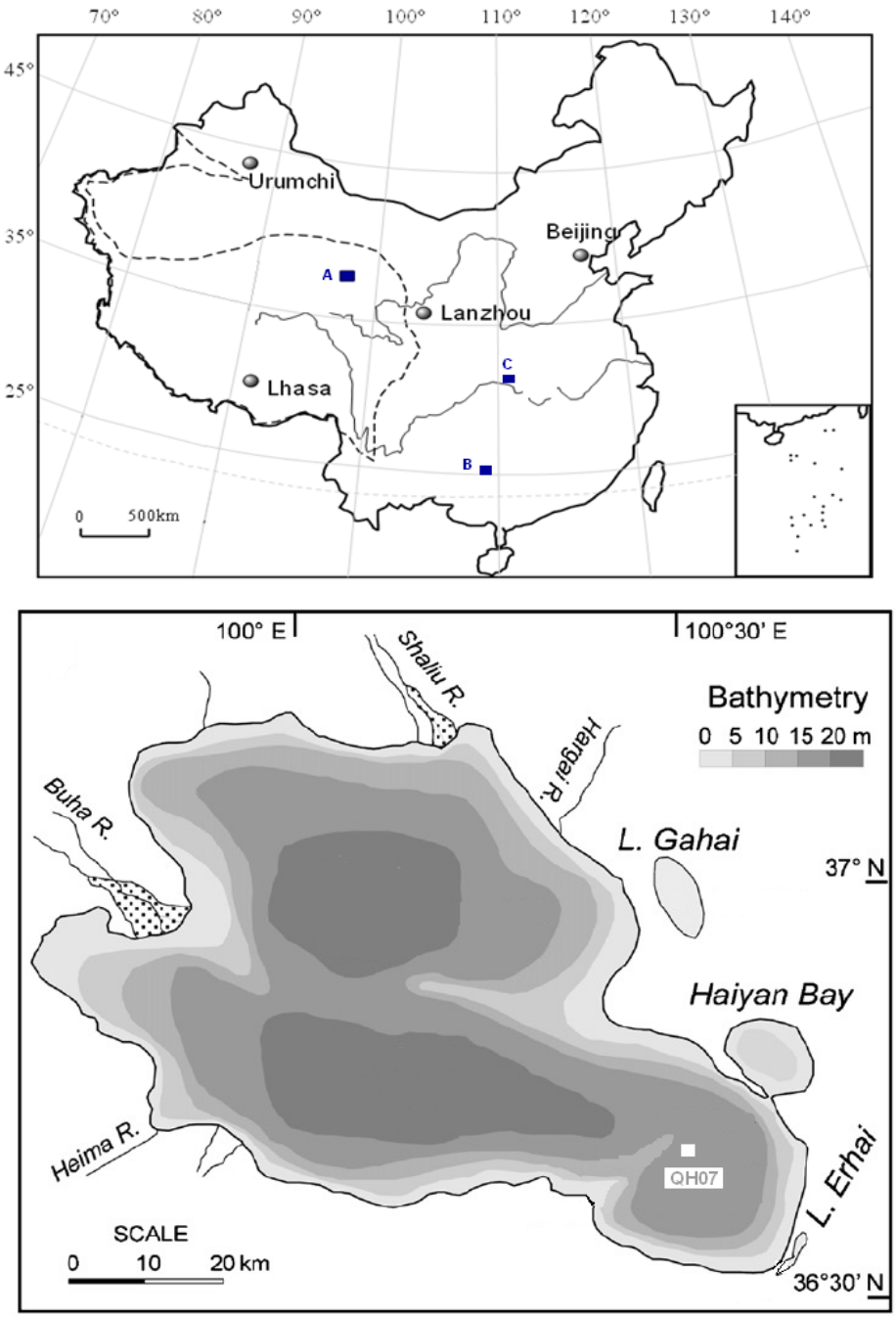

Fig. 2 Age-depth model for QH07 (in calibrated years BP) using a smooth spline model in CLAM (Blaauw, 2010). Mirrored grey histograms show calibrated distributions for individual $^{14}C$ ages. Crosses indicate ages considered outliers. Grey envelops show 95% confidence intervals around the age model. Black curve shows the "best" fit of the age estimates (a modern day age at the surface sediment and a 700-yr reservoir effect were used).

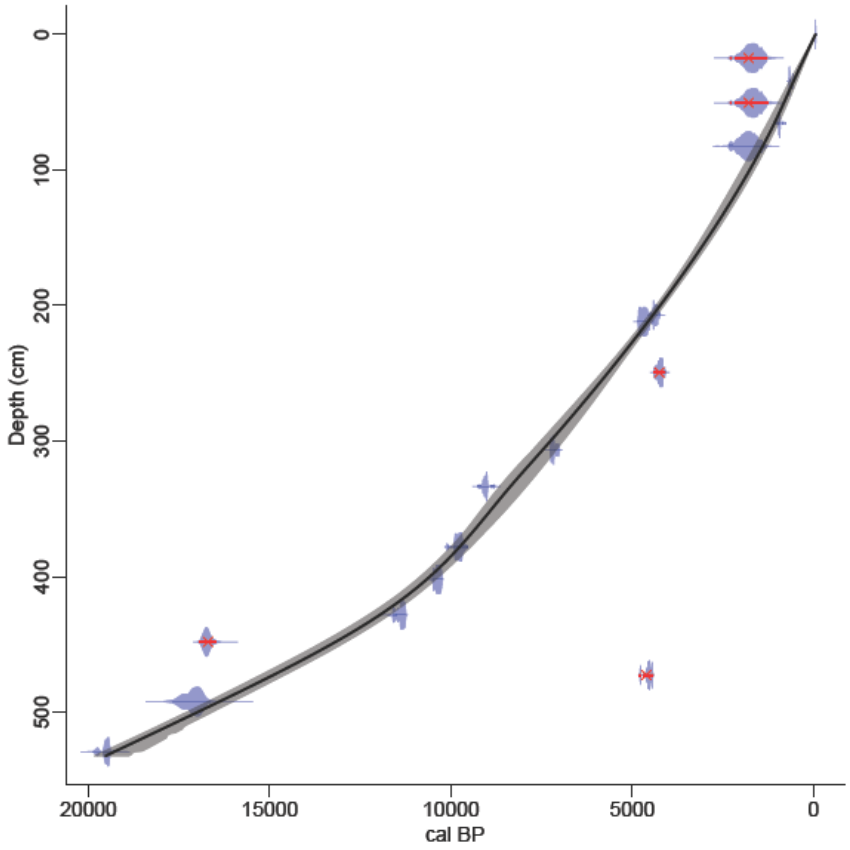

Fig. 3 Results from the lithological and sedimentologic measurements, including water content, Cl/Ti from XRF (water content index), bulk density, carbonate content, and Ca/Ti from XRF (reflecting carbonate content).

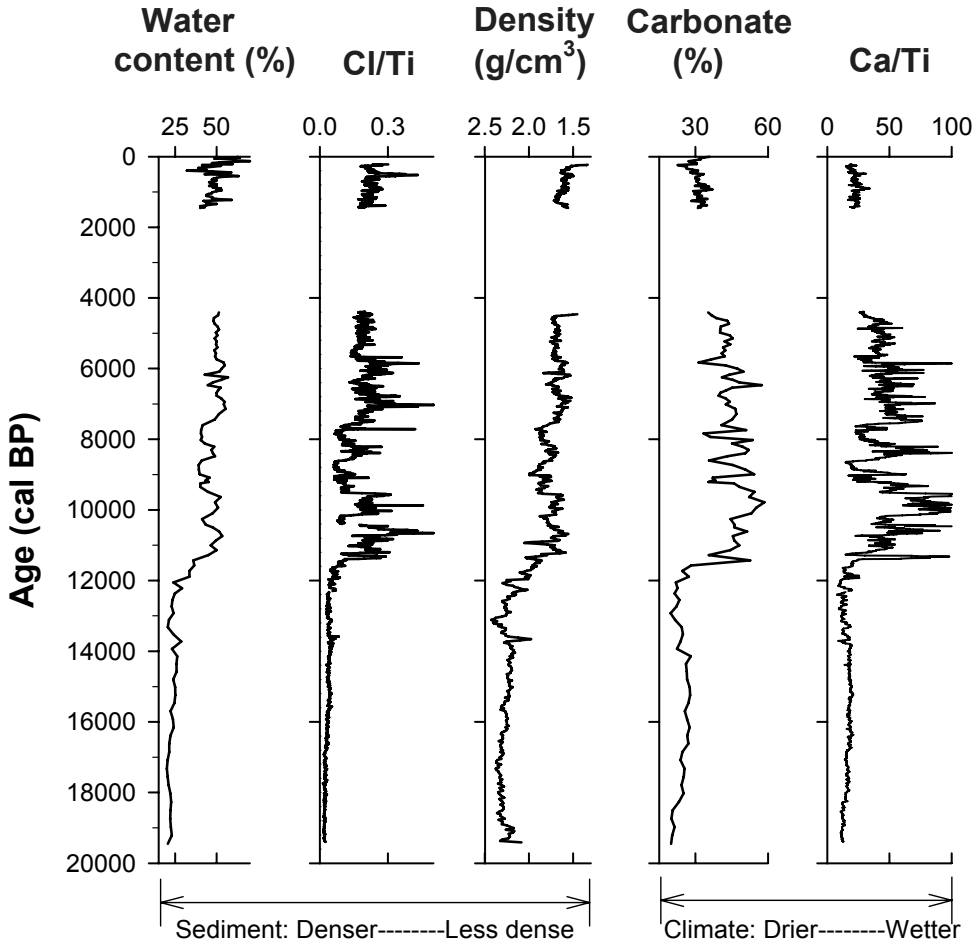

Fig. 4 Results from organic geochemical proxies, including total organic carbon, Inc/Coh ratio from XRF (reflecting total organic matter), total organic nitrogen, C/N, the carbon and nitrogen isotopic composition of bulk organic matter ($\delta^{13}C_{OM}$ and $\delta^{15}N_{OM}$).

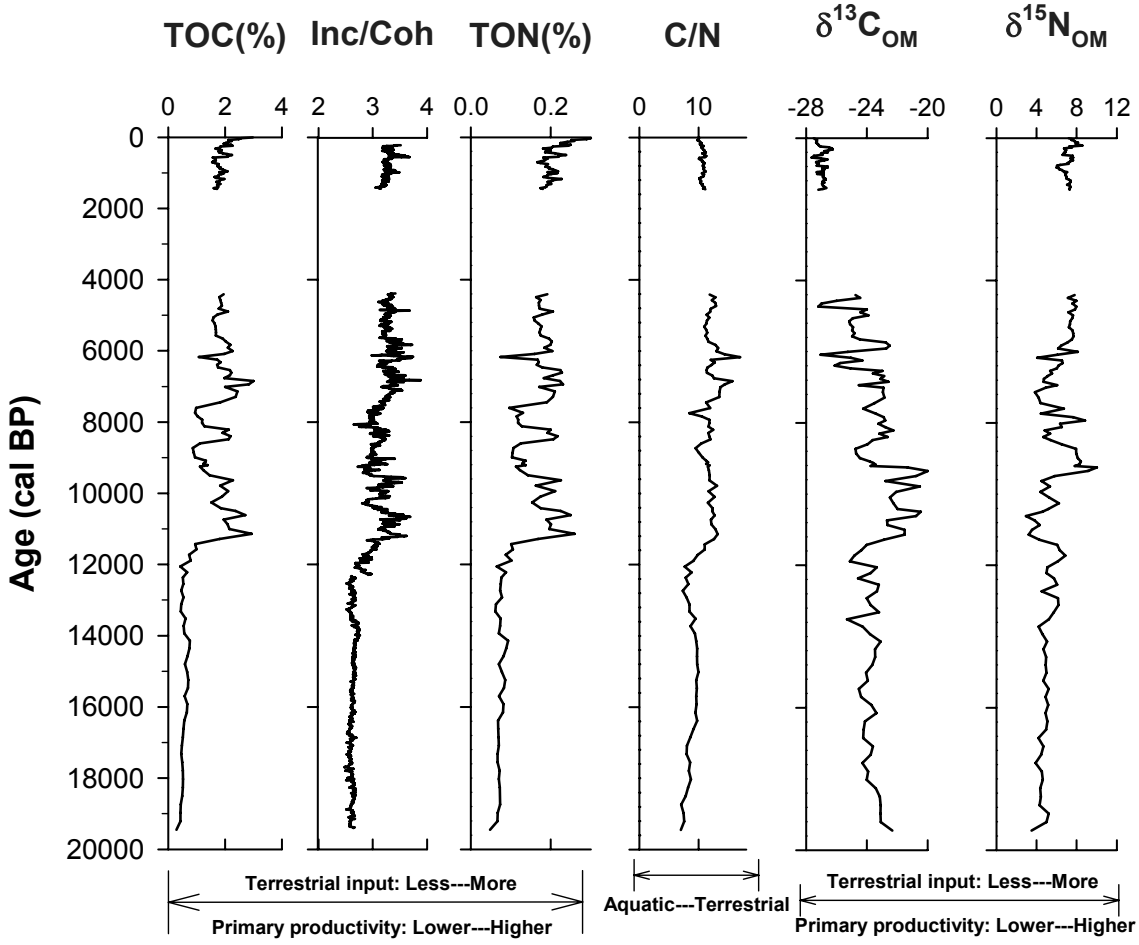

Fig. 5 Cross plots of TOC vs. TN (a), TOC vs. C/N (b), and TOC vs. $\delta^{13}C_{OM}$ (c). Open squares indicate data for the Late Pleistocene and dots indicated those for the Holocene.

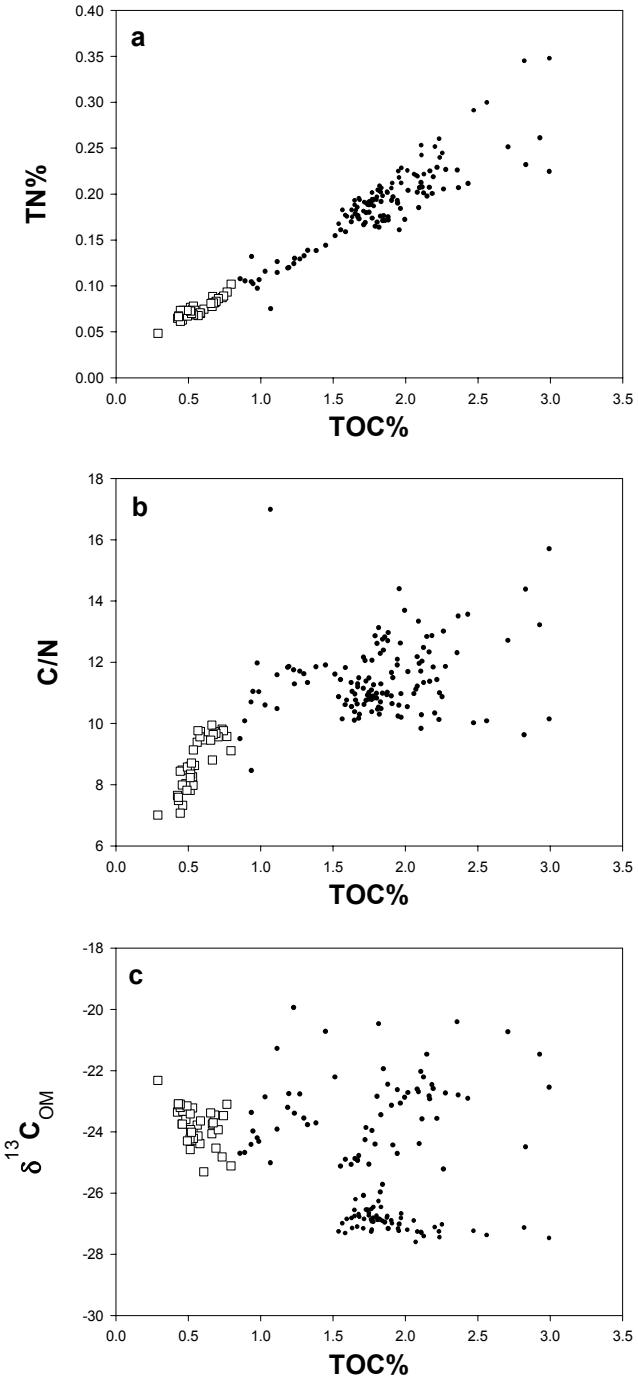

Fig. 6 Results for proxies derived from terrigenous sediment, including magnetic susceptibility, Fe content, Ti content, mean grain size, content of >116 μm fraction of lake sediment, content of 16-116 μm fraction, Si/Ti from XRF (index of quartz content), and K/Ti.

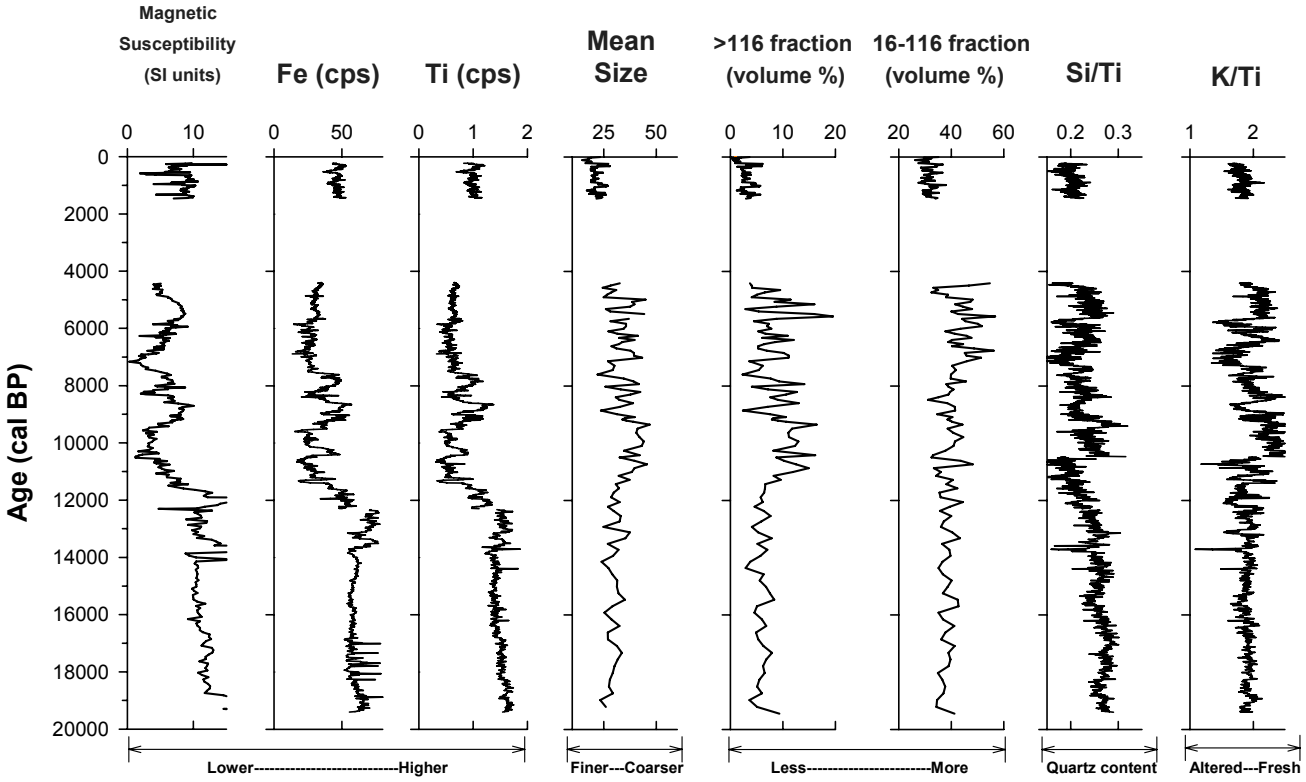

Fig. 7 Comparison of summer monsoon proxies for QH07 (green dotted line: TOM flux; blue solid line: carbonate flux) with Dongge (black solid line) and Sanbao (red dotted line) cave speleothem $\delta^{18}O$ records and June insolation difference between 30˚N and 15˚N. Gray bars indicate the Younger Dryas (YD) and Bølling–Allerød (B/A) periods.

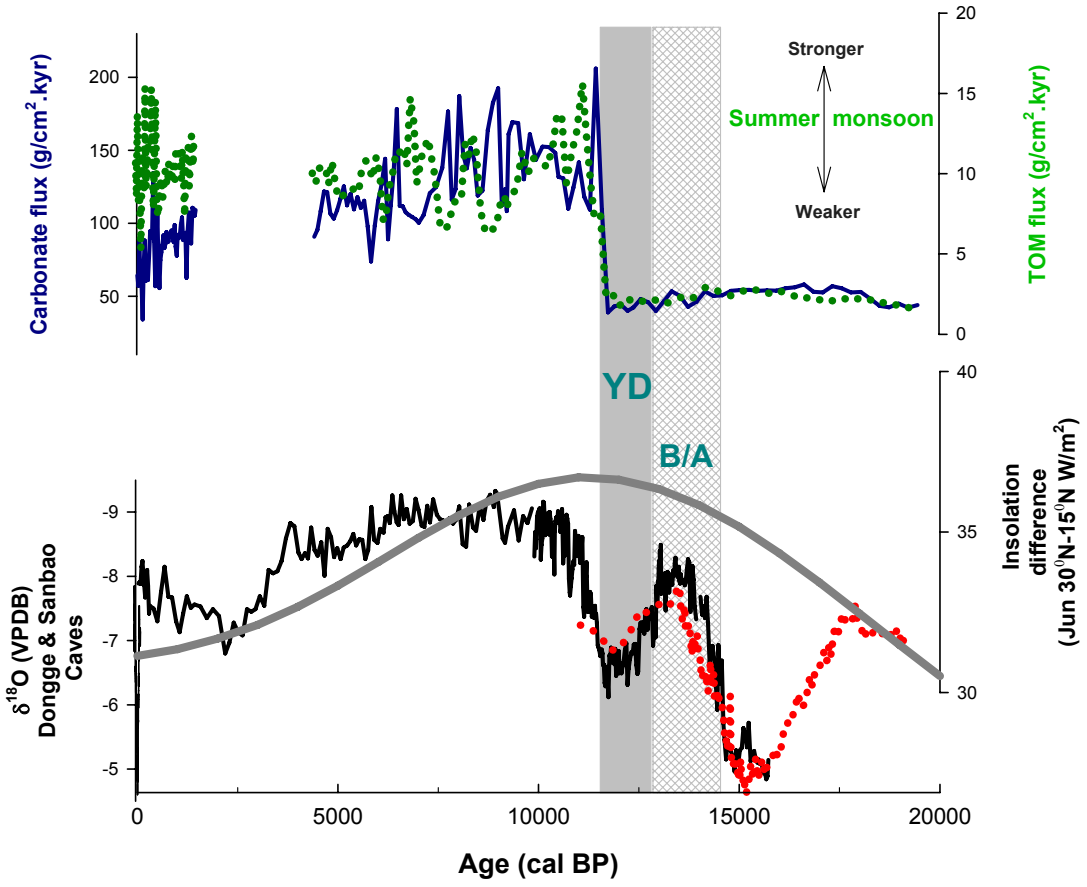

# Chapter 3: Magnetic and geochemical characteristics of the Lake Qinghai sediments and their implications of past climate change

**Liu, Xiuju[1,2], Colman, Steve M.[1,3], Brown, Erik T.[1,3]**

1 Large Lakes Observatory, University of Minnesota Duluth, Duluth MN 55812, USA

2 Department of Earth Sciences, University of Minnesota Twin Cities, Minneapolis MN 55455, USA

3 Department of Geological Sciences, University of Minnesota Duluth, Duluth MN 55812, USA

Magnetic properties and geochemistry of sediments from Lake Qinghai, northeastern Tibetan Plateau, were determined for a set of u-channel samples (total 18.6 m) and several selected discrete samples. These results provide information about changes in magnetic mineral concentration, grain-size distribution, mineralogy, and geochemical composition, as well as implications for paleoclimatology.

The relative abundances of iron and concentration-dependent magnetic parameters reflect higher concentrations of magnetic minerals during glacial times than the Holocene. Hysteresis measurements of the discrete samples show a larger proportion of single domain (SD) minerals relative to multiple domain (MD) particles in Late Pleistocene sediment compared to Holocene sediment, suggesting that the glacial period was dominated by the deposition of fine-grained aeolian materials whereas the Holocene was characterized by increased riverine and shoreline transport of coarse materials to the lake. Furthermore, the greater variability of magnetic parameters and geochemical composition during the Holocene suggests complex and multiple sediment sources.

Magnetite has been identified by temperature-dependent magnetic measurements and S-ratios as the primary ferrimagnetic mineral throughout the core, suggesting the mineralogy is relatively constant. Relatively low magnetite concentration during the Holocene is mainly caused by dilution by increased authigenic carbonate that is strongly associated with riverine runoff. The low-temperature magnetic behavior indicates the presence of monoclinic pyrrhotite ($Fe_7S_8$), which implies reducing depositional environment in the lake. Several lines of evidence suggest the local occurrence of greigite ($Fe_3S_4$), which may indicate relatively low lake level phases and dry climate conditions during the glacial period.

Results from the elemental composition and magnetic properties of the Lake Qinghai sediments are consistent with records derived from lithological and sedimentological proxies, reflecting a distinct Late Pleistocene (relatively stable, cold-dry) and Holocene (relatively unstable, warm-wet) climates.

# 1 Introduction

Magnetic and geochemical properties of sediment contain a wealth of information, providing clues to magnetic mineral concentration, mineralogy, particle grain size distribution, as well as sedimentary environment (Colman et al., 1997; Hilgenfeldt, 2000; Geiss et al., 2003; Zhu et al., 2003; Geiss et al., 2004). Bulk elemental chemistry is largely unbiased by mineralogy and provides details on sediment chemistry, sediment origin, provenance, and past climate changes (Brown et al., 2007). For example, the geochemical composition and magnetic susceptibility have been used to create records of redoxomorphic iron mineral diagenesis in suboxic marine sediments (Funk et al., 2003). Mineral magnetic properties and geochemical data from Lago Verde, East-Central Mexico, have been combined to provide a sedimentary record of past environmental conditions (Ortega et al., 2006). However, studies that address paleoclimatic issues synthesizing magnetic parameters and geochemical data from lacustrine sediments are scarce.

Lake Qinghai (36°32’ to 37°15’ N, 99°36’ to 100°47’ E, Fig. 1), the largest inland water body in China, situated at an elevation of 3194 m, on the northeastern margin of the Tibetan Plateau, is thought to be one of the best archives for exploring the past changes in continental climate (Colman et al., 2007). To investigate the geochemical composition and magnetic properties of the sediments and their paleoclimatic implications, we performed high-resolution, continuous, nondestructive, fast core-scannings of elemental and magnetic analyses for the changing sediment input, on the u-channel samples from a 18.6-meter-long drill core from Lake Qinghai (An et al., 2006). To characterize the magnetic mineralogical and grain size variations, hysteresis and temperature-dependent magnetic properties were examined in several selected discrete samples.

In the Lake Qinghai sediments, several major elements such as iron (Fe), titanium (Ti) and sulfur (S) are associated with magnetic minerals. We specifically present the variations in these elemental concentrations, changes in sediment magnetic parameters that include magnetic susceptibility ($\chi$), natural remanent magnetization (NRM), anhysteretic remanent magnetization (ARM), isothermal remanent magnetization (IRM), and their interparametric ratios, as well as hysteresis and thermomagnetic properties. Our integrated study would help better understand the mineralogy and its implication to climate change in the Lake Qinghai region.

## 2 Study site

Lake Qinghai is a closed basin, surrounded by two high mountain ranges, the Qilian Shan (Datong Shan) to the north, and the Qinghai Nan Shan to the south (Yu, 2005). The drainage area of the lake is about 30,000 $km^2$ (LZCAS, 1994). The lake has a surface area of 4400 $km^2$ and an average water depth of 21 m, with a maximum depth of 27 m. The lake water is brackish to saline (average salinity = 15.5 g/l; pH = 9.06). The mean annual precipitation in this semi-arid region is ~360 mm, most of which falls in summer, while the potential evaporation is up to 1000 mm on lake surface per year. About 75% of the total runoff occurs in the summer time. The catchment is mainly semi-arid grassland. Annual mean temperature is –0.7 °C and monthly means exhibit remarkable seasonality, varying from –11 °C in winter to 12 °C in summer (Lister et al., 1991; Shen et al., 2005; Henderson et al., 2010). Lake Qinghai area is generally considered to be at the intersection of the East Asian monsoon and the Westerlies on the Tibetan Plateau (Zhang, 1997; Henderson et al., 2010; An et al., 2011). Its unique geographical settings make Lake Qinghai very sensitive to environmental and climatic changes and thus largely benefit paleoclimatology studies.

## 3 Materials and methods

### 3.1 Sediments

A 18.6-m-long continuous and undisturbed drill core LQDP05-1F (Fig. 2) was collected from the deepest part of the southwestern Qinghai Lake basin, using the GLAD800 (Global Lake Drilling to 800 m) drilling system in 2005 (An et al., 2006). After splitting the cores, u-channel samples, normally 2×2×150 cm, were collected from individual core sections. This special sampling method provided the convenience of scanning purposes and also avoided the contaminated or deformed sedimentary material near the outside of the core. Accordingly, u-channel sediments are the most representative of the sedimentary sequence.

Eight discrete samples were selected for this study, including two from core LQDP05-1F and six from core QH07 (Fig. 2). Although these two cores were recovered from different sub-basins of Lake Qinghai, they were quite similar in terms of lithology.

### 3.2 Analytical methods

3.2.1 XRF core scanning

Bulk elemental composition of the sediments was analyzed using an ITRAX X-ray Fluorescence (XRF) Core Scanner (Cox Analytical Instruments). The surface of the sediment in split core was carefully smoothed and flattened. A molybdenum X-ray source set to 30 kV and 30 mA was focused to generate a rectangular X-ray beam that covered an area of 0.2 × 20 mm on the surface of sediments (Croudace et al., 2006). Measurements were taken at 5-mm intervals for a counting time of 60 seconds as the core moved by an incremental motion whose direction was perpendicular to the X-ray beam. After core scanning on the instrument was complete, initial XRF spectral data were reprocessed in a standard fitting procedure using the Q-Spec spectral analysis software to refine the fitting of individual elemental peak areas (Croudace et al., 2006). Final XRF data were output as counts per second (cps).

### 3.2.2 Magnetic measurements

Magnetic susceptibility ($\chi$) was measured at 1-cm intervals on the u-channel samples using a susceptometer with point sensors (Geotek MSCL-XYZ). The susceptibility was reported as volume-normalized susceptibility values, with units of $10^{-6}$ SI.

Remanent magnetization investigation of the u-channel samples was conducted at 1-cm intervals using a 2G® Enterprises SQUID pass-through cryogenic magnetometer situated in a magnetically shielded room with background field of <500 nT (inside the magnetometer at the sensors, the background field is <10 nT). The natural remanent magnetization (NRM) was measured before sediment samples were exposed to laboratory-applied magnetic fields. The anhysteretic remanent magnetization (ARM) was acquired through the combined effects of two superimposed magnetic fields: a small, constant direct current (DC) field, $50 \times 10^{-6}$ Tesla (T), and a large, decreasing alternating field (AF) (peak value of 0.1 T). Isothermal remanent magnetization (IRM) was acquired by exposing the sample for a short time in a 2G® core pulse magnetizer with a forward field of 1 T ($IRM_{1000mT}$) and at a backward field of 300 mT ($IRM_{-300mT}$). $IRM_{1000mT}$ was considered the saturation of IRM (SIRM). All the NRM and AF demagnetization data were reprocessed in a deconvolution model that was specially designed for u-channel magnetometer data (Jackson et al., 2010).

The S-ratio ($-IRM_{-300mT}$/SIRM) is a function of the relative contribution of low- to high-coercivity minerals. It is commonly interpreted to represent the proportion of magnetite to hematite; low S-ratios indicate more hematite while high S-ratios indicate more magnetite (Heslop, 2009). Hard isothermal remanent magnetization is calculated using the equation (H'IRM) = (SIRM + $IRM_{-300\ mT}$)/2. Soft isothermal remanent magnetization is calculated by (S'IRM) = (SIRM - $IRM_{-300\ mT}$)/2. These two parameters are measures of relative concentrations of high/low coercivity magnetic minerals, respectively (King and Channell, 1991). Unfortunately, we did not get good deconvolved data for these

parameters, because quite a few intervals in the u-channels, especially below 6 m, had high intensity magnetization. As a result, flux jumps and erroneous drift corrections occurred in the instrument, so that none of the measurements related to these intervals were usable (gaps of data in Fig. 3 and Fig. 5). Therefore, magnetic parameters such as S-ratio, H'IRM, and S'IRM for the u-channel samples were not discussed.

Hysteresis measurements and S-ratios in the discrete samples were determined using a Vibrating Sample Magnetometer (VSM). Hysteresis loops were obtained by cycling the magnetic field from +1 T to -1 T and back again (King and Channell, 1991). S-ratios were calculated

Low temperature (10 K<T<300 K) and high temperature (~25 °C<T<700 °C) measurements were performed on selected freeze-dried discrete samples using a Quantum Designs Magnetic Properties Measurement System (MPMS) and a KappaBridge high-temperature susceptibility bridge, respectively. For low-temperature thermomagnetic characterization, a 2.5 T IRM was imparted at 300K (RT-SIRM). The remanence was then measured on cooling to 10 K and on re-warming to 300K. High-temperature measurements were made in an Ar atmosphere.

# 4 Results

## 4.1 Geochemical composition

We focus on variations in titanium (Ti), iron (Fe), and sulfur (S) contents using the XRF data. Ti is a chemically immobile element and not affected by diagenesis (Thompson et al., 1998). Its relative abundance in sediments largely depends on the amount of primary mineral input from terrestrial sources and on dilution by carbonates and biogenic matter (Yancheva et al., 2007). The Ti profile (Fig. 3a) shows a considerable variability with depth in core LQDP05-1F. The upper 5 m has relatively low Ti contents, the lowest of which occurs at the depth of 3-4 m. Below 5 m, the relative concentration of Ti is much

higher. In addition, the upper 5 m of the Ti profile shows greater variability relative to that at greater depth.

In contrast to Ti, Fe is mobile in reducing and/or acidic aqueous environments. The Fe profile (Fig. 3b) follows the same trend of Ti, with a high correlation coefficient (R) of 0.89 (Fig. 4), suggesting the relative immobility of iron in the sediments, and suggesting that Fe distributions are minimally affected by authigenic or diagenetic processes. Any Fe solubilized during diagenesis is unlikely to have undergone significant vertical migration at the scale of our measurements (5 mm). The Fe content changes significantly along the core, showing much higher values in the lower depths compared to the upper depths. Similar to Ti, the Fe profile also exhibits greater variability in the upper 5 m.

Sulfur behaves quite differently from Fe and Ti (Fig. 3c), showing higher values in the upper 7 m of the core, dropping drastically from 7 to 7.5 m, fluctuating between 7.5 and 8.5 m, and then remaining at fairly low concentrations in the lower part of the core, except at depths of 15.5-17 m where a "plateau-like" interval shows up. The S profile also shows greater variability in the upper part of the core than that of the lower part. This is consistent with the Ti and Fe profiles. In the deeper interval, S concentrations remain relatively stable compared to Ti and Fe.

**4.2 Magnetic properties**

4.2.1 Magnetic susceptibility

In sedimentary environments, magnetic susceptibility values ($\chi$) generally reflect the concentration of magnetic minerals in sediments. Based on types of magnetic behavior, three types of magnetic minerals are defined, ferro-, para- and diamagnetic (Evans and Heller, 2003). Ferromagnetic minerals such as magnetite, hematite, and greigite, have large positive susceptibility and usually are the major contributors to magnetic susceptibility. Paramagnetic and diamagnetic minerals, however, commonly exhibit

weakly positive and negative values in magnetic susceptibility, respectively. Examples of paramagnetic minerals can be siderite, biotite, and pyrite. Substances like quartz, calcite, water, organic matter, containing little or no Fe, are typical diamagnetic minerals (Thompson and Oldfield, 1986).

Lake sediment is a mixture of particles of different origins including terrigenous and authigenic sources. In addition to control by concentration, susceptibility is also grain-size dependent (Oldfield, 2007). For example, larger magnetic grain sizes, such as multi-domain (MD) grains, and very fine magnetic grain sizes, such as superparamagnetic (SP) particles, lead to higher $\chi$ values (Dearing, 1999). Accordingly, interpretation of susceptibility measurements from lacustrine sediments is complex.

The magnetic susceptibility (Fig. 3d) of the u-channel samples changes significantly along the core. $\chi$ values are extremely low throughout the upper 5 m. Between 5 and 8 m, the susceptibility remains relatively low but higher than the upper 5 m. Below 8 m, sediments show a significant increase in susceptibility, about two orders of magnitude higher than the upper depths, especially in two intervals (8-8.5 m and 15.5-16.5 m) where $\chi$ values are remarkably high as much as 140 $\times 10^{-6}$ SI. The upper 5-m record also shows larger variations than the rest of the record.

### 4.2.2 NRM, ARM, IRM, and their interparametric ratios

NRM provides information about the intensity and orientation of the Earth's magnetic field when the sediment was initially deposited (Weeks et al., 1995). ARM and IRM are two artificial magnetizations induced in the samples. NRM, ARM, and IRM together can complement magnetic susceptibility in interpreting variations in concentration, grain size, and mineralogy of magnetic materials (Peck et al., 1994), and providing paleoclimatic and paleoenvironmental information (Geiss et al., 2004; Ortega et al., 2006). ARM/SIRM

and ARM/$\chi$ ratios are widely employed as proxies of magnetic grain-size because the ARM is more sensitive to the finer magnetic grains than the IRM (Richter et al., 2001; Evans and Heller, 2003).

Magnetic parameters NRM (Fig. 3e), ARM (Fig. 3f), and SIRM (Fig. 3g) exhibit parallel changes with $\chi$ (Fig. 3d) throughout the core LQDP05-1F, showing relatively low magnetization in the upper part of the record and two to three orders of magnitude higher values in the lower part. These magnetic parameters display overall smaller variations than magnetic susceptibility, which shows quite different trends at the intervals of 0-1 m and 3-4 m, where susceptibilities are decreasing while relative stability is observed in other magnetic parameters.

The NRM record is more similar to ARM than $\chi$. Both the NRM and ARM show remarkably high values at two intervals of 8-8.5 m and 15.5-16.5 m. The NRM record also shows another high value region in the depth of 11.5-12.2 m.

The ARM record is much like the magnetic susceptibility record but shows relative invariance other than in two major pulses, again, at the depth intervals of 8-8.5 m and 15.5-16.5 m. Low ARM values are found above 6 m and increasing values at greater depth.

The IRM record of LQDP05-1F is not complete. Two gaps in the IRM data are due to instrumental limitations, which were caused by unusually intense magnetic signals during the scanning process (the same reason as for the invalid S-ratios). These intervals also show remarkably high susceptibility. Although discontinuous, the SIRM record still increases down core, which is similar to the susceptibility, NRM, and ARM records.

ARM/SIRM and ARM/χ (Fig. 5) show relatively high values on average with large variations in the upper 8 m. At greater depth down core, except for the interval of 15.5-16.5 m, ARM/χ shows relatively low values. ARM/SIRM and ARM/χ ratios are usually used as proxies of magnetic grain-size (Geiss et al., 2003). However, ARM is sensitive to magnetostatic interactions, which in general increase with concentration. According to the concentration-dependent magnetic parameters, magnetic concentration varies strongly with core depth. Therefore, the grain-size information in ARM/SIRM and ARM/χ may be affected by magnetostatic interactions.

S-ratios measured on the discrete samples are generally close to 1, indicating the dominance of low-coercivity minerals such as magnetite.

4.2.3 Hysteresis loops

The characteristics of a hysteresis loop in a given sample are determined by the magnetic mineralogy, magnetic grain size, and concentration of magnetic minerals (Mischke et al., 2005). Several hysteresis parameters derived from hysteresis measurements can be used as proxies for one of the variables. Saturation magnetization (Ms) is usually a function of magnetic concentration. The ratio of Mr/Ms (Mr is saturation remanent magnetization) is indicative of magnetic grain size distributions where mineralogy does not vary strongly (Dunlop, 2002) .

The hysteresis data (Fig. 6) were summarized in a Theoretical Day Plot of the hysteresis parameters Mr/Ms versus Hcr/Hc, which covers superparamagnetic (SP), single-domain (SD), and multi-domain (MD) magnetite and mixtures of these grain sizes (Dunlop, 2002). Hcr is the coercivity of remanence (measured in zero field). Hc is the bulk coercivity in the field. All the Qinghai data points are situated closely to the SD-MD mixing curves, in a region of $0.1 < Mr/Ms < 0.5$ and $Hcr/Hc < 4$.

4.2.4 Temperature-dependent measurements

Low-temperature magnetic measurements of all the samples (Fig. 7) show that remanence drops sharply on cooling through typical Verwey transitions at ~120 K (Ozdemir et al., 1993) in RT-SIRM curves, suggesting the presence of magnetite. Most samples also show changes through the transitions at ~34 K, indicating the presence of monoclinic pyrrhotite in sediments (Dekkers et al., 1989). Two samples from the glacial deposit with high susceptibility, which may contain greigite, did not show evidence for the monoclinic pyrrhotite transition at ~34 K.

High-temperature measurements (Fig. 8) show a sharp drop at ~550 °C, which also provides evidence of magnetite, whose curie temperature is ~580 °C (Maher and Taylor, 1988). Two samples selected from high magnetic susceptibility ($\chi$) intervals show distinct features at ~250 °C and ~350 °C in high-temperature susceptibility curves (Fig. 9). The former seems to be related to greigite (Roberts et al., 2011).

# 5 Discussion and implication for paleoclimatic changes

Age estimates for core LQDP05-1F indicate that, in a general way, the upper 5-m sediment was deposited during the Holocene period (0~11.5 ka), and that the bottom of the core reaches back to about 32 ka (An et al., 2011). Major changes in magnetic properties are clearly linked to the geochemistry of the sediments. The Fe and Ti contents are correlated with magnetic parameters; Fe correlates with susceptibility (R=0.45, Fig. 4) in LQDP05-1F, where the correlation is stronger in core QH07 (R=0.76). The Fe content also has a positive correlation with the other magnetic parameters including NRM, ARM, and SIRM, but the correlations are relatively weak (Fig. 4), suggesting that Fe contents and magnetic properties reflect the concentration of the iron-bearing minerals from the detrital input in at least a general way. Changes in mineralogy and contributions

from other non-magnetic materials may result in relatively weak correlations (Fig. 4). However, the magnetic and geochemical characteristics of Lake Qinghai sediments of glacial and Holocene age are distinctively different. On the other hand, magnetite, which is identified by the temperature-dependent magnetic properties, is present throughout the core. It is also magnetically the dominant mineral relative to hematite or other high-coercivity minerals, as suggested by S-ratios.

Fluctuations in magnetic parameters can be used to track changes in authigenic or detrital input. Concentration-dependent magnetic parameters $\chi$, ARM, and IRM show a striking shift at the glacial/Holocene transition, suggesting a major change in the source of sediments. Increases in $\chi$, NRM, ARM, and SIRM, as well as Fe abundance indicate higher concentrations of magnetic minerals during the glacial period than in the Holocene. This appears to be a manifestation of the dominance of aeolian material during the glacial period. Smear slide analyses show that glacial sediments contain more clastic, clay-sized minerals than do Holocene sediments. In addition, hysteresis measurements indicate that magnetic minerals during glacial times are mainly SD particles (small grain-size). This is consistent with aeolian processes, which tend to transport relatively small grains. The SD particles also seem to be related to magnetite. According to Middleton (2006), SD magnetite particles are prone to acquiring strong ARM. In addition to the concentration of magnetic minerals, this could partially explain the higher ARM during glacial times relative to the Holocene.

The Holocene is characterized by relatively low Fe and Ti contents, and decreases in the magnetic parameters including $\chi$, NRM, ARM, and SIRM, suggesting relatively low concentrations of magnetic minerals. The hysteresis loops and temperature-dependent properties of the Holocene sediments and the glacial sediments are quite similar, suggesting that the mineralogy throughout the core does not vary significantly. Magnetic hysteresis properties of the sediments imply lower concentrations of ferrimagnetic and paramagnetic minerals in the Holocene compared to the late Pleistocene. The Holocene

sediments contain more MD magnetic grains, which are relatively large. Large variations in magnetic parameters and geochemical composition during the Holocene suggest a complex and variable combination of sediment sources, including both aeolian dust and riverine inputs. Increasing riverine load carries coarser materials including MD grains from the catchment, perhaps through the longshore current system. MD particles acquire comparatively low ARM and IRM (Middleton, 2006). This is consistent with the observations of low ARM and SIRM during the Holocene. Most importantly, the low susceptibility, Fe content, Ti content and decreases in magnetic parameters are primarily ascribed to dilution by other components of the sediments, such as carbonates, organic matter and other diamagnetic minerals.

Iron oxides are chemically stable enough to survive physical transport, suggesting a terrigenous origin (Middleton, 2006). In contrast, iron sulfides are easily oxidized, so that they typically form diagenetically in the sediment column. For example, pyrite ($FeS_2$) is usually formed diagenetically in lake sediments. Its formation is largely determined by the availability of sulphate, reduced or reactive detrital iron, and reducing organic matter (Berner, 1984). Pyrrhotite ($Fe_7S_8$) and greigite ($Fe_3S_4$) are potential intermediate products during pyrite formation (Horng et al., 1998). Conditions with relatively low organic carbon, high ferric iron activity, and fine-grained sediments favor formation of these intermediate magnetic iron sulfides rather than pyrite (Kao et al., 2004). The availability of labile organic matter and reactive iron are the two most important factors controlling the preferential preservation of pyrrhotite or greigite. Moreover, greigite tends to be formed in favor of pyrrhotite in diagenetic environments with higher supplies of reactive iron, lower supplies of labile organic matter, and lower sulfide concentration (Kao et al., 2004).

The water column of Lake Qinghai presently is oxic, but within a few centimeters of the sediment surface, the sediments become anoxic (Ji et al., 2009). This reduced condition, together with biological process mediated by sulfate-reducing bacteria, allows sulfate

reduction and reaction with available iron to form iron sulfides. Sulfur and organic matter relationships in lake sediments have been used to characterize depositional environment, because the biogeochemical cycle of sulfur is closely tied to that of carbon (Sampei et al., 1997; Drevnick et al., 2010). Sulfur abundance correlates positively with total organic matter in Lake Qinghai sediments, showing higher concentrations and greater variability in the Holocene compared to low, relatively constant concentrations during the glacial period. Relatively warm and wet Holocene climate conditions due to strong Asian summer monsoon circulation would enhance the primary productivity of the lake. This would be enhanced by delivery of more terrestrial organic matter to the lake by the increased runoff (An et al., 2011). Remineralization of this increased organic matter would consume a significant amount of oxygen in the water column as well as in the uppermost sediments, resulting in conditions favorable for sulfate reduction, leading to the formation of monoclinic pyrrhotite as observed in the sediments.

Evidence suggests that greigite may be present in some intervals during glacial times. First, gyroremanent magnetization (GRM) is observed in certain sections of the u-channel samples of core LQDP05-1F. GRM is a laboratory remanence that is acquired by anisotropic magnetic samples in alternating fields. GRM acquisition is commonly associated with greigite (Roberts et al., 2011). Second, greigite thermally breaks down above ~280 °C (Roberts et al., 2011). Some Lake Qinghai samples show high-temperature susceptibility curves with an increase at ~250 °C (Fig. 9), but other minerals would also contribute to this increase. Third, greigite lacks a low-temperature magnetic transition (Roberts, 1995), which is consistent with results from the low temperature experiments.

Authigenic greigite occurrence has been considered as an indicator of drought, because evaporative conditions and relatively long water-residence times during drought periods favor increased levels of sulfate for bacterial sulfate reduction (Reynolds et al., 1999). For example, the presence of greigite in sediments from Lake Luanhaizi, on the northeast

side of Lake Qinghai and less than 100 km away, has been interpreted as indicating low lake levels (Mischke et al., 2005). During glacial times, strengthened cold and dry westerly winds brought a significant amount of detrital dust input to the Lake Qinghai area (An et al., 2011). Iron from aeolian materials was abundant, while low reactive organic matter contents and dissolved sulfate concentrations possibly limited iron sulfide formation. Consequently, the occurrence of greigite in the Lake Qinghai sediments during the glacial period is probably associated with relatively arid climate conditions. Relatively concentrated dissolved sulfate stimulates sulfate reduction and the formation of greigite rather than pyrrhotite or pyrite. However, the instability of greigite under laboratory conditions makes detailed interpretation difficult (Snowball, 1991).

The magnetic and geochemical characteristics of Lake Qinghai sediments are consistent with their lithological and sedimentological properties, providing information about magnetic concentration, mineralogy, and particle size, as well as sediment chemistry, sediment origin, and source provenance. This study complements our understanding of the climate history since Late Pleistocene in terms of variations in monsoonal precipitation and intensity of the Westerlies (An et al., 2011).

## 6 Conclusions

Magnetic properties and geochemistry of the sediments from Lake Qinghai were investigated using a 18.6-m-long u-channel sample and several selected discrete samples. We used a combination of geochemical analyses (Fe, Ti and S), together with a set of magnetic parameters, including concentration-dependent parameters ($\chi$, NRM, ARM and SIRM), and grain-size-dependent parameters (ARM/SIRM, ARM/ $\chi$ and hysteresis parameters). Magnetic mineralogy was characterized by a combination of hysteresis, low-temperature and high-temperature magnetic measurements, as well as S-ratios and smear slide analyses.

The results illustrate the changes in magnetic concentration, grain size trends, and mineralogy, as well as variations in geochemical composition of the sediments, reflecting distinctive Holocene and Late Pleistocene sediment depositional processes and correlative climate changes.

- The iron relative abundance (Fe) has a positive correlation with magnetic parameters including $\chi$, NRM, ARM and SIRM. Each of the proxies depends primarily on concentration of magnetic minerals, showing higher concentration during the glacial period compared to the Holocene, which is consistent with the hysteresis results.
- Late Pleistocene sediments contain mainly SD minerals, whereas Holocene sediments comprise a large proportion of MD particles. Magnetic parameters and elemental profiles exhibit greater variability during the Holocene relative to the glacial period. These lines of evidence support the idea that the glacial period is dominated by the deposition of aeolian materials and the Holocene is characterized by increasing riverine and shoreline load.
- Magnetite is the dominant ferrimagnetic mineral throughout the core, suggesting subtle mineralogical difference between the late Pleistocene and the Holocene. Relatively low magnetite concentration during the Holocene is mainly due to the dilution effect from increased authigenic carbonate that is strongly associated with riverine input.
- Monoclinic pyrrhotite was identified in all samples except the two samples from the high-susceptibility regions and greigite seems to be preserved in some intervals during the glacial period. The presence of monoclinic pyrrhotite indicates reducing depositional environment associated with organic matter respiration. The occurrence of greigite may indicate relatively dry climate during

glacial times. However, the unstable nature of greigite in atmosphere creates difficulty in interpretation.

In sum, the geochemical composition and magnetic properties of the Lake Qinghai sediments are consistent with the lithological and sedimentological records, suggesting a relatively unstable warm-humid Holocene condition versus a stable cold-dry Late Pleistocene climate.

**Acknowledgement:** This work was supported by National Science Foundation grant EAR-0602412 to Steve Colman. We thank Ms. Julie Bowles and Mr. Mike Jackson at the Institute for Rock Magnetism (IRM), University of Minnesota-Twin Cities, for laboratory assistance and discussion.

Fig. 1 Map of China showing the location of Lake Qinghai (blue square)

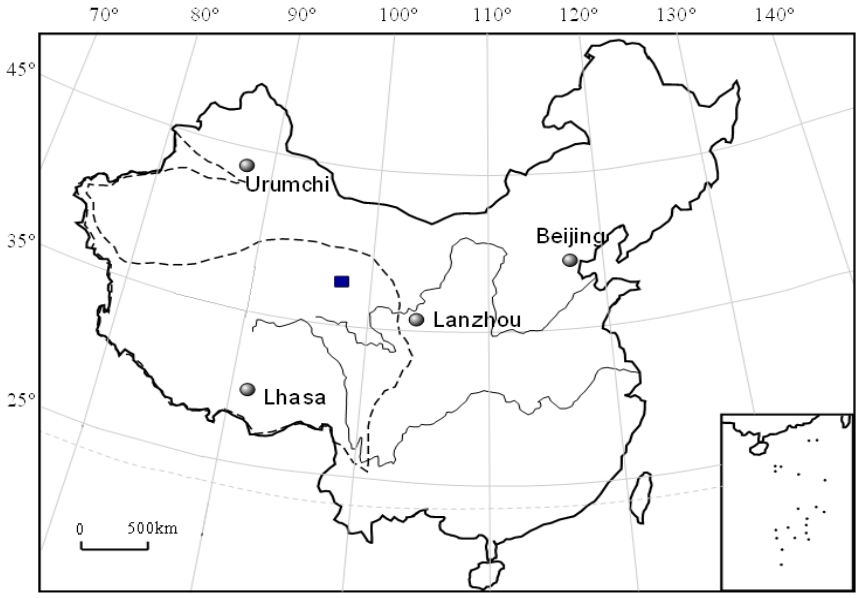

Fig. 2 Bathymetry of Lake Qinghai showing the locations of the sediment cores LQDP05-1F and QH07. The u-channel samples and two discrete samples were from core LQDP05-1F. Six discrete samples were from core QH07.

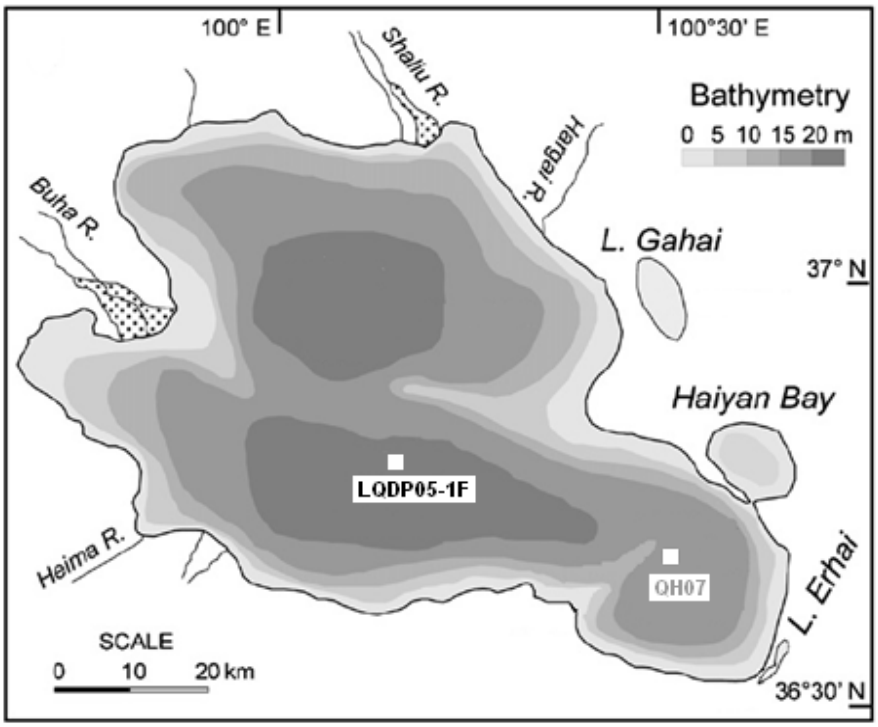

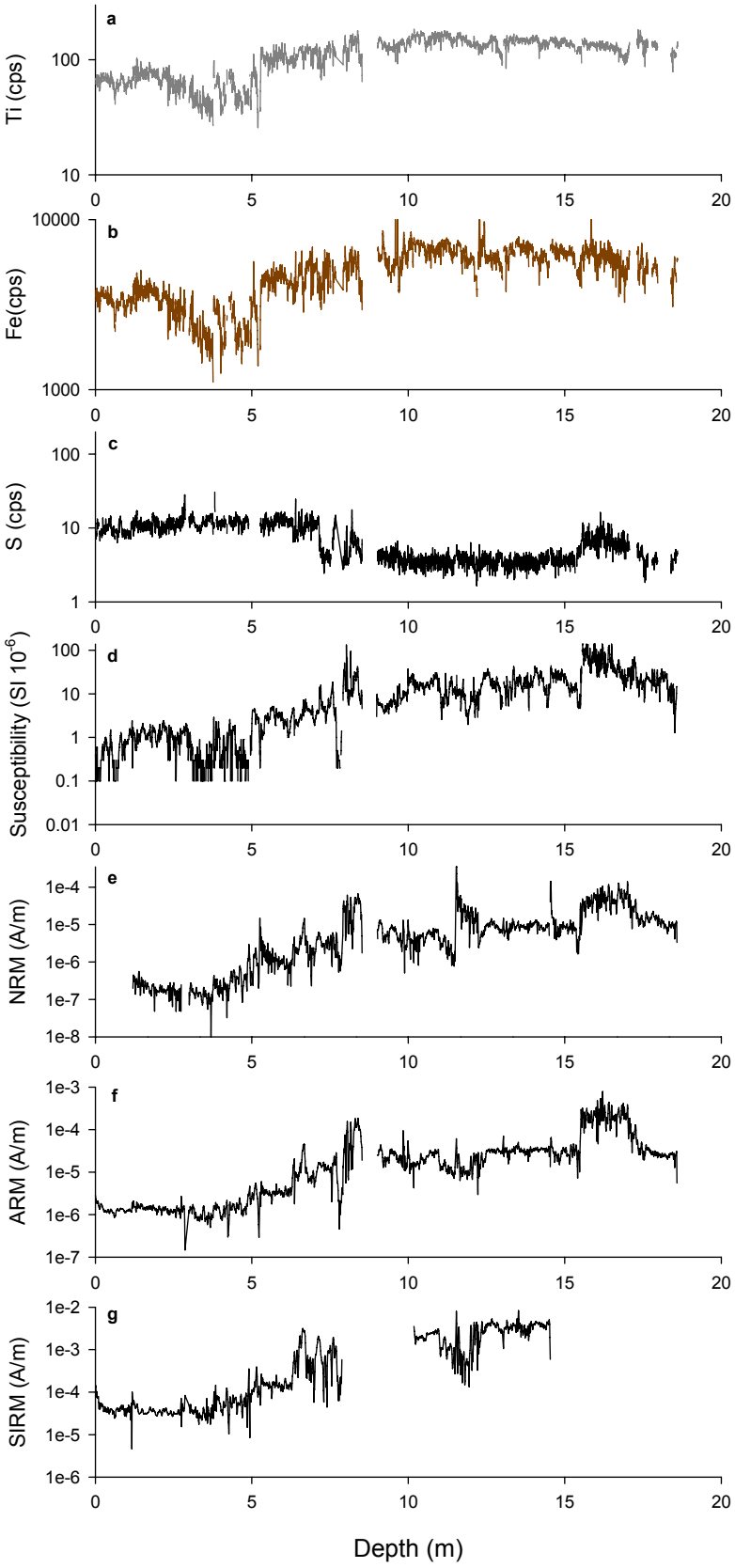


Fig. 3 Elemental profiles (Ti, Fe and S) and magnetic parameters changes with depth, including $\chi$, NRM, ARM and SIRM. All plots are semi-log.

Fig. 4 Correlations between Fe content and Ti content, χ, NRM, ARM and SIRM, respectively

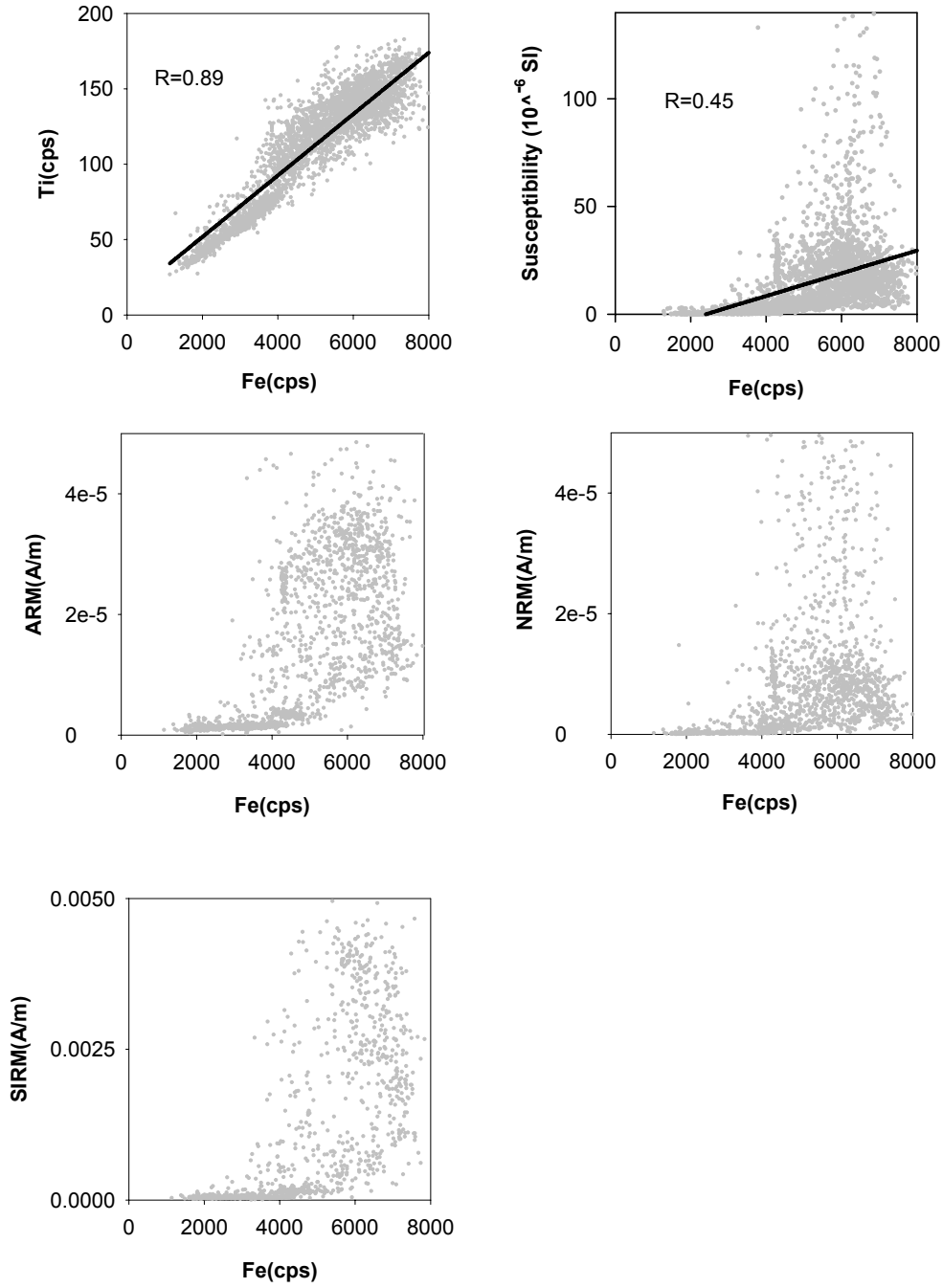

Fig. 5 Elements Fe, S profiles, and magnetic parameters, two discrete samples were taken from each of the gray areas that indicate intervals of high susceptibility.

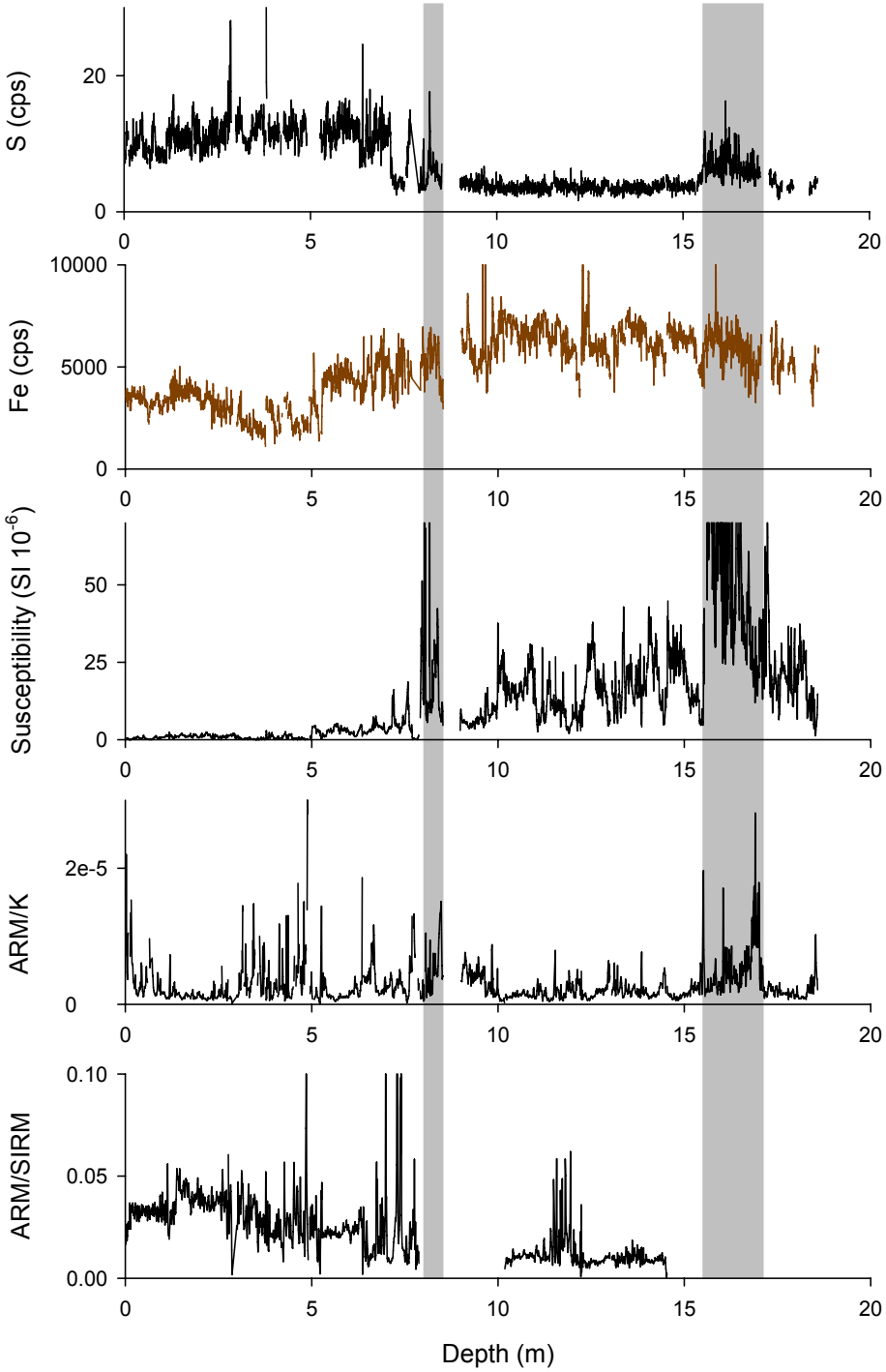

Fig. 6 Summary of the hysteresis loops showing the magnetic grain-size distribution. The upper four black data points are from the glacial deposits. The lower four red data points are from the Holocene-age sediments. The lines are mixing (linear and non-linear) curves of SD-MD and SD-SP (10 nm) for magnetite (Dunlop, 2002). SD: single domain; MD: multi-domain; SP: superparamagnetic; Mr: saturation remanent magnetization; Ms: saturation magnetization; Hcr: coercivity (measured in field); Hc: coercivity of remanence (measured in zero field).

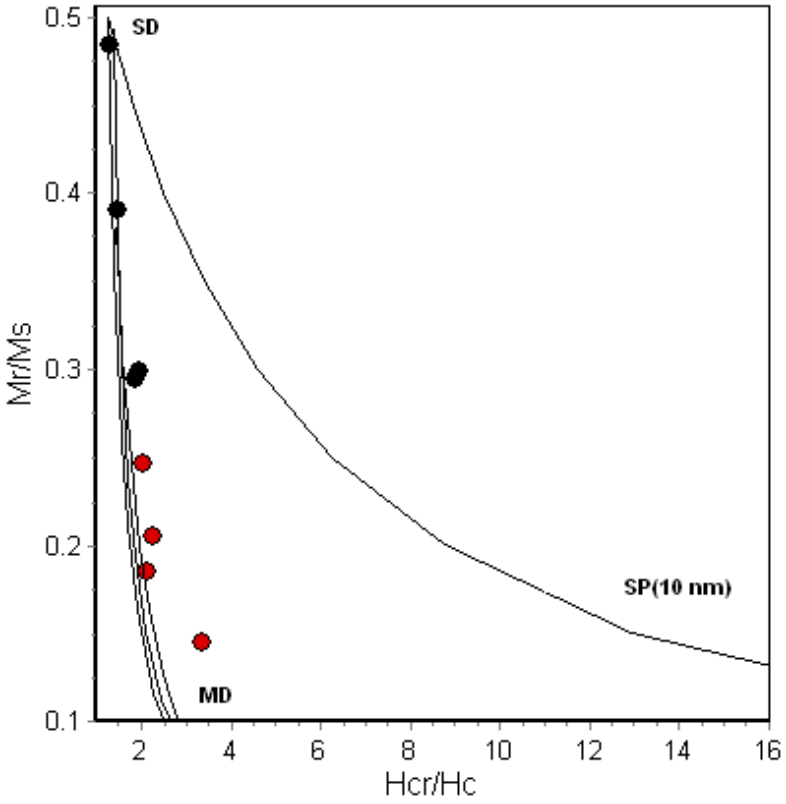

Fig. 7 An example of low-temperature magnetic measurements (cooling curve) suggests the presence of magnetite and pyrrhotite in the Lake Qinghai sediments.

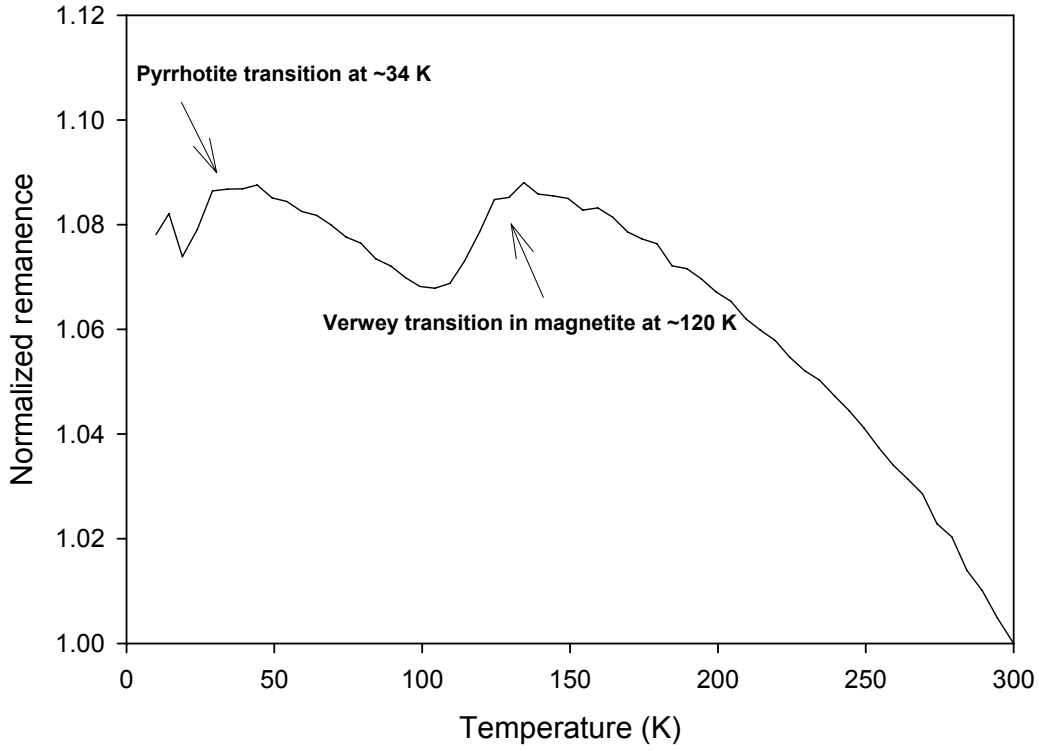

Fig. 8 An example of high-temperature magnetic measurements shows the presence of magnetite in the Lake Qinghai sediments.

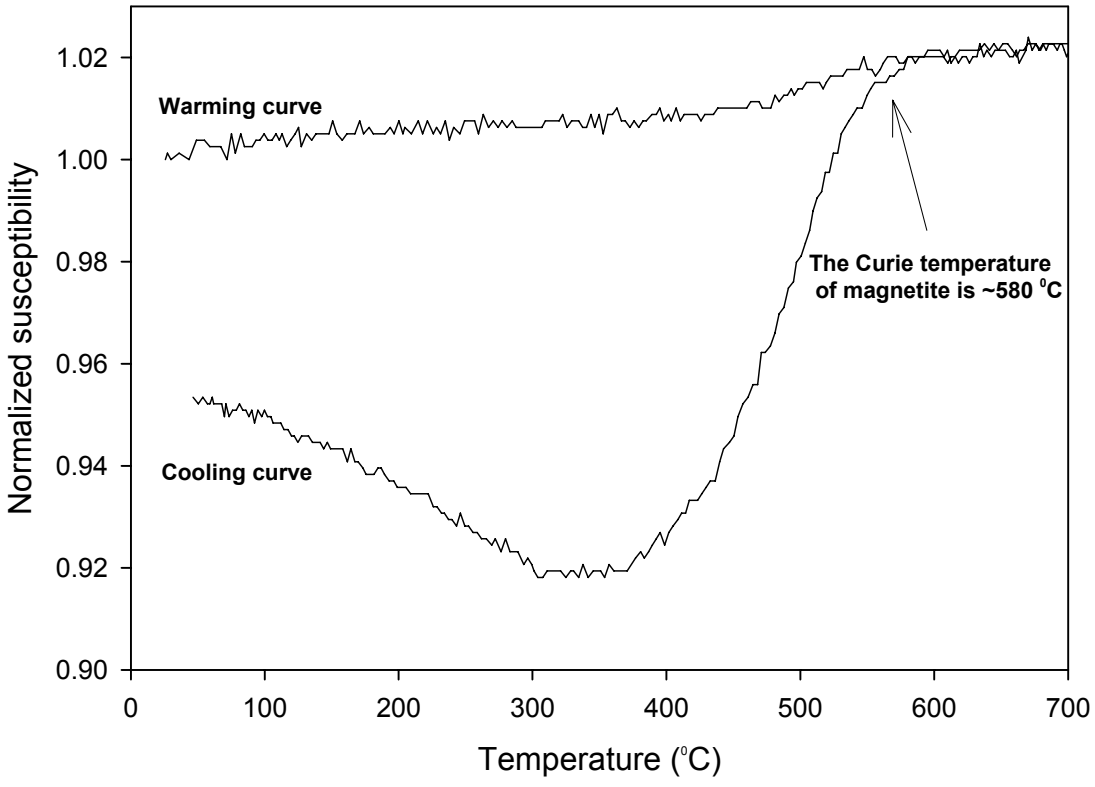

Fig.9 An example of high-temperature magnetic measurements suggests the presence of greigite in the glacial sediments.

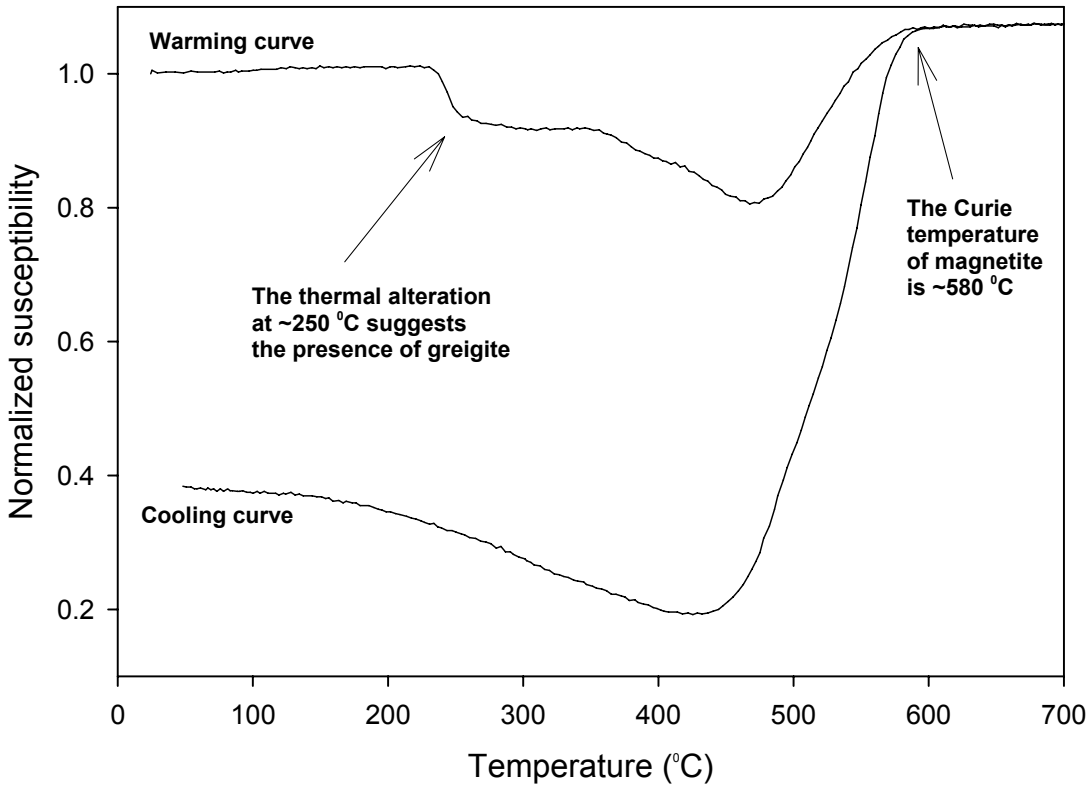

# Chapter 4: Determination of carbonate, total organic matter, and biogenic silica contents by FTIR and XRF techniques on lacustrine sediments

**Liu, Xiuju[1,2], Colman, Steve M.[1,3], Brown, Erik T.[1,3], Minor, Elizabeth C.[1,4]**

1 Large Lakes Observatory, University of Minnesota-Duluth, Duluth MN 55812, USA

2 Department of Earth Sciences, University of Minnesota Twin Cities, Minneapolis MN 55455, USA

3 Department of Geological Sciences, University of Minnesota-Duluth, Duluth MN 55812, USA

4 Department of Department of Chemistry and Biochemistry, University of Minnesota-Duluth, Duluth MN 55812, USA

Major components of lacustrine sediments, such as carbonates, organic matter, and biogenic silica, provide significant paleoenvironmental information about lake systems. Fourier Transform Infrared Spectroscopy (FTIR) and X-ray Fluorescence (XRF) scanning techniques are fast, cost effective, non-destructive, efficient methods to determine the relative abundances of these components. We investigate sediments from two large lakes, Lake Malawi (Africa) and Lake Qinghai (China).

Our results show statistically significant correlations between conventionally measured concentrations of carbonate (%$CaCO_3$), total organic carbon (%TOC), and biogenic silica (%BSi), and absorbance in the corresponding FTIR spectral regions, as well as between conventional measurements and XRF elemental ratios including calcium: titanium (Ca/Ti), incoherent: coherent X-ray scatter intensities (Inc/Coh), and silicon: titanium (Si/Ti). The correlation coefficients (R) range from 0.86 to 0.96 between FTIR results and conventional measurements, and from 0.75 to 0.91 between XRF results and conventional measurements. Both FTIR and XRF techniques exhibit great potential to quantitatively assess concentrations of inorganic and organic contents of lacustrine sediments. The results from statistical analysis of the data suggest that if carbonate or biogenic silica are the major components in sediments, absorbances in regions of 1300-1600 $cm^{-1}$ and 1050-1250 $cm^{-1}$, are good predictors of their respective concentrations in lakes with different sittings particularly with respect to biogeochemistries. A high positive correlation between TOC and absorbance in the 2800-3000 $cm^{-1}$ region is observed in Lake Malawi samples, which have relatively high TOC, whereas weak correlation is found in Lake Qinghai sediments, where TOC is low and carbonate is high. XRF ratios (Ca/Ti, Inc/Coh, Si/Ti) are quantitatively related to the contents of carbonates, total organic carbon, and biogenic silica. The regression results suggest internal calibrations of the relationship between XRF ratios and abundances of corresponding components in sediments are needed for individual lakes.

# 1 Introduction

Lakes, especially large lakes, often contain long-term sedimentary sequences that record evidence of past climatic and environmental changes on the continents. A number of large lake studies have used a variety of proxies in sediments to reconstruct climate history for understanding the mechanisms of climatic variations and their impact on humans. A few examples are Lake Baikal (Colman et al., 1995), Lake Malawi (Johnson et al., 2002), Lake Tanganyika (Stager et al., 1997), Lake Victoria (Johnson et al., 2000), Lake Biwa (Xiao et al., 1997), and Lake Qinghai (An et al., 2011). Major sedimentary components such as carbonate, organic carbon, and biogenic silica contain a wealth of information about the environment of deposition of lake sediments, and multi-proxy analysis on sediments from the same core has been commonly adopted (Allen et al., 1994; Curtis et al., 1998; Sayer et al., 1999; Reed et al., 2001; Korhola et al., 2002; Hodgson et al., 2005; Shen et al., 2005; An et al., 2011). One major benefit of a multi-proxy approach is in the correlations and relationships between different proxies and processes. Another major benefit is that inter-proxy comparisons are relatively less dependant on the chronology than inter-core comparisons, since the multiple proxy data are derived from the same core (Henderson and Holmes, 2009).

Common climatic proxies include total inorganic carbon, total organic matter, magnetic susceptibility, grain size, elemental compositions, stable isotope ratios, and organic biogeochemical properties. Among these various proxies, major sediment components such as carbonate content (%$CaCO_3$), total organic carbon content (%TOC) and biogenic silica concentration (%BSi) are essentials for understanding the history of geological, geochemical, biological, and hydrological processes in lake systems. Conventional methods to determine these properties are relatively time consuming and expensive. Moreover, these traditional analyses normally require relatively large amounts of sediment, which may not be available in high-resolution multi-proxy studies.

Fourier transform infrared spectroscopy (FTIR), a biophysical characterisation technique, has been widely used in material analysis (Allen et al., 1994; Alvarado et al., 1999; Griffiths and de Hasseth, 2007; Coury and Dillner, 2008). The physical principle of FTIR is that covalent chemical bonds absorb infrared energy by vibrations at specific frequencies (or wavelengths), so that the spectral locations of infrared absorption are indicative of specific chemical bonds or functional groups. Absorption intensity can be measured by either reflectance or transmittance over a wide range of wavelengths within only a few minutes. This capability allows a rapid and cost-effective analysis for extracting distributions of chemical moieties and their corresponding paleoclimatic information from sediments.

FTIR has been applied in both marine and lacustrine studies for analysis of inorganic and organic components of sediments, as well as particulate matter and dissolved organic matter from the water column (Bertaux et al., 1998; Maria et al., 2002; Rosen and Persson, 2006; Rosen and Hammarlund, 2007; Mecozzi et al., 2009; Abdulla et al., 2010; Palmucci et al., 2011; Swann and Patwardhan, 2011). While many of these studies involve qualitative characterization of sample composition, some have used Lambert-Beer's law (Harris, 2005), a linear relationship between the strength of absorption of infrared radiation and the concentration of the absorbing compounds (Harris, 2005; Hornback, 2005) along with appropriate calibrations for differences in band strength (response factor) as a function of functional group. For example, FTIR has been used to quantify the relative abundance of quartz, clay, and calcite in marine sediments (Herbert et al., 1992), and to estimate total inorganic and total organic carbon, total organic nitrogen, and biogenic silica in lacustrine sediments (Vogel et al., 2008; Rosen et al., 2010).

X-ray Fluorescence (XRF) core scanning provides bulk elemental composition of sediment (Andrews and Haroardottir, 2009; Brown et al., 2010; Liu et al., 2011a). It is high-resolution, non-destructive, automatic, fast and needs nearly no sample preparation.

When an external X-ray from an X-ray source strikes sediment, the X-ray can be absorbed by the atom in the sediment. Due to the absorption, the atom transfers all of its energy to innermost electrons, which are accordingly ejected from the inner shells, creating vacancies. The atom subsequently becomes unstable. As the atom tends to return to its stable condition, these vacancies are soon filled by electrons from the outer shells. These electrons release a pulse of X-radiation, which is the energy difference between the two binding energies of the corresponding shells. This process of emissions of secondary X-radiation is called "X-ray Fluorescence" (XRF) (Rothwell, 2006). Because each element has a unique set of energy levels, each element produces characteristic X-ray spectrum. This makes measurement of elemental composition of sediments possible. Moreover, the intensity of the energy at different wavelengths allows determination of relative abundance for a wide range of elements down to limits of a few ppm (Rothwell, 2006).

The XRF technique has been so far extensively used in paleolimnological studies, including metal pollution/tephra layer detection, varve counting, and provenance studies, such as for estimation of past lake primary productivity and past weathering/erosion/redox conditions (Holmes et al., 2004; Shanahan et al., 2008; Ziegler et al., 2008; Jaccard et al., 2011).

In our study, we use FTIR and XRF data to estimate carbonate, total organic carbon and biogenic silica contents. Calibrations are established using orthogonal (Type Ⅱ) linear least-square regression of conventional measurements against FTIR spectral variations, and against XRF ratios. We examined sediments from two lakes, Lake Malawi and Lake Qinghai. The results contribute to an understanding of the feasibility of utilizing FTIR and XRF analyses to quantitatively determine biogeochemical properties of lake sediments and the advantages and limitations of each analytical technique.

## 2 Sediment and methods

## 2.1 Samples

Lake Malawi is the third largest lake in Africa and southernmost of the Great Rift Valley system of East Africa (9˚–14˚S, 35˚E). Climatically, it is located near the present southernmost extent of the Intertropical Convergence Zone (ITCZ). Core M98-1P was taken at 10˚15.9' S, 34˚19.1' E, and a 403-m depth. Core MAL05-2A (at 10˚01.1' S, 34˚11.2' E and a 345-m depth) was recovered by the Lake Malawi Drilling Project (Johnson et al., 2002; Brown et al., 2007; Castaneda et al., 2007). Sediment samples from M98-1P and MAL05-2A were used to assess the correlations between FTIR data or XRF data, and conventional measurements of carbonate, total organic carbon and biogenic silica concentrations. The sediment from the calibration set (MAL05-2A) has carbonate contents varying between 0% to 30%, and TOC values ranging from 1% to 10%. The calibration set from M98-1P has biogenic silica concentrations from 5% to 40%.

Lake Qinghai, the largest inland water body in China, at an elevation of 3194 m, is situated on the northeastern margin of the Tibetan Plateau, where the climate conditions are mainly controlled by the interplay of the East Asian monsoon and the Westerlies. It lies near by the limit of penetration of the Asian Summer monsoon, i.e., the transition from the arid to the semi-arid zone (An et al., 2006; Liu et al., 2011b). A Uwitec sediment core (QH07) was collected from the southeastern basin of Lake Qinghai (36° 43′ 36.7" N, 100° 29′ 28.1" E). The calibration sample set from QH07 was used to focus on assessing the correlations between FTIR data or XRF ratios, and conventional measurements of carbonate, and total organic carbon, but not biogenic silica because of its scarcity in the sediment. TOC in Qinghai sediments is generally low, less than 3.5%, while carbonate content is relatively high, varying from 20% to 60%.

## 2.2 Laboratory methods

2.2.1 Traditional analyses for carbonate, total organic carbon and biogenic silica contents

Carbonate content in the study sediments was measured by coulometry. Samples were freeze-dried and ground into fine, homogeneous powder and desiccated overnight. Carbon dioxide gas evolved by reaction of carbonates in the powdered sample with acid (30 mg sediment and 5 ml 2N HCl) was carried by a $CO_2$-free gas stream into a coulometer cell, and was detected and recorded as micrograms of carbon. Blanks and standards were run after every 10 samples. The amount of carbonate (%$CaCO_3$) was calculated using the conversion: Carbonate content = (μg carbon in sample − μg carbon in blank) / (μg sample weight) × 100/12 by assuming all inorganic carbon is present as calcium carbonate.

For Lake Malawi, TOC was determined by the difference between total inorganic carbon and total carbon. The analysis procedure for determining total inorganic carbon (TIC) using coulometry was the same as the description in the paragraph above. As for total carbon (TC) analysis, samples were freeze-dried and ground into fine, homogeneous powder and desiccated overnight. About 30 mg sediment was loaded into an empty platinum container, which was then placed into a ladle. The ladle was inserted into the furnace for combustion at 950 ℃. The amount of carbon dioxide released from the combustion of sediment was detected by titration and recorded. Blanks and standards were run after every 10 samples. TOC was calculated by subtracting TIC from TC, reported as weight percentages.

TOC in Lake Qinghai samples was measured by elemental analysis (EA). Samples were freeze-dried, ground into fine powder, oven-dried at 60˚C overnight. About 20 mg sediment was treated by acid fumigation for 9 hrs to remove inorganic carbon and leave behind organic matter. The fumigated samples were then oven dried at 60˚C for 6 hours and enclosed in tin capsules, and placed in a desiccator prior to EA. To confirm the accuracy of TOC measurements from EA, we measured TOC and TC using elemental analysis, TIC and TC using coulometry, on the same set of samples. The lab procedure of measuring TC using EA was similar to that of measuring TOC using EA except without

the fumigation process. We compared the TOC contents, which were determined in three different ways: 1) direct from EA; 2) subtraction from $TC_{coulometry}$ -$TIC_{coulometry}$; 3) subtraction from $TC_{EA}$ -$TIC_{coulometry}$. The comparisons showed that TOC contents direct from EA were very close to the ones from the other two calculating methods. Therefore, we concluded that the TOC measurements direct from EA were relatively accurate.

For biogenic silica determination, the analytical procedure described in (DeMaster, 1979) was applied with minor modification for Lake Malawi sediment samples. Samples were digested in 0.5 M NaOH at 85˚C for 42.5 minutes. This timing of the extraction was determined after examining the results of 168 analyses of samples.

2.2.2 XRF analysis

Bulk elemental composition of the sediments was analyzed using an ITRAX X-ray Fluorescence (XRF) Core Scanner (Cox Analytical Instruments). The surface of the sediment in split core was carefully smoothed and flattened. A molybdenum X-ray source set to 30 kV and 30 mA was used to generate a rectangular X-ray beam that covered an area of 200 μm × 2 cm on the surface of sediments (Croudace et al., 2006). Optimized peak-fitting functions were chosen by defining the likely elements in the sediment as well as adjusting and refining the peak-fitting parameters based on a representative part of the core section. Measurements were taken at 2-mm interval for a counting time of 90 seconds as the core moved by an incremental motion whose direction was perpendicular to the X-ray beam. After core scanning on the instrument was complete, initial XRF spectral data were reprocessed in a standard fitting procedure using the Q-Spec spectral analysis software to refine the fitting of individual elemental peak areas (Croudace et al., 2006). Final XRF data were output as counts per second (cps).

2.2.3 FTIR analysis

Samples were freeze-dried, ground and mixed with potassium bromide (KBr), which is transparent in the infrared region, to form a very fine powder. The weight ratio between sediment and KBr (in 1:100-1:200 dilution) was to keep absorbance within the sensitivity range of the detector. The powder was compressed into a thin pellet, which was stored in a dessicator for a few hours before being analyzed. Transmittance of samples was measured using a Nicolet Magna IR 560 FTIR ESP. To avoid interferences from atmospheric moisture and $CO_2$, sample pellets were placed in the instrument chamber, which was swept with $CO_2$-$H_2O$-free gas, at least 4 minutes before scanning. During each sample run, a pure KBr pellet was measured as background and subtracted from the sample measurement. Each sample spectrum was comprised of 936 increments for wavelengths between 400 and 4000 $cm^{-1}$. Omnic software (V. 3.1a) was used on the spectral data to convert transmittance (T) to absorption (A), according to the equation: A=log (1/T). For comparison among samples, initial FTIR spectra data were normalized to percentages.

## 3 Results and discussion

### 3.1 Carbonate

Carbonate ion consists of one carbon atom surrounded by three oxygen atoms (one double bond to a neutral oxygen and two single bonds to negative oxygen atoms, although electron resonance can distribute the negative charges throughout the entire molecule), in a trigonal planar arrangement. FTIR spectra of pure calcite show a maximal absorption band centered at 1435 $cm^{-1}$, ranging from approximately 1300 to 1600 $cm^{-1}$, along with a narrow peak at 900 $cm^{-1}$ (Herbert et al., 1992). Other previous studies on carbonate minerals also show absorption due to carbon-oxygen double bond (C=O) at about 713, 877, 1425, 1460, 1800 and 2500 $cm^{-1}$ (Gaffey, 1986; Mecozzi et al., 2001; Kovac et al., 2005). Absorption bands (m−moderate; s−strong; vs−very strong) include 700-725 (m), 860-890 (s), 1300-1560 (vs), 1780-1810 (m), and 2460-2640 (m) were reported as the most important carbonate-related wave numbers in carbonate-rich

sediment (Rosen et al., 2010). Based on these previous results and preliminary inspection of our data, we propose using the infrared absorption band of 1300-1600 $cm^{-1}$ to assess the C=O molecular vibrations in carbonates.

FTIR results from Lake Malawi and Lake Qinghai sediment containing carbonates show a remarkable absorption band centered at 1432 $cm^{-1}$ (Fig. 1). Carbonate free sediments, however, show no obvious peaks in this spectral region. Correlations between individual bands (936 total) in the FTIR spectra of the sediment and conventionally-measured concentrations of carbonate show that the absorption band of 1300-1600 $cm^{-1}$ has significantly high correlation coefficients (R) for both Lake Malawi (R= ~0.98, shaded area, Fig. 2a) and Lake Qinghai (R= ~0.9, shaded area, Fig. 2b). Another high correlation area is around 873 $cm^{-1}$, suggesting high absorbance linked to carbonates, but this area is very narrow.

Ca/Ti derived from XRF measurements is related to the relative abundance of carbonates, if carbonates present in the sediment are mainly calcium carbonate, which applies to many lacustrine sediments, and if the Ca/Ti ratio of the other sediment components is relatively constant. Carbonates in Lake Malawi sediments are mainly calcite (Brown et al., 2007) and Lake Qinghai sediments are mainly aragonite (Shen et al., 2005). Because carbonates contain abundant Ca and little Ti, Ca/Ti can reflect the relative abundance of carbonates.

FTIR spectral variations at 1300-1600 $cm^{-1}$ related to C=O bond and XRF Ca/Ti ratios compare favorably with conventional measurements of carbonates (Fig. 3). Regression between FTIR C=O absorbance in the 1300-1600 $cm^{-1}$ region and conventionally measured carbonate contents yields R= 0.94 for Lake Malawi and R= 0.86 for Lake Qinghai. All correlation coefficients are statistically significant with p-values smaller than 0.001. The non-zero intercepts suggest that, in addition to carbonates, other components of the sediment also contribute some absorption at the region of 1300-1600

$cm^{-1}$. Regardless of the fact that Lake Malawi and Lake Qinghai sediments contain different amounts and types of carbonate minerals, the two regression lines for Lake Malawi and Lake Qinghai have similar slopes, i.e., 2.03 vs. 2.29, indicating that absorbance in the infrared spectral region of 1300-1600 $cm^{-1}$ works well on estimating changes in relative carbonate content in different lakes. The different intercepts suggest that a calibration will need to be performed on individual lake for quantitative estimation of carbonate content.

The correlations between XRF Ca/Ti and conventionally measured carbonate contents are R= 0.91 for Lake Malawi and R= 0.85 for Lake Qinghai, indicating that Ca/Ti predicts relative carbonate concentration quite well. The slopes of the regression lines for the two lakes are quite different, namely that, 2.05 (Lake Malawi) versus 0.49 (Lake Qinghai), suggesting that internal calibrations are needed when applying Ca/Ti to estimate carbonate contents in different lakes. The different slopes suggest that either Ca is associated with other substances such as clay minerals, or other carbonates, such as siderite, magnesite, may be present in the sediment.

### 3.2 Total organic carbon

The organic fraction of lake sediments is a mixture of organic compounds, including carbohydrates, lipids, proteins and other humic substances. These components in turn contain a range of organic functional groups in differing within molecule "environments" (Hedges and Oades, 1997). Therefore, for lake organic matter, infrared absorption bands are relatively wide due to overlap of bands from this plethora of functional groups. For instance, O-H vibrations of carbohydrates, proteins, and fatty acids are attributed to the spectral absorption band between 3400-3460 $cm^{-1}$ (Kovac et al., 2005). However, the band at ~3430 $cm^{-1}$ is also associated with the O-H vibration of water. C-H stretching in –CH from unsaturated hydrocarbon chains are related to the band at 3010-3030 $cm^{-1}$; C-H stretching modes at 2850-2950 $cm^{-1}$ are due to –CH, $–CH_2$, $–CH_3$ groups of aliphatic

chains of carbohydrates, proteins, and lipids (Mecozzi et al., 2009; Rosen et al., 2010). Due to the presence of C=O bond in proteins (Amide I and Amide II) and fatty acids, absorption in the region of 1500-1700 $cm^{-1}$ overlaps with that of the C=O bond in carbonates; C-O-C of carbohydrate vibrations may cause a peak in the spectral band centered around 1250 and 1100 $cm^{-1}$ where absorption from the Si-O bond may also occur (Mecozzi et al., 2009).

Based on these considerations of organic compounds, we used spectral variations at 2800-3000 $cm^{-1}$, which, while lower in intensity can be more clearly ascribed to organic matter precursors, an index to organic carbon contents. The FTIR spectra from Lake Malawi and Lake Qinghai show distinctive double peaks in the region of 2800-3000 $cm^{-1}$ when TOC in sediments is relatively high (Fig.1). Conventionally-measured TOC is positively correlated with absorbance of C-H bond at 2800-3000 $cm^{-1}$ (R= ~0.91) for Lake Malawi (shaded area, Fig. 2d). The equivalent correlation for Lake Qinghai, however, is different than that for Lake Malawi. The wave number correlation pattern for TOC (Fig. 2c) at Lake Qinghai actually resembles that for $\%CaCO_3$ in Lake Qinghai (Fig. 2b). This may be related to the fact that Lake Qinghai sediments are carbonate-rich (about 50% on average) and organic-matter-poor (less than 4%). Because the FTIR analysis was done on bulk sediments, the organic matter absorption signal in the 2800-3000 $cm^{-1}$ region may be overwhelmed by the carbonate absorption in this region, because the absorption for the two materials overlaps in this particular spectral region (the IR spectra of pure calcite show an absorption peak at 2875 $cm^{-1}$).

Incoherent and coherent X-ray scatter data were obtained during XRF scanning. Coherent (Rayleigh) scattering happens when primary X-ray collides with an atom and deviates without a loss in energy. Incoherent (Compton) scattering is a process during which the incident X-ray loses some of its energy to the scattering electron (Jenkins, 1999). XRF scattering relates to the average atomic number of a material, where coherent scattering occurs more often in high atomic number material and incoherent scattering occurs more

often in low atomic number material. Because organic matter generally has a lower average atomic mass than other constituents such as carbonates, aluminosilicates, and quartz, the ratio of incoherence to coherence scattering (Inc/Coh) would increase with greater organic matter content, and vice versa. Therefore, if inorganic sediment composition is relatively invariant, Inc/Coh can be used as an indicator of total organic matter content (Allen et al., 1994; Saez et al., 2009; Burnett, 2010; Giralt et al., 2011)

In our samples, conventionally-measured TOC compares well with XRF Inc/Coh ratios (Fig. 4). Lake Malawi sediments exhibit good correlation (R= 0.94) between %TOC and FTIR absorbance (2800-3000 $cm^{-1}$, C-H bond), whereas Lake Qinghai sediments show almost no correlation (R= 0.086). This striking difference in R values between Lake Malawi and Lake Qinghai may imply that organic matter in these two lakes is complex and very different, such that they have distinctive characteristics in their infrared spectra. It may also be that different proportion of other components in the sediments, such as carbonates, aluminosilicates, and biogenic silica, also affect the absorption signal. Note that the patterns of TOC and carbonate correlation bands (Fig. 2b and 2c) are similar. If the Lake Qinghai sediment samples were decalcified prior to the FTIR analysis, a better correlation between absorbance at 2800-3000 $cm^{-1}$ and TOC might be expected. The Lake Qinghai results suggest that further research on the FTIR signals of organic-rich sediments from different lakes, especially those with significant carbonates is needed.

The correlation between conventionally measured TOC and Inc/Coh is relatively high (R= 0.75, Lake Malawi; R= 0.89, Lake Qinghai). This result supports the feasibility of using Inc/Coh in statistical models as an indicator of organic matter content. However, the slopes of the regression lines are quite different, 8.41 (Lake Malawi) versus 2.36 (Lake Qinghai), suggesting that when the XRF Inc/Coh is used to infer organic matter content, internal calibrations for individual lakes are necessary.

**3.3 Biogenic silica**

Generally $SiO_2$ minerals have absorbance peaks at 471, 520, 1030, 1083, and 1165 $cm^{-1}$. For example, quartz absorption bands appear at 1083, 695, and 469 $cm^{-1}$ with a unique doublet at 800 and 780 $cm^{-1}$ (Kovac et al., 2005). Biogenic silica, a hydrated form of $SiO_2$ is contributed to lake sediments by diatoms, plant phytoliths, radiolaria, and siliceous sponges. In Lake Malawi sediments, diatoms form the major part of biogenic silica (Johnson et al., 2011). In Lake Qinghai, due to the high pH of the lake water, biogenic silica concentration in sediments is very low (Liu et al., 2010). FTIR measurements on individual diatom shells show that diatoms absorb mainly in the region 1050-1250 $cm^{-1}$ (Rosen et al., 2010). Si-O-Si vibrations in biogenic silica are responsible for an absorbance maximum centered at 1100 $cm^{-1}$ (Stehfest et al., 2005). Sediments with high diatom concentration show strong absorbance between 1050 and 1250 $cm^{-1}$, while sediments with low diatom concentration show weak absorption in this region (Rosen et al., 2010). Thus we used FTIR spectral variations between 1050 and 1250 $cm^{-1}$ related to Si-O bond to represent variability in biogenic silica.

Our findings in Lake Malawi (relatively high biogenic silica) and Lake Qinghai (low biogenic silica) sediments are consistent with the spectral features described in previous studies (Fig.1). The correlation of conventionally-measured biogenic silica (%BSi) to FTIR spectral data for Lake Malawi is high (R= ~0.9) at the selected absorption band, 1050-1250 $cm^{-1}$, for biogenic silica (shaded area, Fig. 2e). A set of fifteen samples were initially diluted with KBr with a ratio of 1:100 (sediment: KBr). Measurements of six samples that have biogenic silica concentration greater than 25% were unexpectedly low compared with the other nine measurements. These six samples were then resampled and treated with a new dilution ratio of 1:200 (sediment: KBr) (Fig. 5). These results suggest that samples with high %BSi need to be diluted appropriately to obtain reliable FTIR measurements.

The Si/Ti in Lake Malawi sediments as determined by XRF has been used as an index of changes in biogenic silica concentration. It was suggested that appropriate internal calibration is needed when calculating BSi% from Si/Ti (Brown et al., 2007). Unfortunately, core M98-1P was subsampled previously and no sediments were left for scanning XRF analysis. Consequently, no comparison of conventional %BSi could be made with Si/Ti for core M98-1P. For core MAL05-2A, no conventional %BSi measurements were available. Consequently, we compared Si-O absorbance (FTIR) with Si/Ti (Fig. 5).

The correlation of the Si-O FTIR absorbance with conventional measurements in core M98-1P is excellent (R=0.96, Fig. 5). The relationship between Si-O absorbance and Si/Ti in MAL05-2A also shows high correlation (R=0.86, Fig. 5). These results demonstrate the potential of both FTIR and XRF methods for providing quantitative estimates of biogenic silica concentrations in sediments.

## 4 Advantages and limitations of FTIR and XRF techniques

FTIR technique is fast, cost effective, and requires a small amount of sediments. The FTIR spectra are informative, providing quantitative information on the biogeochemical properties of sediments. Different compounds have different individual spectra, but overlapping peaks and bands from different components in the sediment can complicate the interpretation of FTIR spectra. Thus, quantitative analyses using FTIR technique are restricted to the dominant components or those with unique absorption bands.

Compared with conventional XRF analysis, the XRF core scanner allows high-resolution, continuous, non-destructive, automated, fast and cost effective analysis without significant sample pretreatment. The scanning technique performs very well for profiling elemental composition with depth. The main disadvantages are that analyses are generally restricted to elements heavier than aluminum and difficulty in vigorous

calibration. The XRF data can normally be considered semi-quantitative and as such need to be interpreted with caution (Croudace et al., 2006). The data quality, however, strongly depends on sample conditions, i.e., it requires smooth and flat surface, as well as homogeneous samples. In reality, for split cores, variations in lithostratigraphic phases and changes in water content, sediment texture, and porosity all modify the effectiveness of XRF scanning.

Among the elemental ratios available in XRF data, Ca/Ti is suitable for estimating carbonate content if all calcium is associated with carbonate, but if significant amounts of other carbonate minerals (for example, siderite, magnesite, high/low-Mg calcite) are involved, the relationship between Ca/Ti and carbonate content does not apply. Similarly, Si/Ti reflects total silica concentration, but it can not distinguish among the sources of silica, including siliceous microfossils or silicate minerals, such as quartz. Although Inc/Coh ratio is strongly correlated with total organic carbon, one should note that each component of a given sediment sample, such as carbonates, clay minerals, water, and organic matter, has its own Inc/Coh value. The detected Inc/Coh by XRF, however, is a bulk ratio, which means the Inc/Coh ratio is affected by all the components of the sediment according to their respective abundances.

## 5 Conclusions

In our case study, the high correlation between infrared absorption in the wave number band related to the C=O bond and conventionally measured carbonate contents (R= 0.94, Lake Malawi; R= 0.91, Lake Qinghai), indicates that 1300-1600 $cm^{-1}$ spectral band represents carbonate content well in both Lake Malawi and Lake Qinghai sediments. Spectral variations at 1050-1250 $cm^{-1}$, are similarly well correlated with biogenic silica concentration (R= 0.96, Lake Malawi). C-H bond absorption at 2800-3000 $cm^{-1}$, correlates well with TOC in Lake Malawi (R= 0.94) but not in Lake Qinghai (R= 0.086). The contrast in results for correlation to TOC contents may be related to two possible

reasons. First, compared to carbonates and biogenic silica, the composition of organic matter is more complicated and can vary from lake to lake. Second, due to low TOC and high carbonate in Lake Qinghai, the C-H absorption signal in 2800-3000 $cm^{-1}$ region might be overwhelmed by the carbonates.

In short, our results suggest that if carbonate or biogenic silica is the major component in sediments, absorbance in regions of 1300-1600 $cm^{-1}$, and 1050-1250 $cm^{-1}$, can well predict concentrations of carbonate and biogenic silica, respectively. With respect to the relationship between TOC and absorbance in 2800-3000 $cm^{-1}$ region, further research is needed to confirm their correlations in different lakes where organic rich sediment materials are available.

The correlation between Ca/Ti and carbonate content is high (R= 0.91, Lake Malawi; R= 0.85, Lake Qinghai). Inc/Coh and total organic carbon show high correlation as well (R= 0.75, Lake Malawi; R= 0.89, Lake Qinghai). Si/Ti and Si-O absorption are strongly correlated (R=0.86, Lake Malawi). All these results show the potential of XRF ratios in estimating the concentrations of major components in sediments. The comparisons of the regression results between Lake Malawi and Lake Qinghai suggest that appropriate calibrations of the relationship between XRF ratios and abundances of corresponding components in sediments are needed for individual lakes.

**Acknowledgement:** This work was supported by National Science Foundation grant EAR-0602412 to Colman. We thank Dr. Tomas C. Johnson for providing Malawi sediment samples. We also thank Hongyu Li for laboratory assistance.

Fig. 1 Typical FTIR spectra from sediment samples with different relative concentrations of carbonate ($CaCO_3$), total organic carbon (TOC), and biogenic silica (BSi), from one core in Lake Qinghai (QH07: sediments that contain high $CaCO_3$, 28~60%, and low TOC content, 2~4%) and two cores in Lake Malawi (M98-1P: sediments that have BSi; MAL05-2A-a: sediments that contain relatively high $CaCO_3$ and no TOC; MAL05-2A-a: sediments that contain relatively high TOC and no $CaCO_3$). Three grey bars indicate the selected absorption bands related to organic carbon, carbonate, and biogenic silica, respectively. C-H: carbon-hydrogen bond; C=O: carbon-oxygen double bond; Si-O: silica-oxygen bond.

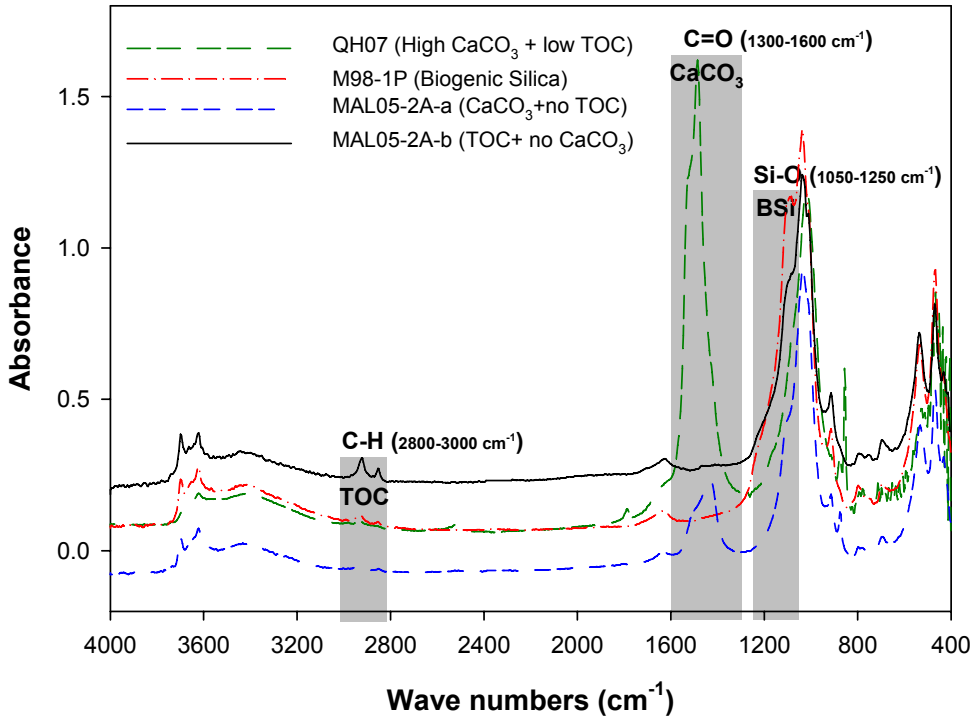

Fig. 2 Correlation between individual bands (936 total) in the FTIR spectra of the sediment and conventionally-measured concentrations of carbonate, total organic carbon, and biogenic silica from different cores (Lake Qinghai: QH07; Lake Malawi: M98-1P and MAL05-2A). Y axis shows values of the correlation coefficients R. Grey/black bars indicate the selected absorption bands related to carbonate, organic carbon, and biogenic silica.

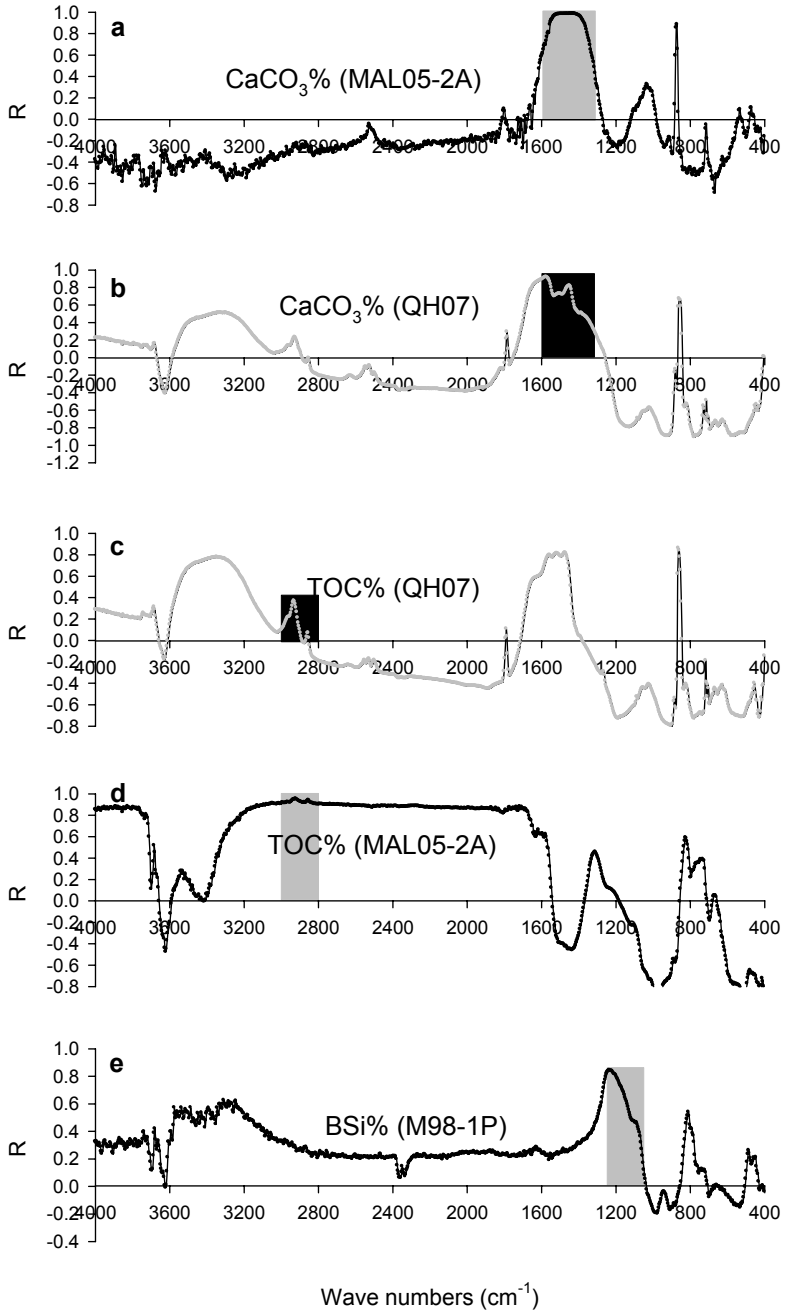

Fig. 3 Cross plots and orthogonal (type **II**) linear least-square regression of conventionally-measured carbonate contents versus FTIR absorbance in the 1300-1600 $cm^{-1}$ region (C=O bond), and conventionally-measured carbonate contents versus Ca/Ti, for Lake Malawi and Lake Qinghai, respectively.

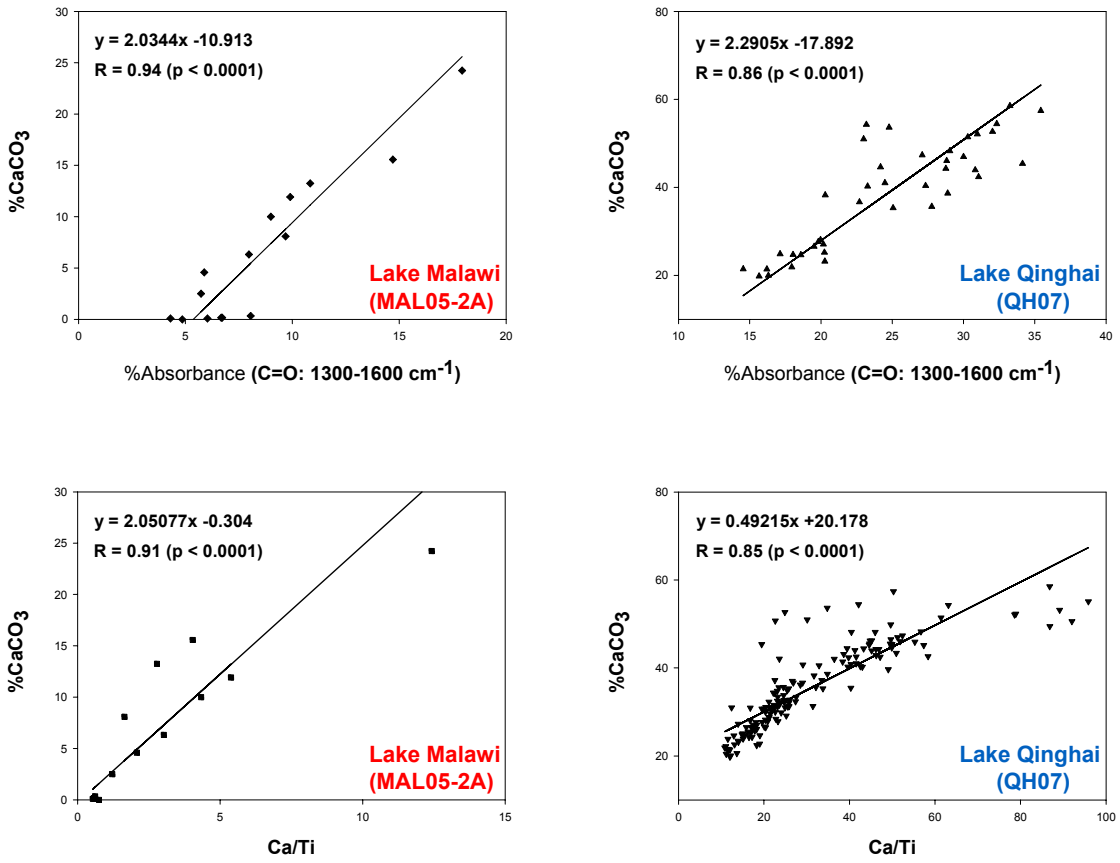

Fig. 4 Cross plots and least-square regression of conventionally-measured TOC versus FTIR absorbance in the 2800-3000 $cm^{-1}$ region (C-H bond), and conventionally-measured TOC versus Inc/Coh, for Lake Malawi and Lake Qinghai, respectively.

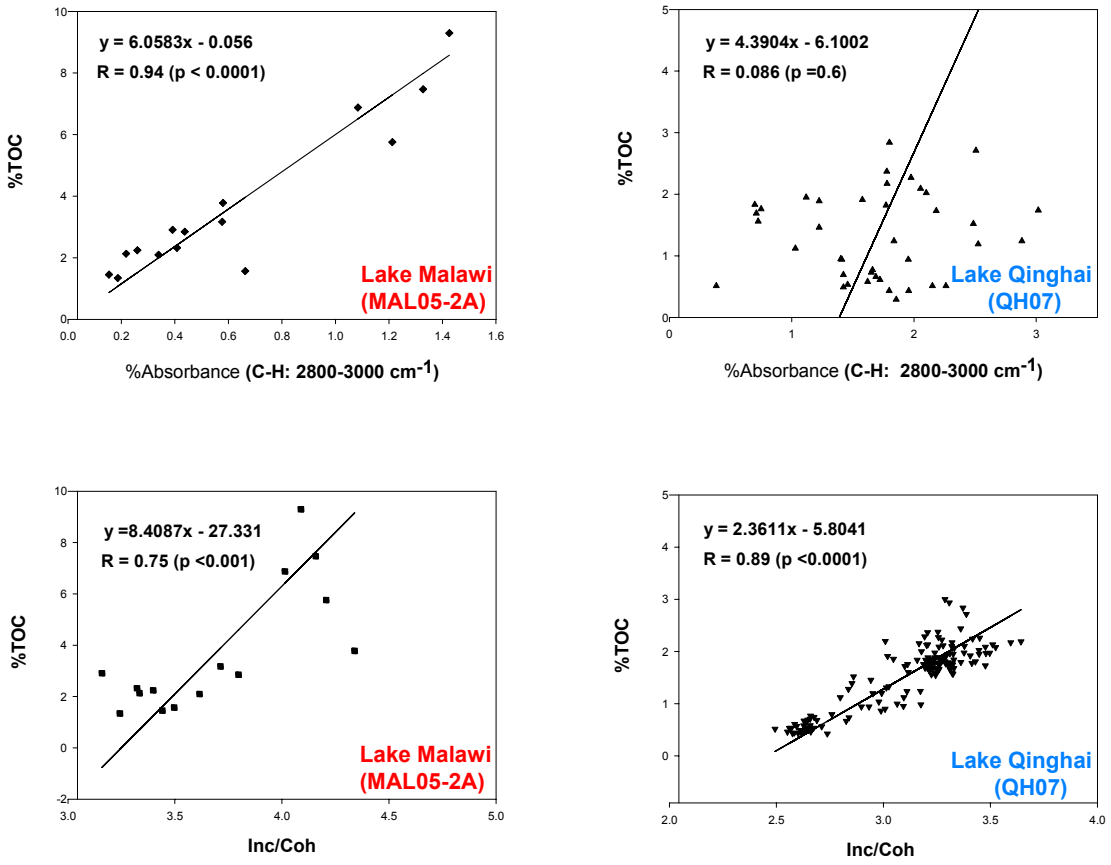

Fig. 5 Cross plots and least-square regression of conventionally-measured biogenic silica content versus FTIR absorbance in the 1050-1250 $cm^{-1}$ region (Si-O bond) for M98-1P, and absorbance in the 1050-1250 $cm^{-1}$ region (Si-O bond) versus Si/Ti for MAL05-2A.

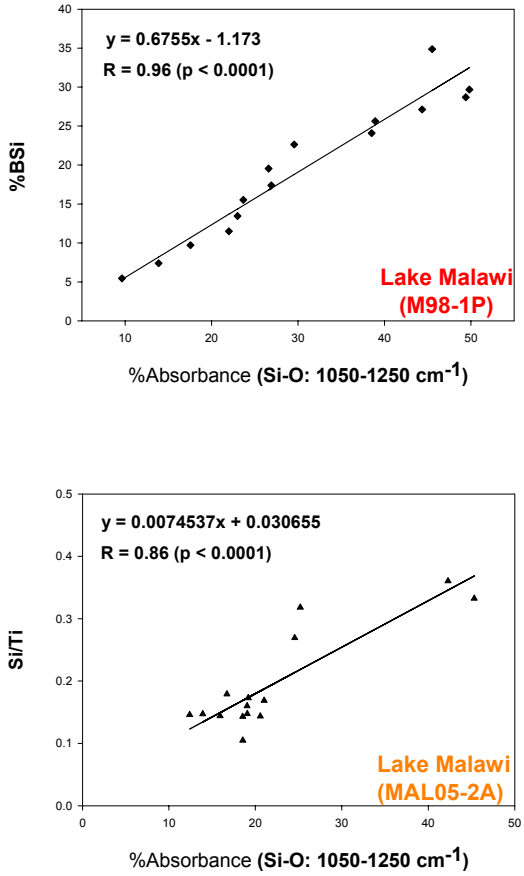

# Bibliography


Abdulla, H. A. N., Minor, E. C., and Hatcher, P. G. (2010). Using two dimensional correlations of 13C-NMR and FTIR to investigate changes in the chemical composition of dissolved organic matter along an estuarine transect. *Environmental Science and Technology* **44,** 8044-8049.

Allen, D. T., Palen, E. J., Haimov, M. I., Hering, S. V., and Young, J. R. (1994). Fourier-Transform Infrared-Spectroscopy Of Aerosol Collected In A Low-Pressure Impactor (Lpi/Ftir) - Method Development And Field Calibration. *Aerosol Science And Technology* **21,** 325-342.

Alvarado, A., Tuazon, E. C., Aschmann, S. M., Arey, J., and Atkinson, R. (1999). Products and mechanisms of the gas-phase reactions of OH radicals and O-3 with 2-methyl-3-buten-2-ol. *Atmospheric Environment* **33,** 2893-2905.

An, Z. H., Kukla, G. J., Porter, S. C., and Xiao, J. L. (1991). Magnetic-Susceptibility Evidence Of Monsoon Variation On The Loess Plateau Of Central China During The Last 130,000 Years. *Quaternary Research* **36,** 29-36.

An, Z. S. (2000). The history and variability of the East Asian paleomonsoon climate. *Quaternary Science Reviews* **19,** 171-187.

An, Z. S., Clemens, S. C., Shen, J., Qiang, X. K., Jin, Z. D., Sun, Y. B., Prell, W. L., Luo, J. J., Wang, S. M., Xu, H., Cai, Y. J., Zhou, W. J., Liu, X. D., Liu, W. G., Shi, Z. G., Yan, L. B., Xiao, X. Y., Chang, H., Wu, F., Ai, L., and Lu, F. Y. (2011a). Glacial-Interglacial Indian Summer Monsoon Dynamics. *Science* **333,** 719-723.

An, Z. S., Colman, S. M., Zhou, W. J., Li, X. Q., Brown, E. T., Julll, T., Cai, Y. J., and Huang, Y. S., et al. (2011b). Climate change at the confluence of the Westerlies and Asian Monsoon since 32 ka. *Nature***,** (In review).

An, Z. S., Kutzbach, J. E., Prell, W. L., and Porter, S. C. (2001). Evolution of Asian monsoons and phased uplift of the Himalayan Tibetan plateau since Late Miocene times. *Nature* **411,** 62-66.

An, Z. S., Wang, P., Shen, J., Zhang, Y. X., Zhang, P. Z., Wang, S. M., Li, X. Q., Sun, Q. L., Song, Y. G., Al, L., Zhang, Y. C., Jiang, S. R., Liu, X. Q., and Wang, Y. (2006). Geophysical survey on the tectonic and sediment distribution of Qinghai Lake basin. *Science In China Series D-Earth Sciences* **49,** 851-861.

Anderson, L. (2011). Holocene record of precipitation seasonality from lake calcite delta O-18 in the central Rocky Mountains, United States. *Geology* **39,** 211-214.

Andrews, J. T., and Haroardottir, J. (2009). A comparison of Holocene sediment- and paleo-magnetic characteristics from the margins of Iceland and East Greenland. *Jokull* **59,** 51-66.

Berner, R. A. (1984). Sedimentary Pyrite Formation - An Update. *Geochimica Et Cosmochimica Acta* **48,** 605-615.

Bertaux, J., Frohlich, F., and Ildefonse, P. (1998). Multicomponent analysis of FTIR spectra: Quantification of amorphous and crystallized mineral phases in synthetic and natural sediments. *Journal Of Sedimentary Research* **68,** 440-447.

Blaauw, M. (2010). Methods and code for 'classical' age-modelling of radiocarbon sequences. *Quaternary Geochronology* **5,** 512-518.

Braconnot, P., Otto-Bliesner, B., Harrison, S., Joussaume, S., Peterchmitt, J. Y., Abe-Ouchi, A., Crucifix, M., Driesschaert, E., Fichefet, T., Hewitt, C. D., Kageyama, M., Kitoh, A., Laine, A., Loutre, M. F., Marti, O., Merkel, U., Ramstein, G., Valdes, P., Weber, S. L., Yu, Y., and Zhao, Y. (2007). Results of PMIP2 coupled simulations of the Mid-Holocene and Last Glacial Maximum - Part 1: experiments and large-scale features. *Climate Of The Past* **3,** 261-277.

Brown, E. T., Johnson, T. C., Scholz, C. A., Cohen, A. S., and King, J. W. (2007). Abrupt change in tropical African climate linked to the bipolar seesaw over the past 55,000 years. *Geophysical Research Letters* **34**.

Brown, E. T., Werne, J. P., Rubesch, M., Fawcett, P. J., Ortega, B., Caballero, M., and Lozano, S. (2010). Lacustrine sedimentary evidence of millennial scale variability in North America and Africa revealed by XRF core scanning. *Geochimica Et Cosmochimica Acta* **74,** A124-A124.

Burnett, A. P., Soreghan,Michael J., Scholza, Christopher A. and Brown, Erik T. (2010). Tropical East African climate change and its relation to global climate: A record from Lake Tanganyika, Tropical East Africa, over the past 90+ kyr. *Palaeogeography, Palaeoclimatology, Palaeoecology* **doi:10.1016/j.palaeo.2010.02.011**.

Castaneda, I. S., Werne, J. P., and Johnson, T. C. (2007). Wet and arid phases in the southeast African tropics since the Last Glacial Maximum. *Geology* **35,** 823-826.

Chen, F. H., Chen, J. H., Holmes, J., Boomer, I., Austin, P., Gates, J. B., Wang, N. L., Brooks, S. J., and Zhang, J. W. (2010). Moisture changes over the last millennium in arid central Asia: a review, synthesis and comparison with monsoon region. *Quaternary Science Reviews* **29,** 1055-1068.

Chen, F. H., Yu, Z. C., Yang, M. L., Ito, E., Wang, S. M., Madsen, D. B., Huang, X. Z., Zhao, Y., Sato, T., Birks, H. J. B., Boomer, I., Chen, J. H., An, C. B., and Wunnemann, B. (2008). Holocene moisture evolution in arid central Asia and its out-of-phase relationship with Asian monsoon history. *Quaternary Science Reviews* **27,** 351-364.

Chen, F. H., Zhu, Y., Li, J. J., Shi, Q., Jin, L. Y., and Wunemann, B. (2001). Abrupt Holocene changes of the Asian monsoon at millennial- and centennial-scales: Evidence from lake sediment document in Minqin Basin, NW China. *Chinese Science Bulletin* **46,** 1942-1947.

Clemens, S. C., Prell, W. L., and Sun, Y. B. (2010). Orbital-scale timing and mechanisms driving Late Pleistocene Indo-Asian summer monsoons: Reinterpreting cave speleothem delta(18)O. *Paleoceanography* **25**.

Colman, S., Grachev, M., Hearn, P., Horie, S., Kawai, T., Kuzmin, M., Logachov, N., Fialkov, V., Gorigljad, A., Tomilov, B., Khakhaev, B., Kochikov, S., Lykov, V., Pevzner, L., Bucharov, A., Karabanov, E., Logachev, N., Mats, V., Bardardinov, A., Baranova, E., Khlystov, O., Khrachenko, V., Shimaraeva, M., Stolbova, E., Komakova, E., Efremova, S., Gvozdkov, A., Kravchinski, V., Peck, J., Fileva, T., Kashik, S., Khramtsova, T., Kalashnikova, I., Rasskazova, T., Tatarnikova, V., Yuretich, R., Mazilov, V., Takemura, K., Bobrov, V., Gunicheva, T., Haraguchi, H., Ito, S., Kocho, T., Markova, M., Pampura, V., Proidakova, O., Ishiwatari, R., Sawatari, H., Takeuchi, A., Toyoda, K., Vorobieva, S., Ikeda, A., Marui, A., Nakamura, T., Ogura, K., Ohta, T., King, J., Sakai, H., Yokoyama, T., Hayashida, A., Bezrukova, E., Fowell, S., Fuji, N., Letunova, P., Misharina, V., Miyoshi, N., Chernyaeva, G., Ignatova, I., Likhoshvai, E., Stoermer, E., Granina, L., Levina, O., Dolgikh, P., Lazo, F., Lutskaia, N., Orem, W., Wada, E., Williams, D., Yamada, K., Yamada, S., Callander, E., Golobokoval, L., Shanks, P., Dorofeeva, R., and Duchkov, A. (1997). Preliminary results of the first scientific drilling on Lake Baikal, Buguldeika site, southeastern Siberia. *Quaternary International* **37,** 3-17.

Colman, S. M., Peck, J. A., Hatton, J., Karabanov, E. B., and King, J. W. (1999). Biogenic silica records from the BDP93 drill site and adjacent areas of the Selenga Delta, Lake Baikal, Siberia. *Journal Of Paleolimnology* **21,** 9-17.

Colman, S. M., Peck, J. A., Karabanov, E. B., Carter, S. J., Bradbury, J. P., King, J. W., and Williams, D. F. (1995). Continental Climate Response To Orbital Forcing From Biogenic Silica Records In Lake Baikal. *Nature* **378,** 769-771.

Colman, S. M., Yu, S. Y., An, Z., Shen, J., and Henderson, A. C. G. (2007). Late Cenozoic climate changes in China's western interior: a review of research on Lake Qinghai and comparison with other records. *Quaternary Science Reviews* **26,** 2281-2300.

Conroy, J. L., Overpeck, J. T., Cole, J. E., Shanahan, T. M., and Steinitz-Kannan, M. (2008). Holocene changes in eastern tropical Pacific climate inferred from a Galapagos lake sediment record. *Quaternary Science Reviews* **27,** 1166-1180.

Coury, C., and Dillner, A. M. (2008). A method to quantify organic functional groups and inorganic compounds in ambient aerosols using attenuated total reflectance FTIR spectroscopy and multivariate chemometric techniques. *Atmospheric Environment* **42,** 5923-5932.

Croudace, I. W., Rindby, A., and Rothwell, R. G. (2006). ITRAX: description and evaluation of a new multi-function X-ray core scanner. In: R.G. Rothwell, Editor. *New Techniques in Sediment Core Analysis, London, Geological Society, Special Publications* **267,** 51-63.

Curtis, J. H., Brenner, M., Hodell, D. A., Balser, R. A., Islebe, G. A., and Hooghiemstra, H. (1998). A multi-proxy study of Holocene environmental change in the Maya lowlands of Peten, Guatemala. *Journal Of Paleolimnology* **19,** 139-159.

Dearing, J. (1999). Magnetic susceptibility. In Walden, J., Oldfield, F. and Smith, J. P. (eds.), Environmental magnetism: a practical guide. Technical Guide. *Quaternary Research Association* **6,** 35-62.

Dekkers, M. J., Mattei, J. L., Fillion, G., and Rochette, P. (1989). Grain-Size Dependence Of The Magnetic-Behavior Of Pyrrhotite During Its Low-Temperature Transition At 34-K. *Geophysical Research Letters* **16,** 855-858.

DeMaster, D. J. (1979). thesis. *Yale University*.

DeNiro, M. (1987). Stable Isotopy and Archaeology. *American Scientist***,** 182-191.

Drevnick, P. E., Muir, D. C. G., Lamborg, C. H., Horgan, M. J., Canfield, D. E., Boyle, J. F., and Rose, N. L. (2010). Increased Accumulation of Sulfur in Lake Sediments of the High Arctic. *Environmental Science & Technology* **44,** 8415-8421.

Dunlop, D. J. (2002). Theory and application of the Day plot (M-rs/M-s versus H-cr/H-c) 1. Theoretical curves and tests using titanomagnetite data. *Journal Of Geophysical Research-Solid Earth* **107**.

Evans, M. E., and Heller, F. (2003). Environmental Magnetism: Principles and Applications of Enviromagnetics.

Feng, S., and Hu, Q. (2005). Regulation of Tibetan Plateau heating on variation of Indian summer monsoon in the last two millennia. *Geophysical Research Letters* **32**.

Funk, J. A., Dobeneck, T. v., and Reitz, A. (2003). Integrated Rock Magnetic and Geochemical Quantification of Redoxomorphic Iron Mineral Diagenesis in Late Quaternary Sediments from the Equatorial Atlantic. 237-260.

Gaffey, S. J. (1986). Spectral Reflectance Of Carbonate Minerals In The Visible And Near-Infrared (0.35-2.55 Microns) - Calcite, Aragonite, And Dolomite. *American Mineralogist* **71,** 151-162.

Geiss, C. E., Banerjee, S. K., Camill, P., and Umbanhowar, C. E. (2004). Sediment-magnetic signature of land-use and drought as recorded in lake sediment from south-central Minnesota, USA. *Quaternary Research* **62,** 117-125.

Geiss, C. E., Umbanhowar, C. E., Camill, P., and Banerjee, S. K. (2003). Sediment magnetic properties reveal Holocene climate change along the Minnesota prairie-forest ecotone. *Journal Of Paleolimnology* **30,** 151-166.

Giralt, S., Rico-Herrero, M. T., Vega, J. C., and Valero-Garces, B. L. (2011). Quantitative climate reconstruction linking meteorological, limnological and XRF core scanner datasets: the Lake Sanabria case study, NW Spain. *Journal of Paleolimnology***,** DOI 10.1007/s10933-011-9509-x.

Griffiths, P., and de Hasseth, J. A. (2007). Fourier Transform Infrared Spectrometry (2nd ed.).

Harris, D. C. (2005). Exploring Chemical Analysis (3rd ed.).

Harrison, T. M., Copeland, P., Kidd, W. S. F., and Yin, A. (1992). Raising Tibet. *Science* **255,** 1663-1670.

Hayes, J. M. (1993). Factors Controlling C-13 Contents Of Sedimentary Organic-Compounds - Principles And Evidence. *Marine Geology* **113,** 111-125.

Hedges, J. I., and Oades, J. M. (1997). Comparative organic geochemistries of soils and marine sediments. *Organic Geochemistry* **27,** 319-361.

Henderson, A. C. G., and Holmes, J. A. (2009). Palaeolimnological evidence for environmental change over the past millennium from Lake Qinghai sediments: A review and future research prospective. *Quaternary International* **194,** 134-147.

Henderson, A. C. G., Holmes, J. A., and Leng, M. J. (2010). Late Holocene isotope hydrology of Lake Qinghai, NE Tibetan Plateau: effective moisture variability and atmospheric circulation changes. *Quaternary Science Reviews* **29,** 2215-2223.

Henderson, A. C. G., Holmes, J. A., Zhang, J. W., Leng, M. J., and Carvalho, L. R. (2003). A carbon- and oxygen-isotope record of recent environmental change from Qinghai Lake, NE Tibetan Plateau. *Chinese Science Bulletin* **48,** 1463-1468.

Herbert, T. D., Tom, B. A., and Burnett, C. (1992). Precise Major Component Determinations In Deep-Sea Sediments Using Fourier-Transform Infrared-Spectroscopy. *Geochimica Et Cosmochimica Acta* **56,** 1759-1763.

Herzschuh, U. (2006). Palaeo-moisture evolution in monsoonal Central Asia during the last 50,000 years. *Quaternary Science Reviews* **25,** 163-178.

Heslop, D. (2009). On the statistical analysis of the rock magnetic S-ratio. *Geophysical Journal International* **178,** 159-161.

Hilgenfeldt, K. (2000). Diagenetic dissolution of biogenic magnetite in surface sediments of the Benguela upwelling system. *International Journal Of Earth Sciences* **88,** 630-640.

Hodgson, D. A., Verleyen, E., Sabbe, K., Squier, A. H., Keely, B. J., Leng, M. J., Saunders, K. M., and Vyverman, W. (2005). Late Quaternary climate-driven environmental change in the Larsemann Hills, East Antarctica, multi-proxy evidence from a lake sediment core. *Quaternary Research* **64,** 83-99.

Hoefs, J. (1988). Stable Isotope Geochemistry, 3 rd ed.

Holmes, M. A., Watkins, D. K., and Norris, R. D. (2004). Paleocene cyclic sedimentation in the western North Atlantic, ODP Site 1051, Blake Nose. *Marine Geology* **209,** 31-43.

Hornback, J. M. (2005). Organic geochemistry.

Horng, C. S., Torii, M., Shea, K. S., and Kao, S. J. (1998). Inconsistent magnetic polarities between greigite- and pyrrhotite/magnetite-bearing marine sediments from the Tsailiao-chi section, southwestern Taiwan. *Earth And Planetary Science Letters* **164,** 467-481.

Hou, J. Z., Huang, Y. S., Brodsky, C., Alexandre, M. R., McNichol, A. P., King, J. W., Hu, F. S., and Shen, J. (2010). Radiocarbon Dating of Individual Lignin Phenols: A New Approach for Establishing Chronology of Late Quaternary Lake Sediments. *Analytical Chemistry* **82,** 7119-7126.

Huang, Q., and Sun, N. J. (1989). Preliminary-Study On Depositing Rate Of Qinghai Lake And Its Evolution Of Paleoclimate. *Chinese Science Bulletin* **34,** 1457-1462.

Huang, Y. S., Shuman, B., Wang, Y., and Webb, T. (2002). Hydrogen isotope ratios of palmitic acid in lacustrine sediments record late Quaternary climate variations. *Geology* **30,** 1103-1106.

Huybers, P. (2006). Early Pleistocene glacial cycles and the integrated summer insolation forcing. *Science* **313,** 508-511.

Jaccard, S. L., Galbraith, E. D., Sigman, D. M., and Haug, G. H. (2011). A pervasive link between Antarctic ice core and subarctic Pacific sediment records over the past 800 kyrs. *Quaternary Science Reviews* **29,** 206-212.

Jackson, M., Bowles, J. A., Lascu, I., and Solheid, P. (2010). Deconvolution of u channel magnetometer data: Experimental study of accuracy, resolution, and stability of different inversion methods. *Geochemistry Geophysics Geosystems* **11**.

Jenkins, R. (1999). X-ray fluorescence spectrometry. **2nd edition**.

Ji, J. F., Balsam, W., Shen, J., Wang, M., Wang, H. T., and Chen, J. (2009). Centennial blooming of anoxygenic phototrophic bacteria in Qinghai Lake linked to solar and monsoon activities during the last 18,000 years. *Quaternary Science Reviews* **28,** 1304-1308.

Ji, J. F., Shen, J., Balsam, W., Chen, J., Liu, L. W., and Liu, X. Q. (2005). Asian monsoon oscillations in the northeastern Qinghai-Tibet Plateau since the late glacial as interpreted from visible reflectance of Qinghai Lake sediments. *Earth And Planetary Science Letters* **233,** 61-70.

Jin, Z. D., You, C. F., Wang, Y., and Shi, Y. W. (2010). Hydrological and solute budgets of Lake Qinghai, the largest lake on the Tibetan Plateau. *Quaternary International* **218,** 151-156.

Johnson, T. C., Brown, E. T., McManus, J., Barry, S., Barker, P., and Gasse, F. (2002). A high-resolution paleoclimate record spanning the past 25,000 years in southern East Africa. *Science* **296,** 113-+.

Johnson, T. C., Brown, E. T., and Shi, J. M. (2011). Biogenic silica deposition in Lake Malawi, East Africa over the past 150,000 years. *Palaeogeography Palaeoclimatology Palaeoecology* **303,** 103-109.

Johnson, T. C., Kelts, K., and Odada, E. (2000). The holocene history of Lake Victoria. *Ambio* **29,** 2-11.

Kao, S. J., Horng, C. S., Roberts, A. P., and Liu, K. K. (2004). Carbon-sulfur-iron relationships in sedimentary rocks from southwestern Taiwan: influence of geochemical environment on greigite and pyrrhotite formation. *Chemical Geology* **203,** 153-168.

Kelts, K., Zao, C. K., Lister, G., Qing, Y. J., Hong, G. Z., Niessen, F., and Bonani, G. (1989). Geological Fingerprints Of Climate History - A Cooperative Study Of Qinghai Lake, China. *Eclogae Geologicae Helvetiae* **82,** 167-182.

King, J. W., and Channell, J. E. T. (1991). Sedimentary Magnetism, Environmental Magnetism, And Magnetostratigraphy. *Reviews Of Geophysics* **29,** 358-370.

Konert, M., and Vandenberghe, J. (1997). Comparison of laser grain size analysis with pipette and sieve analysis: A solution for the underestimation of the clay fraction. *Sedimentology* **44,** 523-535.

Korhola, A., Sorvari, S., Rautio, M., Appleby, P. G., Dearing, J. A., Hu, Y., Rose, N., Lami, A., and Cameron, N. G. (2002). A multi-proxy analysis of climate impacts on the recent development of subarctic Lake Saanajarvi in Finnish Lapland. *Journal Of Paleolimnology* **28,** 59-77.

Kovac, N., Fraganeli, J., Bajt, O., Orel, B., and Vuk, A. S. (2005). Investigation of sediment samples from the Gulf of Trieste (northern Adriatic) by FTIR spectroscopy. *Materials and Geoenvironment* **52,** 81-85.

Li, C. F., and Yanai, M. (1996). The onset and interannual variability of the Asian summer monsoon in relation to land sea thermal contrast. *Journal Of Climate* **9,** 358-375.

Lister, G. S., Kelts, K., Zao, C. K., Yu, J. Q., and Niessen, F. (1991). Lake Qinghai, China - Closed-Basin Lake Levels And The Oxygen Isotope Record For Ostracoda Since The Latest Pleistocene. *Palaeogeography Palaeoclimatology Palaeoecology* **84,** 141-162.

Liu, B., Xu, H., Lan, J. H., Liu, X. Y., Hou, Z. H., and Dong, J. B. (2010). A preliminary study on the environmental significance of biogenic silica in Qinghai Lake (In Chinese with English abstract). *Quaternary Sciences*.

Liu, K. B., Yao, Z. J., and Thompson, L. G. (1998). A pollen record of Holocene climatic changes from the Dunde ice cap, Qinghai-Tibetan Plateau. *Geology* **26,** 135-138.

Liu, W. G., Liu, Z. H., Wang, H. Y., He, Y. X., Wang, Z., and Xu, L. M. (2011a). Salinity control on long-chain alkenone distributions in lake surface waters and sediments of the northern Qinghai-Tibetan Plateau, China. *Geochimica Et Cosmochimica Acta* **75,** 1693-1703.

Liu, X. D., and Yin, Z. Y. (2002). Sensitivity of East Asian monsoon climate to the uplift of the Tibetan Plateau. *Palaeogeography Palaeoclimatology Palaeoecology* **183,** 223-245.

Liu, X. J., Colman, S. M., and Brown, E. T. (2011b). High-resolution core-scanning based lacustrine sediment study of Lake Qinghai: bridge the geochemical proxies and magnetic properties. *(in preparation)*.

Liu, X. J., Colman, S. M., Brown, E. T., Henderson, A. C. G., and Holmes, J. A. (2011c). Multi-proxy evidence for climate history since the LGM from Lake Qinghai sediments (in preparition).

Liu, X. M., An, Z. S., Rolph, T., Qiang, X. K., Hesse, P., Lu, H. Y., Zhou, J., and Cai, Y. J. (2001). Magnetic properties of the Tertiary red clay from Gansu Province, China and its paleoclimatic significance. *Science in China, Series D* **44,** 635-651.

Liu, X. Q., Shen, J., Wang, S. M., Wang, Y. B., and Liu, W. G. (2007). Southwest monsoon changes indicated by oxygen isotope of ostracode shells from sediments in Qinghai Lake since the late Glacial. *Chinese Science Bulletin* **52,** 539-544.

Liu, Z. H., Henderson, A. C. G., and Huang, Y. S. (2006). Alkenone-based reconstruction of late-Holocene surface temperature and salinity changes in Lake Qinghai, China. *Geophysical Research Letters* **33**.

LZCAS. (1994). (Lanzhou Branch of Chinese Academy Sciences) Evolution of Recent Environments in Qinghai Lake and Its Prediction. *West Center of Resource and Environment, Chinese Academy of Sciences, Science Press, Beijing (in Chinese with English abstracts)*.

Maher, B. A., and Taylor, R. M. (1988). Formation of ultrafine-grained magnetite in soils. *Nature* **336,** 368-370.

Maria, S. F., Russell, L. M., Turpin, B. J., and Porcja, R. J. (2002). FTIR measurements of functional groups and organic mass in aerosol samples over the Caribbean. *Atmospheric Environment* **36,** 5185-5196.

Mecozzi, M., Pietrantonio, E., Amici, M., and Romanelli, G. (2001). Determination of carbonate in marine solid samples by FTIR-ATR spectroscopy. *Analyst* **126,** 144-146.

Mecozzi, M., Pietrantonio, E., and Pietroletti, M. (2009). The roles of carbohydrates, proteins and lipids in the process of aggregation of natural marine organic matter investigated by means of 2D correlation spectroscopy applied to infrared spectra. *Spectrochimica Acta Part A-Molecular And Biomolecular Spectroscopy* **71,** 1877-1884.

Metivier, F., Gaudemer, Y., Tapponnier, P., and Meyer, B. (1998). Northeastward growth of the Tibet plateau deduced from balanced reconstruction of two depositional areas: The Qaidam and Hexi Corridor basins, China. *Tectonics* **17,** 823-842.

Meyers, P. A. (1994). Preservation Of Elemental And Isotopic Source Identification Of Sedimentary Organic-Matter. *Chemical Geology* **114,** 289-302.

Meyers, P. A., and Ishiwatari, R. (1993). Lacustrine Organic Geochemistry - An Overview Of Indicators Of Organic-Matter Sources And Diagenesis In Lake-Sediments. *Organic Geochemistry* **20,** 867-900.

Meyers, P. A., and Lallier-Verges, E. (1999). Lacustrine sedimentary organic matter records of Late Quaternary paleoclimates. *Journal Of Paleolimnology* **21,** 345-372.

Middleton, G. V. (2006). Encyclopedia of Sediments and Sedimentary Rocks.

Mischke, S., Herzschuh, U., Zhang, C., Bloemendal, J., and Riedel, F. (2005). A Late Quaternary lake record from the Qilian Mountains (NW China): lake level and salinity changes inferred from sediment properties and ostracod assemblages. *Global And Planetary Change* **46,** 337-359.

Molnar, P., England, P., and Martinod, J. (1993). Mantle dynamics, uplift of the Tibetan Plateau, and the Indian monsoon. *Reviews of Geophysics* **31,** 357-396.

Muller, J., Oberhansli, H., Melles, M., Schwab, M., Rachold, V., and Hubberten, H. W. (2001). Late Pliocene sedimentation in Lake Baikal: implications for climatic and tectonic change in SE Siberia. *Palaeogeography Palaeoclimatology Palaeoecology* **174,** 305-326.

O'Leary, M. H. (1988). Carbon isotopes in photosynthesis. *Bioscience* **38,** 328-336.

Oldfield, F. (2007). Sources of fine-grained magnetic minerals in sediments: a problem revisited. *Holocene* **17,** 1265-1271.

Ortega, B., Caballero, M., Lozano, S., Vilaclara, G., and Rodriguez, A. (2006). Rock magnetic and geochemical proxies for iron mineral diagenesis in a tropical lake: Lago Verde, Los Tuxtlas, East-Central Mexico. *Earth And Planetary Science Letters* **250,** 444-458.

Ozdemir, O., Dunlop, D. J., and Moskowitz, B. M. (1993). The Effect Of Oxidation On The Verwey Transition In Magnetite. *Geophysical Research Letters* **20,** 1671-1674.

Palmucci, M., Ratti, S., and Giordano, M. (2011). Ecological And Evolutionary Implications Of Carbon Allocation In Marine Phytoplankton As A Function Of Nitrogen Availability: A Fourier Transform Infrared Spectroscopy Approach. *Journal Of Phycology* **47,** 313-323.

Pausata, D. S. B., Nisancioglu, K. H., and Bitz, C. M. (2011). Chinese stalagmite δ18O controlled by changes in the Indian monsoon during a simulated Heinrich event. *Nature* **DOI: 10.1038/NGEO1169**.

Peck, J. A., King, J. W., Colman, S. M., and Kravchinsky, V. A. (1994a). A Rock-Magnetic Record From Lake Baikal, Siberia - Evidence For Late Quaternary Climate-Change. *Earth And Planetary Science Letters* **122,** 221-238.

Peck, J. A., King, J. W., Colman, S. M., and Kravchinsky, V. A. (1994b). A Rock Magnetic Record From Lake Baikal, Siberia - Evidence For Late Quaternary Climate-Change (Vol 123, Pg 221, 1994). *Earth And Planetary Science Letters* **128,** 703-703.

Porter, S. C., and An, Z. S. (1995). Correlation Between Climate Events In The North-Atlantic And China During Last Glaciation. *Nature* **375,** 305-308.

Prell, W. L., and Kutzbach, J. E. (1992). Sensitivity Of The Indian Monsoon To Forcing Parameters And Implications For Its Evolution. *Nature* **360,** 647-652.

Ramirez, E., Hoffmann, G., Taupin, J. D., Francou, B., Ribstein, P., Caillon, N., Ferron, F. A., Landais, A., Petit, J. R., Pouyaud, B., Schotterer, U., Simoes, J. C., and Stievenard, M. (2003). A new Andean deep ice core from Nevado Illimani (6350 m), Bolivia. *Earth And Planetary Science Letters* **212,** 337-350.

Raymo, M. E., and Ruddiman, W. F. (1992). Tectonic forcing of late Cenozoic climate. *Nature* **359,** 117-122.

Rea, D. K., Snoeckx, H., and Joseph, L. H. (1998). Late Cenozoic eolian deposition in the North Pacific: Asian drying, Tibetan uplift, and cooling of the northern hemisphere. *Paleoceanography* **13,** 215-224.

Reed, J. M., Stevenson, A. C., and Juggins, S. (2001). A multi-proxy record of Holocene climatic change in southwestern Spain: the Laguna de Medina, Cadiz. *Holocene* **11,** 707-719.

Reynolds, R. L., Rosenbaum, J. G., van Metre, P., Tuttle, M., Callender, E., and Goldin, A. (1999). Greigite (Fe3S4) as an indicator of drought - The 1912-1994 sediment magnetic record from White Rock Lake, Dallas, Texas, USA. *Journal Of Paleolimnology* **21,** 193-206.

Richter, C., Blum, P., and Rohl, U. (2001). Data report:magnetic properties abd XRF-scanner data of Site 1075 (lower Congo Basin). *Proceedings of the Ocean Drilling Program, Scientific Results* **175,** 1-31.

Roberts, A. P. (1995). Magnetic-Properties Of Sedimentary Greigite (Fe3s4). *Earth And Planetary Science Letters* **134,** 227-236.

Roberts, A. P., Chang, L., Rowan, C. J., Horng, C.-S., and Florindo, F. (2011). MAGNETIC PROPERTIES OF SEDIMENTARY GREIGITE (Fe3S4): AN UPDATE. *Rev. Geophys.* **49,** doi:10.1029/2010RG000336.

Rosen, P., and Hammarlund, D. (2007). Effects of climate, fire and vegetation development on Holocene changes in total organic carbon concentration in three boreal forest lakes in northern Sweden. *Biogeosciences* **4,** 975-984.

Rosen, P., and Persson, P. (2006). Fourier-transform infrared spectroscopy (FTIRS), a new method to infer past changes in tree-line position and TOC using lake sediment. *Journal Of Paleolimnology* **35,** 913-923.

Rosen, P., Vogel, H., Cunningham, L., Reuss, N., Conley, D. J., and Persson, P. (2010). Fourier transform infrared spectroscopy, a new method for rapid determination of total organic and inorganic carbon and biogenic silica concentration in lake sediments. *Journal Of Paleolimnology* **43,** 247-259.

Rothwell, R. G. (2006). New techniques in sediment core analysis.

Ruddiman, W. F., and Kutzbach, J. E. (1989). Forcing of late Cenozoic Northern Hemisphere climate by plateau uplift in southern Asia and the American west. *Journal of Geophysical Research* **94,** 18,409-18,427.

Russell, J. M., and Johnson, T. C. (2007). Little Ice Age drought in equatorial Africa: Intertropical Convergence Zone migrations and El Nino-Southern Oscillation variability. *Geology* **35,** 21-24.

Saez, A., Valero-Garces, B. L., Giralt, S., Moreno, A., Bao, R., Pueyo, J. J., Hernandez, A., and Casas, D. (2009). Glacial to Holocene climate changes in the SE Pacific. The Raraku Lake sedimentary record (Easter Island, 27 degrees S). *Quaternary Science Reviews* **28,** 2743-2759.

Sampei, Y., Matsumoto, E., Kamei, T., and Tokuoka, T. (1997). Sulfur and organic carbon relationship in sediments from coastal brackish lakes in the Shimane peninsula district, southwest Japan. *Geochemical Journal* **31,** 245-262.

Sayer, C., Roberts, N., Sadler, J., David, C., and Wade, P. M. (1999). Biodiversity changes in a shallow lake ecosystem: a multi-proxy palaeolimnological analysis. *Journal Of Biogeography* **26,** 97-114.

Schiemann, R., Luthi, D., and Schar, C. (2009). Seasonality and Interannual Variability of the Westerly Jet in the Tibetan Plateau Region. *Journal Of Climate* **22,** 2940-2957.

Schulz, H. D., and Zabel, M. (2009). Marine Geochemistry.

Shan, F. S., Du, N. Q., and Kong, Z. C. (1993). Vegetational and environmental changes in the last 350 ka in Erlangjian, Qinghai Lake (In Chinese with English abstract). *Journal of Lake Sciences* **5,** 9-17.

Shanahan, T. M., Overpeck, J. T., Hubeny, J. B., King, J., Hu, F. S., Hughen, K., Miller, G., and Black, J. (2008). Scanning micro-X-ray fluorescence elemental mapping: A new tool for the study of laminated sediment records. *Geochemistry Geophysics Geosystems* **9**.

Shen, J., Liu, X. Q., Wang, S. M., and Matsumoto, R. (2005a). Palaeoclimatic changes in the Qinghai Lake area during the last 18,000 years. *Quaternary International* **136,** 131-140.

Shen, J., Liu, X. Q., Wang, S. M., and Matsumotob, R. (2005b). Palaeoclimatic changes in the Qinghai Lake area during the last 18,000 years. *Quaternary International* **136,** 131-140.

Snowball, I. F. (1991). Magnetic Hysteresis Properties Of Greigite (Fe3s4) And A New Occurrence In Holocene Sediments From Swedish Lappland. *Physics Of The Earth And Planetary Interiors* **68,** 32-40.

Stager, J. C., Cumming, B., and Meeker, L. (1997). A high-resolution 11,400-yr diatom record from Lake Victoria, East Africa. *Quaternary Research* **47,** 81-89.

Stager, J. C., Ryves, D. B., Chase, B. M., and Pausata, F. S. R. (2011). Catastrophic Drought in the Afro-Asian Monsoon Region During Heinrich Event 1. *Science* **331,** 1299-1302.

Stehfest, K., Toepel, J., and Wilhelm, C. (2005). The application of micro-FTIR spectroscopy to analyze nutrient stress-related changes in biomass composition of phytoplankton algae. *Plant Physiology And Biochemistry* **43,** 717-726.

Sun, D. P., Tang, Y., Xu, Z., and Han, Z. (1991). A preliminary investigation on chemical evolution of the Lake Qinghai water (in Chinese). *Chinese Science Bulletin* **C,** 1172–1174.

Swann, G. E. A., and Patwardhan, S. V. (2011). Application of Fourier Transform Infrared Spectroscopy (FTIR) for assessing biogenic silica sample purity in geochemical analyses and palaeoenvironmental research. *Climate Of The Past* **7,** 65-74.

Talbot, M. R., and Kelts, K. (1986). Primary And Diagenetic Carbonates In The Anoxic Sediments Of Lake Bosumtwi, Ghana. *Geology* **14,** 912-916.

Thompson, L. G., Yao, T., Davis, M. E., Henderson, K. A., MosleyThompson, E., Lin, P. N., Beer, J., Synal, H. A., ColeDai, J., and Bolzan, J. F. (1997). Tropical climate instability: The last glacial cycle from a Qinghai-Tibetan ice core. *Science* **276,** 1821-1825.

Thompson, L. G., Yao, T., Mosley-Thompson, E., Davis, M. E., Henderson, K. A., and Lin, P. N. (2000). A high-resolution millennial record of the South Asian Monsoon from Himalayan ice cores. *Science* **289,** 1916-1919.

Thompson, R., and Oldfield, F. (1986). Environmental Magnetism.

Verosub, K. L., Fine, P., Singer, M. J., and Tenpas, J. (1993). Pedogenesis And Paleoclimate - Interpretation Of The Magnetic-Susceptibility Record Of Chinese Loess-Paleosol Sequences. *Geology* **21,** 1011-1014.

Vogel, H., Rosen, P., Wagner, B., Melles, M., and Persson, P. (2008). Fourier transform infrared spectroscopy, a new cost-effective tool for quantitative analysis of biogeochemical properties in long sediment records. *Journal Of Paleolimnology* **40,** 689-702.

Wang, P. X., Clemens, S., Beaufort, L., Braconnot, P., Ganssen, G., Jian, Z. M., Kershaw, P., and Sarnthein, M. (2005). Evolution and variability of the Asian monsoon system: state of the art and outstanding issues. *Quaternary Science Reviews* **24,** 595-629.

Wang, Y. J., Cheng, H., Edwards, R. L., An, Z. S., Wu, J. Y., Shen, C. C., and Dorale, J. A. (2001). A high-resolution absolute-dated Late Pleistocene monsoon record from Hulu Cave, China. *Science* **294,** 2345-2348.

Wang, Y. J., Cheng, H., Edwards, R. L., Kong, X. G., Shao, X. H., Chen, S. T., Wu, J. Y., Jiang, X. Y., Wang, X. F., and An, Z. S. (2008). Millennial- and orbital-scale changes in the East Asian monsoon over the past 224,000 years. *Nature* **451,** 1090-1093.

Weeks, R. J., Laj, C., Endignoux, L., Mazaud, A., Labeyrie, L., Roberts, A. P., Kissel, C., and Blanchard, E. (1995). Normalized Natural Remanent Magnetization Intensity During The Last 240000 Years In Piston Cores From The Central North-Atlantic Ocean - Geomagnetic-Field Intensity Or Environmental Signal. *Physics Of The Earth And Planetary Interiors* **87,** 213-229.

Werne, J. P., and Hollander, D. J. (2004). Balancing supply and demand: controls on carbon isotope fractionation in the Cariaco Basin (Venezuela) Younger Dryas to present. *Marine Chemistry* **92,** 275-293.

Wetzel, R. G. (2001). Limnology, 3rd ed. *San Diego: Elsevier*.

Xiao, J., Porter, S. C., An, Z. S., Kumai, H., and Yoshikawa, S. (1995). Grain-Size Of Quartz As An Indicator Of Winter Monsoon Strength On The Loess Plateau Of Central China During The Last 130,000-Yr. *Quaternary Research* **43,** 22-29.

Xiao, J. L., Inouchi, Y., Kumai, H., Yoshikawa, S., Kondo, Y., Liu, T. S., and An, Z. S. (1997). Eolian quartz flux to Lake Biwa, central Japan, over the past 145,000 years. *Quaternary Research* **48,** 48-57.

Xu, H., Ai, L., Tan, L. C., and An, Z. S. (2006). Stable isotopes in bulk carbonates and organic matter in recent sediments of Lake Qinghai and their climatic implications. *Chemical Geology* **235,** 262-275.

Yan, J. P., Hinderer, M., and Einsele, G. (2002). Geochemical evolution of closed-basin lakes: general model and application to Lakes Qinghai and Turkana. *Sedimentary Geology* **148,** 105-122.

Yancheva, G., Nowaczyk, N. R., Mingram, J., Dulski, P., Schettler, G., Negendank, J. F. W., Liu, J. Q., Sigman, D. M., Peterson, L. C., and Haug, G. H. (2007). Influence of the intertropical convergence zone on the East Asian monsoon. *Nature* **445,** 74-77.

Yu, J. Q. (2005a). Lake Qinghai, China: A multi-proxy investigation on sediment cores for the reconstructions of paleoclimate and paleoenvironment since the Marine Isotope Stage 3 (PhD thesis).

Yu, J. Q. (2005b). Lake Qinghai, China: A multi-proxy investigation on sediment cores for the reconstructions of paleoclimate and paleoenvironment since the Marine Isotope Stage 3 (PhD thesis, University of Technology, Darmstadt).

Yu, J. Q., and Zhang, L. (2008). Lake Qinghai-Paleoenvironment and Paleoclimate.

Yuan, D. X., Cheng, H., Edwards, R. L., Dykoski, C. A., Kelly, M. J., Zhang, M. L., Qing, J. M., Lin, Y. S., Wang, Y. J., Wu, J. Y., Dorale, J. A., An, Z. S., and Cai, Y. J. (2004). Timing, duration, and transitions of the Last Interglacial Asian Monsoon. *Science* **304,** 575-578.

Zhang, E. L., Shen, J., Wang, S. M., Yin, Y., Zhu, Y. X., and Xia, W. L. (2004). Quantitative reconstruction of the paleosalinity at Qinghai Lake in the past 900 years. *Chinese Science Bulletin* **49,** 730-734.

Zhang, J. W., Jin, M., Chen, F. H., Battarbee, R. W., and Henderson, A. C. G. (2003a). High-resolution precipitation variations in the Northeast Tibetan Plateau over the last 800 years documented by sediment cores of Qinghai Lake. *Chinese Science Bulletin* **48,** 1451-1456.

Zhang, P. Z., Cheng, H., Edwards, R. L., Chen, F. H., Wang, Y. J., Yang, X. L., Liu, J., Tan, M., Wang, X. F., Liu, J. H., An, C. L., Dai, Z. B., Zhou, J., Zhang, D. Z., Jia, J. H., Jin, L. Y., and Johnson, K. R. (2008). A Test of Climate, Sun, and Culture Relationships from an 1810-Year Chinese Cave Record. *Science* **322,** 940-942.

Zhang, Q. B., Cheng, G. D., Yao, T. D., Kang, X. C., and Huang, J. G. (2003b). A 2,326-year tree-ring record of climate variability on the northeastern Qinghai-Tibetan Plateau. *Geophysical Research Letters* **30**.

Zhang, Y., Gou, X. H., Chen, F. H., Tian, Q. H., Yang, M. L., Peng, J. F., and Fang, K. Y. (2009). A 1232-Year Tree-Ring Record Of Climate Variability In The Qilian Mountains, Northwestern China. *Iawa Journal* **30,** 407-420.

Zhang, Y., K. Sperber,et al. (1997). Climatology and interannual variantion of the East Asian winter monsoon: Results from the 1979-95 NCEP/NCAR reanalysis. *Monthly Weather Review* **125,** 2605-2619.

Zhao, Y., Yu, Z. C., Chen, F. H., Ito, E., and Zhao, C. (2007). Holocene vegetation and climate history at Hurleg Lake in the Qaidam Basin, northwest China. *Review Of Palaeobotany And Palynology* **145,** 275-288.

Zhao, Y., Yu, Z. C., Chen, F. H., Zhang, J. W., and Yang, B. (2009). Vegetation response to Holocene climate change in monsoon-influenced region of China. *Earth-Science Reviews* **97,** 242-256.

Zhao, Y., Yu, Z. C., Liu, X. J., Zhao, C., Chen, F. H., and Zhang, K. (2010). Late Holocene vegetation and climate oscillations in the Qaidam Basin of the northeastern Tibetan Plateau. *Quaternary Research* **73,** 59-69.

Zhu, L. P., Zhang, P. Z., Xia, W. L., Li, B. Y., and Chen, L. (2003). 1400-year cold/warm fluctuations reflected by environmental magnetism of a lake sediment core from the Chen Co, southern Tibet, China. *Journal Of Paleolimnology* **29,** 391-401.

Ziegler, M., Jilbert, T., de Lange, G. J., Lourens, L. J., and Reichart, G. J. (2008). Bromine counts from XRF scanning as an estimate of the marine organic carbon content of sediment cores. *Geochemistry Geophysics Geosystems* **9**.

# APPENDIX

## Lake Qinghai Drilling Project

The Lake Qinghai Drilling Project (LQDP), under the auspices of the International Continental Drilling Program (ICDP) and the Chinese Academy of Science (CAS), aims to uncover past variations in Asia monsoon and climate, on both orbital and millennial time scales. Drilling on Lake Qinghai was commenced in late July, 2005, using the GLAD 800 drilling system operated by DOSECC (Drilling, Observations, and Sampling of the Earth's Continental Crust, Inc.) (Fig. 1- 3). In the summer of 2007, a set of u-channel samples were subsampled from core LQDP05-1F in Xi'an and shipped to the Limnological Research Center (LRC), University of Minnesota Twin Cities.

To supplement the project with records of larger volumes of modern to Holocene sediments, in May/June 2007, we recovered a 3.55-m-long Uwitec sediment core (QH07-1A) and a 85-cm-long Mackereth core (QH07-1B) from the southeastern basin of Lake Qinghai, at LQDP05 site 2 (Fig. 4-5).

Fig. 1 Seismic survey lines and drill sites

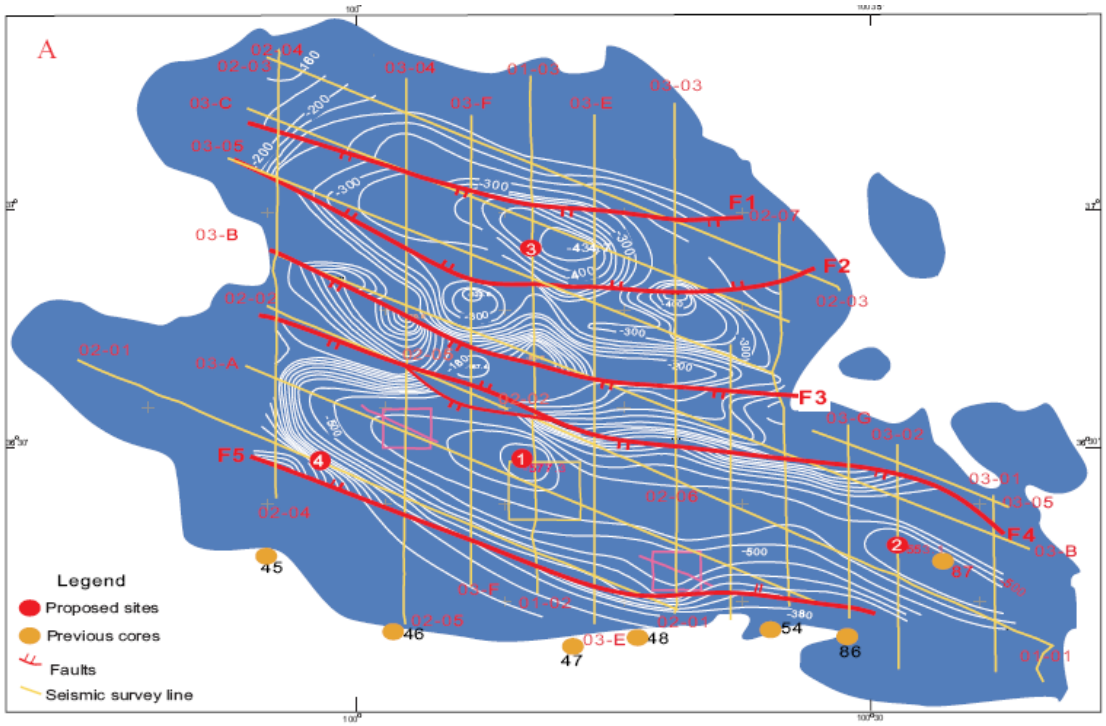

Fig. 2 Drilling platform, 2005

Fig. 3 Core descriptions of LQDP cores from sites 1 and 2. This dissertation focused on a 18.6m drill core from site 1 (LQDP05-1F)

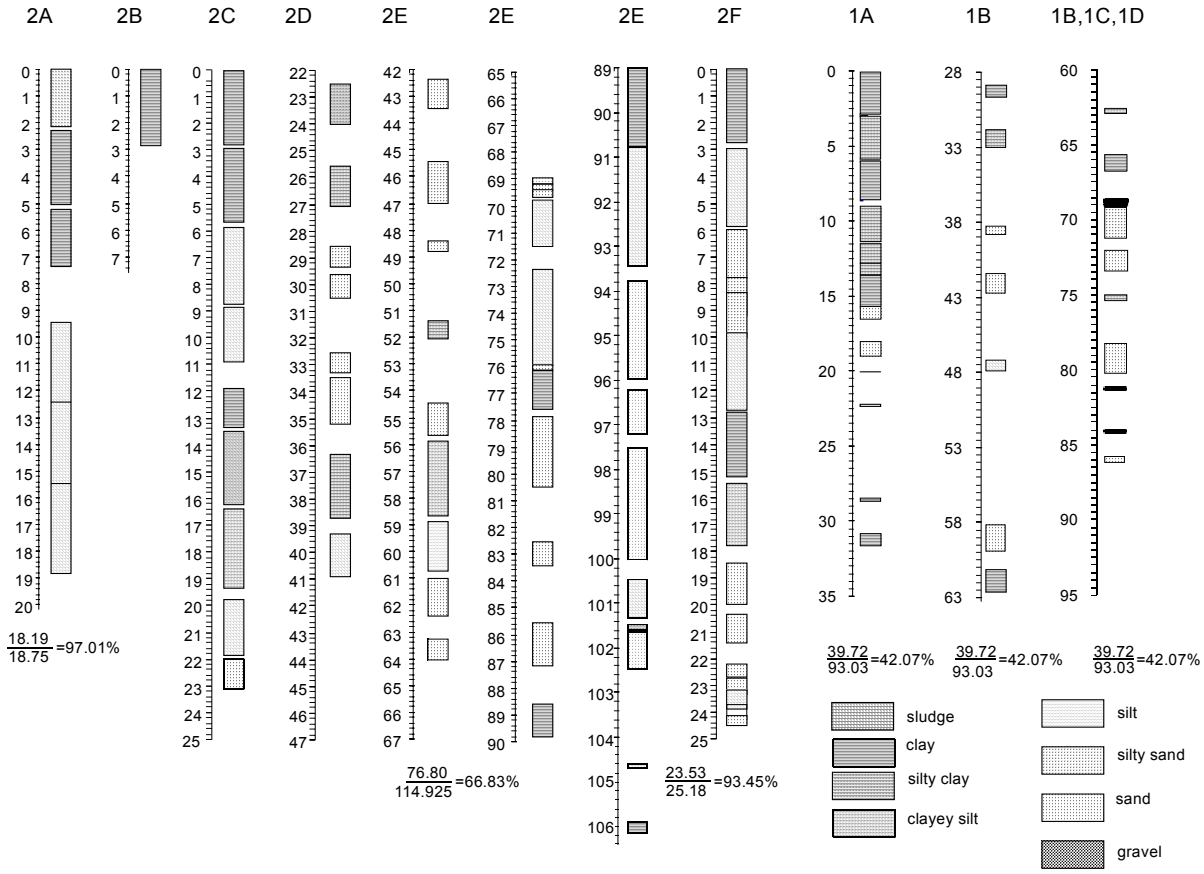

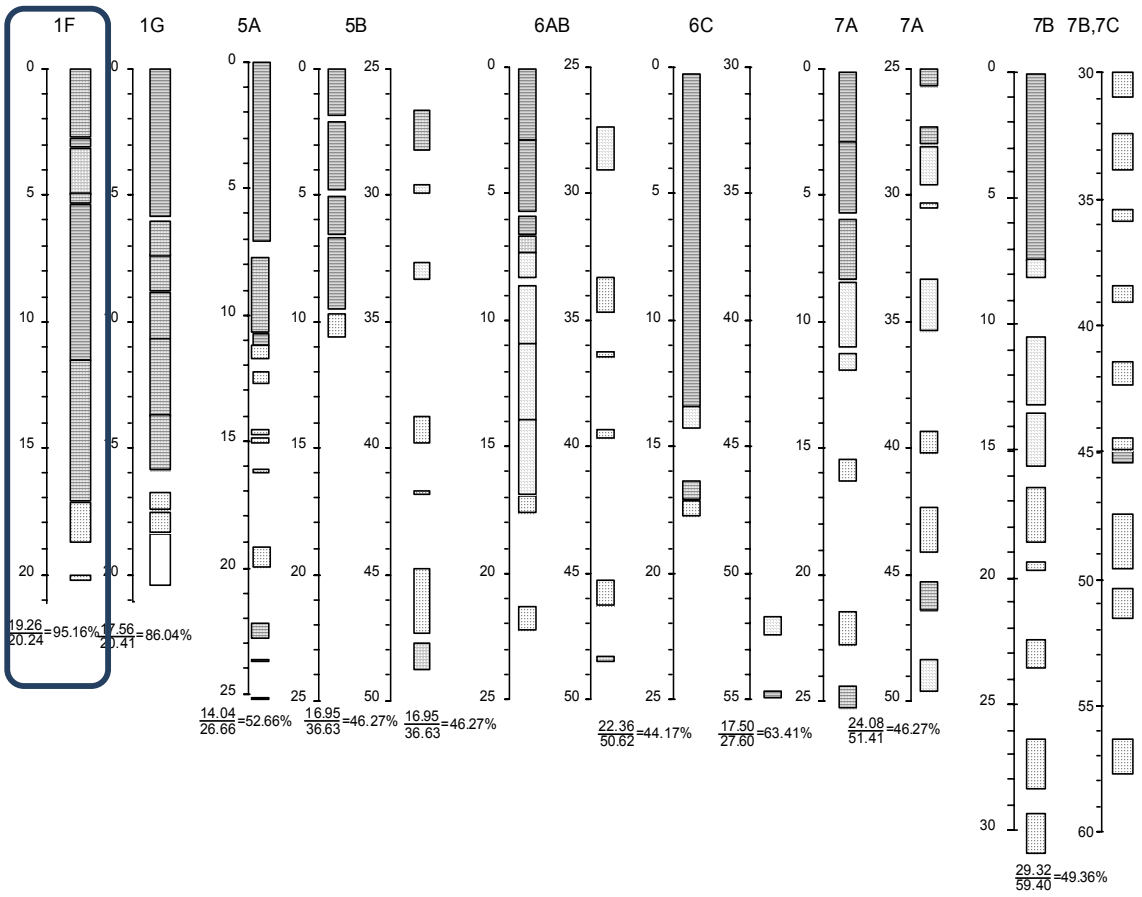
1F
1G
5A
5B
6AB
6C
7A
7A
7B
7B,7C
19.26/20.24=95.16%
17.56/20.41=86.04%
14.04/26.66=52.66%
16.95/36.63=46.27%
16.95/36.63=46.27%
22.36/50.62=44.17%
17.50/27.60=63.41%
24.08/51.41=46.27%
29.32/59.40=49.36%

Fig. 4 Coring (QH07) using a Piston corer, 2007

Fig. 5 Image of core QH07, total 5.3 m, including a 2-m gap between the 85-cm-long mini-Mackereth core (QH07-1B-1MM, section 1, the top 15 cm sediment was subsampled in the field) and the 3.55-m-long Uwitec piston core (QH07-1A, section 2-5). The green box (top) indicates the overlap subsection between section 3 and section 4. The green box (bottom) indicates the disturbed sediment in section 4. Seventeen uncalibrated $^{14}C$ ages are indicated by yellow triangles.